CHALMERS

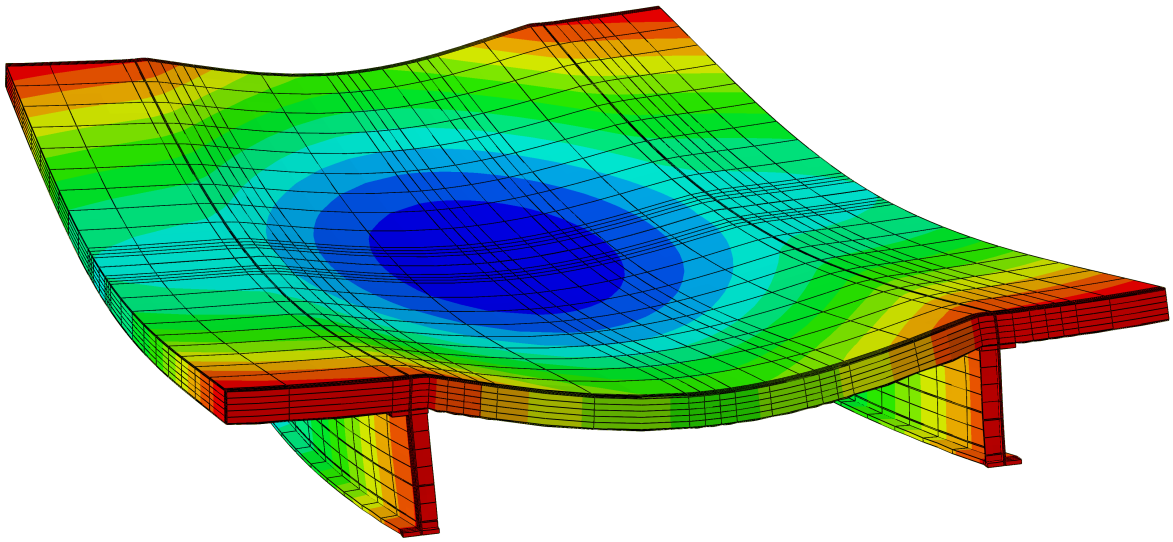

Evaluation and optimization of orthotropic sandwich plate systems with regard to global deflection

Finite element simulation and analytical evaluation

Master of Science Thesis in the Master's Programme Structural Engineering and Building Performance Design

ANDERBERG VIKTOR
BJÖRHAG ISAK

Department of Civil and Environmental Engineering
Division of Structural Engineering
Steel and Timber Structures
CHALMERS UNIVERSITY OF TECHNOLOGY
Göteborg, Sweden 2012

Master's thesis 2012:127

MASTER'S THESIS IN STRUCTURAL ENGINEERING AND BUILDING PERFORMANCE DESIGN

Evaluation and optimization of orthotropic sandwich plate systems with regard to global deflection

Finite element simulation and analytical evaluation

ANDERBERG VIKTOR
BJÖRHAG ISAK

Department of Civil and Environmental Engineering
Division of Structural Engineering
Steel and Timber Structures
CHALMERS UNIVERSITY OF TECHNOLOGY

Göteborg, Sweden 2012

Evaluation and optimization of orthotropic sandwich plate systems with regard to global deflection
Finite element simulation and analytical evaluation
ANDERBERG VIKTOR
BJÖRHAG ISAK

Master's thesis 2012:127
ISSN 1652-8557
Department of Civil and Environmental Engineering
Division of Structural Engineering
Steel and Timber Structures
Chalmers University of Technology
SE-412 96 Göteborg
Sweden
Telephone: +46 (0)31-772 1000

Cover:
The figure shows the studied bridge model and the displacement in the z-direction.

Chalmers Reproservice
Göteborg, Sweden 2012

Evaluation and optimization of orthotropic sandwich plate systems with regard to global deflection
Finite element simulation and analytical evaluation
Master's thesis in Structural Engineering and Building Performance Design
ANDERBERG VIKTOR
BJÖRHAG ISAK
Department of Civil and Environmental Engineering
Division of Structural Engineering
Steel and Timber Structures
Chalmers University of Technology

Abstract

New types of light weight sandwich plate system bridge decks may be an adequate alternative for short span bridges with regard to construction time and load capacity. These types of structural elements has been widely used in the aeronautics industry since the 1940s, mainly because of their high strength/stiffness to weight ratio. Due to recent developments in manufacturing techniques, it may be economically feasible to use sandwich plate systems within bridge-building in civil engineering. The main motivation is to use them in areas where the dead weight of the structure is critical and where strengthening or replacement of existing constructions is needed. In this thesis the focus is to use sandwich structures to serve as a deck plate for a two-girder short span bridge. However, the knowledge of using sandwich structures in the civil engineering area is limited.

Therefore, the main goal of this thesis is to achieve a better understanding of how to optimize the stiffness relations for an orthotropic sandwich plate with regard to global deflection. The examination is done with a parametric study where the different stiffnesses are altered and the global behavior of the beam-plate system is analyzed. To be able to perform such a sensible parametric study the number of parameters have to be reduced. This is done by transforming the structure to a one layered equivalent orthotropic plate.

The transformation process is performed in two main steps; first the structure is translated into a three layered homogeneous sandwich plate with orthotropic material properties; then these three layers are transformed into a single layer equivalent orthotropic plate. The two steps of transformation are performed by both finite element analysis (FEA) and analytical evaluation.

The second step of the transformational process is performed in two different methods to get the equivalent properties, Transformation based on Axial Load Deformation (TALD) and Transformation based on Constant Flexural Rigidity (TCFR). These two methods are generally very similar, but for two of the elastic constants the basis for the assumptions are different. TALD is based on a simple force equilibrium and TCFR calculates the elastic constants based on equilibrium of bending. The two methods are verified for different material parameters and support conditions. The result shows that the TCFR method is superior to the TALD method, with better correlation compared to the untranslated reference plate.

Different conceptual designs of sandwich structures are transformed and compared with the optimized relations obtained from the parametric study. The concepts are modified in order to utilize the material better. The commercial product Asset deck, made of FRP, is also evaluated and modified in order to get a more optimally used structure.

A general method for optimizing deck structures is also presented. One should be aware that the optimization method requires basic knowledge of the engineer on how to improve the stiffness of the structure in different directions. The method presented is only an evaluation tool and does not offer any suggestions of how to improve the structure.

Keywords: Asset deck, evaluation tool, finite element analysis, global deflection, orthotropic bridge deck, sandwich plate, stiffness optimization, transformation

Utvärdering och optimering av ortotropa sandwich-plattor med hänsyn till global nedböjning
Simluering med hjälp av finita element analyser och analytiska uttryck
Examensarbete i Structural Engineering and Building Performance Design
ANDERBERG VIKTOR
BJÖRHAG ISAK
Institutionen för bygg- och miljöteknik
Avdelning för konstruktionsteknik
Stål- och träbyggnad
Chalmers tekniska högskola

Sammanfattning

Nya typer av sandwich-platt-element kan vara ett tillfredställande alternativ för mindre broar med avseende på byggtid och lastkapacitet. Dessa typer av element har använts inom flygindustrin sen 1940-talet, på grund av deras höga förhållande mellan hållfasthet/styvhet och vikt. Nya tillverkningsmetoder, gällande svetsning och sammanfogning, har gjort det mer ekonomiskt att använda dessa för väg- och vattenbyggnadsändamål. Det huvudsakliga användningsområdet är främst där egenvikten spelar en avgörande roll och i fall där förstärkningsåtgärder är nödvändiga. I detta examensarbete undersöks främst hur en sandwich-platta kan användas som brodäck för en mindre bro bestående av tvåprimärbalkar. Dock är kunskaperna att använda sådan inom samhällsbyggnadsområdet väldigt begränsade.

Därav är det huvudsakliga målet med denna rapport att försöka fåen bättre förståelse av hur styvhetsförhållandena för en ortotropisk sandwich-platta kan optimeras med avseende påglobal nedböjning. Denna undersökning görs genom en parametrisk studie där de olika materialparametrarna ändras samtidigt som det globala beteendet studeras.

För att göra en betydelsefull parameterstudie krävs det att antalet parametrar minskas. Detta är gjort genom att transformera en plattstruktur till en motsvarande homogen ortotropisk platta. En effektiv struktur erhålls genom att töjningsfördelningen över höjden av plattan är linjär under böjdeformation. Detta är det huvudsakliga området som undersöks i den parametriska studien.

Transformationsprocessen är uppdelad i två huvudsakliga steg; i första steget transformeras strukturen till tre homogena lager med ortotropiska materialegenskaper; i andra steget transformeras dessa tre lager till en ekvivalent ortotrop platta. Dessa två steg genomförs med finit element-analys och handberäkning med hjälp utav analytiska plattmodeller.

Det andra steget i transformationsprocessen resulterade i två olika metoder, TALD och TCFR, för att erhålla de ekvivalenta egenskaperna. De två metoderna skiljer sig inte särskilt mycket ifrån varandra men för några av de elastiska konstanterna har de olika grundantaganden. TALD är baserad enbart på kraftjämvikt och TCFR på jämvikt för böjning. Dessa två metoders noggranhet är verifierad med olika typer av materialparametrar och stödförhållanden. Resultatet från detta visar att TCFR-metoden är överlägsen gentemot TALD-metoden, när deras nedböjning jämförs med referensplattans.

Olika koncept av sandwich-strukturer är transformerade och jämförs sedan med de optimala förhållandena av styvhetsmodulerna från parameterstudien. Koncepten ändras sedan för att utnyttja materialet bättre. Den redan tillgängliga produkten Asset deck, tillverkad av glasfiber, är också utvärderad och optimerad.

En generell metod för att optimera brodäckstrukturer är också framtagen och presenterad i arbetet. Metoden bygger dock på att ingenjören har tillräckliga kunskaper för att ändra och justera de olika styvheterna. Metoden skall enbart ses som ett utvärderingshjälpmedel och ger inga anvisningar om hur strukturen skall ändras.

Nyckelord: Asset deck, utvärderingsverktyg, finit element analys, global nedböjning, ortotrop brobaneplatta, sandwich-platta, styvhetsoptimering, transformation

Preface

This master's thesis main subject is evaluation and optimization of orthotropic sandwich plate systems with regard to deflection. The project corresponds to 30 higher education credits and has been carried out between January and July 2012 at the Department of Structural Engineering, Division of Steel and Timber Structures, Chalmers University of Technology, Sweden.

We especially want to thank our supervisor and examiner Mohammad Al-Emrani, who has responded to our thoughts and questions. We would also like to thank Valbona Mara because of her help in specific areas of the project and proofreading of the thesis. A little recognition to our roommate Marco Pagliarin for his endurance during our constant window ventilating of the room.

Finally we would like to thank our opponents, Ula Alwan and Diana Järve for their feedback to our project and review along the whole process and also Joakim Carlberg and Binyam Toyib for their answers to random questions regarding our project during the semester.

Göteborg June 2012-06-06

Viktor Anderberg and Isak Björhag

Nomenclature

Abbreviations and technical terms

Anisotropic material	Material that can be described by 21/36 elastic constants
B	Bottom layer of sandwich plate
FE	Finite Element
FEA	Finite Element Analysis
FEM	Finite Element Method
FRP	Fiber Reinforced Polymer
I	Interface layer of sandwich plate
Isotropic material	Material that can be described by two elastic constants
LM1	Load Model 1 from Eurocode
Orthotropic material	Material that can be described by nine elastic constants
REF	Reference
T	Top layer of sandwich plate
TALD	Transformation based on Axial Load Deformation
TCFR	Transformation based on Constant Flexural Rigidity

Roman upper case letters

A_{ii}^{jj}	Area in direction ii, where $i = x, y, z$ or $i = 1, 2, 3$ and $j = T, I, B$.
D_{ii}	Bending stiffness of a plate in direction ii, where $i = x, y, z$ or $i = 1, 2, 3$.
E_{ii}	Elastic modulus in direction ii, where $i = x, y, z$ or $i = 1, 2, 3$.
F_j	Force on sandwich panel part, $j = T, I, B$ and where none is the resulting force.
G_{ii}	Shear modulus in direction ii, where $i = x, y, z$ or $i = 1, 2, 3$.
H^j	Height of sandwich panel part, $j = T, I, B$ and where none is the total height.
P_{ii}^{jj}	Force vector in direction i, where $i = x, y, z$ or $i = 1, 2, 3$ and $j = T, I, B$.
U_i	Displacement, where $i = x, y, z$ or $i = 1, 2, 3$.
W	Width of sandwich panel

Roman lower case letters

b	Width
h	Height
m_i	Moment per unit length in direction i, where $i = x, y, z$ or $i = 1, 2, 3$.
q_i	Distributed load in direction i, where $i = x, y, z$ or $i = 1, 2, 3$.
u_i	Displacement, where $i = x, y, z$ or $i = 1, 2, 3$.

Greek letters

α_j	Ratio of H^j and H.
δ_i^j	Displacement in direction i, where $i = x, y, z$ and part $j = T, I, B$.
ϵ_i	Strain in direction i, where $i = x, y, z$ or $i = 1, 2, 3$.
γ_{ij}	Shear strain in direction ij, where $i, j = x, y, z$ or $i, j = 1, 2, 3$.
$\gamma^{'}, \gamma^{''}$	Angular distortion [Rad]
ν_i	Poisons ratio in direction i, where $i = x, y, z$ or $i = 1, 2, 3$.
ω	Deflection
ω	Angular frequency [Rad/s]
∂	Differential operator
σ_i	Stress in direction i, where $i = x, y, z$ or $i = 1, 2, 3$.
τ_{ij}	Shear stress in direction ij, where $i, j = x, y, z$ or $i, j = 1, 2, 3$.
υ	Angel of rotation [Rad]

Contents

List of Figures

List of Tables

1 Introduction

1.1 Background

In Sweden, the infrastructural freeway network was heavily expanded during the 1950s and 60s, (*väg* 2012). Many roads were constructed and with these followed a lot of bridges and viaducts. The bridges' structures were designed to last for a specific period of time, but due to poor bridge deck construction (mainly made of reinforced concrete) and frequent use of de-icing agents, the bridge deck deteriorated faster than the main bearing structure. This has become a major problem today when a lot of bridge decks have to be rehabilitated or replaced by new ones. In addition the traffic pattern has changed during the years, with more and heavier traffic on the roads today than some time ago. This growing problem can be solved by either strengthening of the main girders, or lowering of the dead weight of the structure.

Until recently there have not been any good options of creating a light weight - high strength bridge deck. However, with the introduction of composite sandwich plate systems, new possibilities are presented. This new deck consists of thin, high strength outer sheet faces, and a much weaker low-density core, which gives a high strength to weight ratio. This type of structural element has been used for a long time in the aeronautic industry, but is still uncharted within the bridge civil engineering field.

Sandwich plate systems are mainly prefabricated which is beneficial when replacing old bridge decks. It will greatly speed up the construction time compared to casting a new reinforced concrete deck. Factory production is often optimized because of the controlled environment and mass production of the specific element. However, there is very limited information on the behavior and optimization of this new sandwich plate system for usage in bridges.

The core of a sandwich plate can be constructed by materials of different shapes, such as honeycomb, trapezoidals or tubulars. These structures are hard to model and analyze in FE programs due to the complex geometry. Furthermore, performing changes and adjustments to a complex core structure is a very time consuming process, where the whole structure has to be remodeled. Instead of modeling the whole structure, a transformation could be made which turns this complex structure into one equivalent homogeneous layer. This will be particularly useful when performing a parametric study where the number of variables are greatly reduced.

1.2 Aim and Objectives

The motivations of this thesis are: to achieve a better understanding how a simple bridge deck made of a sandwich structure behaves when altering the material parameters, i.e. adjusting the stiffnesses in the different directions; to identify which relations between different stiffnesses are needed in order to get a desired global behavior; and to discover how to perform an accurate transformation from a multi layered plate into an equivalent one, if this is possible.

The main objectives for this thesis are:

1. Establish a model that transforms a multi layered sandwich structure into a single layered equivalent plate.

2. Perform a parametric study for a single layered orthotropic plate and establish usable ratios and relations for important stiffness parameters.

3. Find a way to optimize a specific bridge structure with regard to global deflection by altering the sandwich plate.

4. Analyze the commercial product Asset and present possible improvements.

5. Propose an optimization method for a sandwich deck plate in a bridge structure.

1.3 Method

The work flow for this thesis can be seen in figure 1.3.1. It is started with a study of analytical solutions for isotropic and orthotropic plates to give a basic understanding of methods to solve plate equations, and to get a sense of how the plates behave when altering different stiffness parameters. This is followed by establishing different ways of transforming a multi layered structure into a single equivalent one. This produces two different transformation methods for establishing the equivalent Young's modulus, TALD (Transformation based on Axial Loaded Deformation) and TCFR (Transformation based on Constant Flexural Rigidity). These two need to be verified to ensure a good transformation and to compare and evaluate the two transformation methods. This is done by Finite Element analysis in Abaqus CAE and features both modeling with shell and solid elements. A parametric study, which regards all concerned stiffnesses, is then carried out in order to get the optimal relations between different moduli, and to form a basis which can be used to improve existing concepts.

Mathematical algorithms and calculations are developed in MATLAB. Preliminary sizing and load cases for the full scale bridge model is constructed in MathCAD and the FE-modeling is performed in Abaqus CAE. This thesis is written in LaTeX.

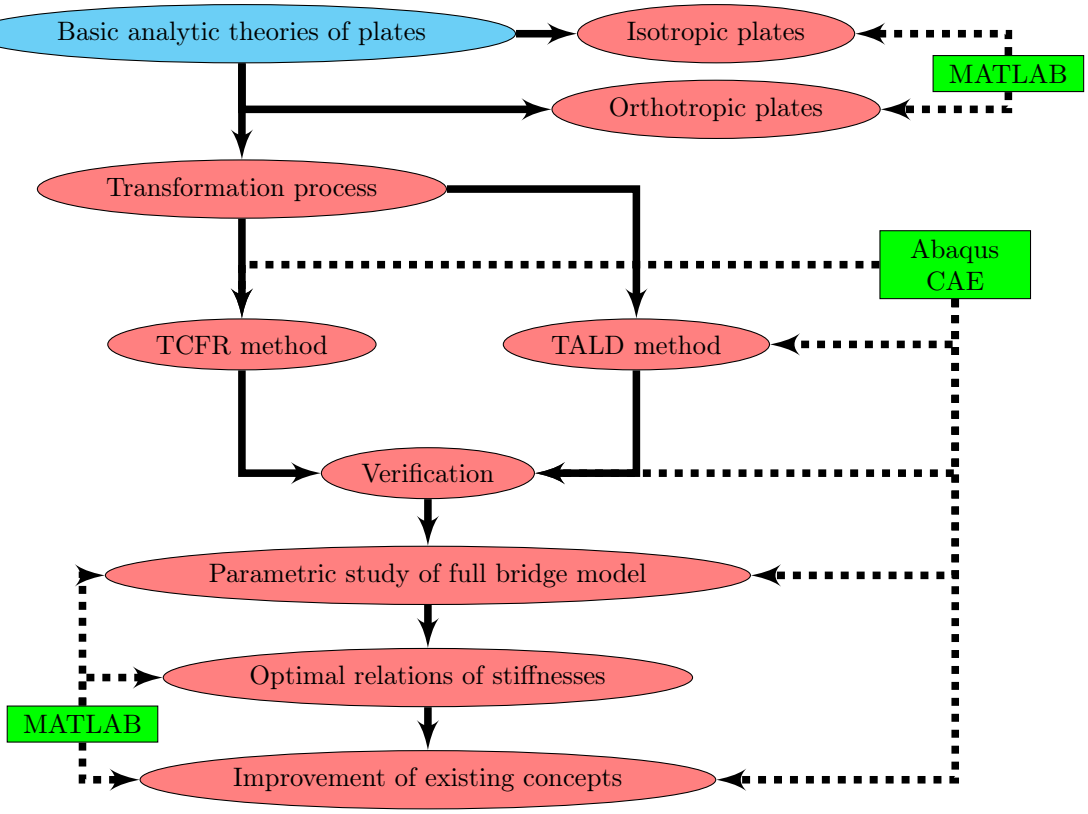

Figure 1.3.1: *Main work flow of the project*

1.4 Limitation

There is a clear time limitation of the study since the master's thesis is to be completed in 20 weeks. All FE-modeling is done with linear analysis, i.e. no local behaviors such as buckling and/or plasticity are considered. Different stiffnesses as well as parameters coupled to these are studied. Strengths and failures are not considered. The parametric study is limited to only include a very specific case where the sandwich plate is resting on two longitudinal main girders. The choice of materials is not important since the only considerations are the numerical values of the stiffnesses.

1.5 Outline of the master's thesis

The introduction of this thesis is followed by chapter 2, which treats analytical solutions of plate equations for isotropic and orthotropic plates. The governing differential equations for both type of plates are derived. Limitations and applicability of these equations are presented and discussed. This chapter also features methods to solve them with help of Fourier approximation and Navier's solution.

The following chapter 3 is about how to transform a multi layered sandwich into a single equivalent plate. A thorough explanation and mathematical derivation is presented. The thoughts behind the different methods of transforming are explained and discussed. These transformations are then verified in chapter 4 for two different cases with randomized material properties. The results from the transformed plates are presented and compared with the reference models and the best method is chosen.

The parametric study of the bridge is then presented in chapter 5 where important relations and ratios are explained. Different concepts are tested and geometrically changed and optimized (chapter 6) to fit the derived relations from the parametric study. This will improve the material efficiency and give a better global behavior with regard to the deflection.

The final chapters of this thesis features a discussion and conclusions. Recommendations for future studies are presented together with advice for improvements of the results.

2 Fundamental Theories of Plate Analysis

The fundamental plate theories are divided into two different parts, the first is isotropic plates where the material has the same properties in all directions for, example steel. The second part threats orthotropic plates where the stiffness varies depending on the direction, for example timber or Fiber Reinforced Polymer (FRP). Basic assumptions are established and the governing differential equations are derived and solved with Fourier analysis for the two cases.

2.1 Isotropic plates

This section treats the simple case of isotropic plates, Kirchoff-Love plates and his *small deflection theory of thin plates*. It is a simplification that translates the three-dimensional plate into a two-dimensional and is based on the assumptions below.

2.1.1 Assumptions

The Kirchoff-Love theory is based on the following assumptions Szilard (2004):

1. Only in-plane stresses and strains are considered.
2. The material has to obey Hooke's law, i.e. it has to be linear elastic, isotropic and homogeneous.
3. The plate has to be initially flat.
4. The middle surface (same as neutral axis for beam theory) of the plate has to stay unstrained during bending.
5. The thickness of the plate has to be constant and less than a tenth of the length (or width depending on which is the smaller) of the plate.
6. The transverse deflection (z-direction) has to be less than a tenth of the thickness, in order to fulfill the requirements of small-deflection-theory.
7. The deflected middle surface's slopes has to be small compare to unity ($\upsilon \ll 1$)
8. The normal stress component σ_z in the transverse direction to the plates surface should be neglected.
9. Shear deformations in the transverse direction to the plates surface should be neglected.

2.1.2 Governing differential equation for bending in Cartesian coordinate system

The derivation of the governing differential equation for isotropic plates is performed by establishing equilibrium equations for a small element of the plate, seen in figure 2.1.1, Szilard (2004).

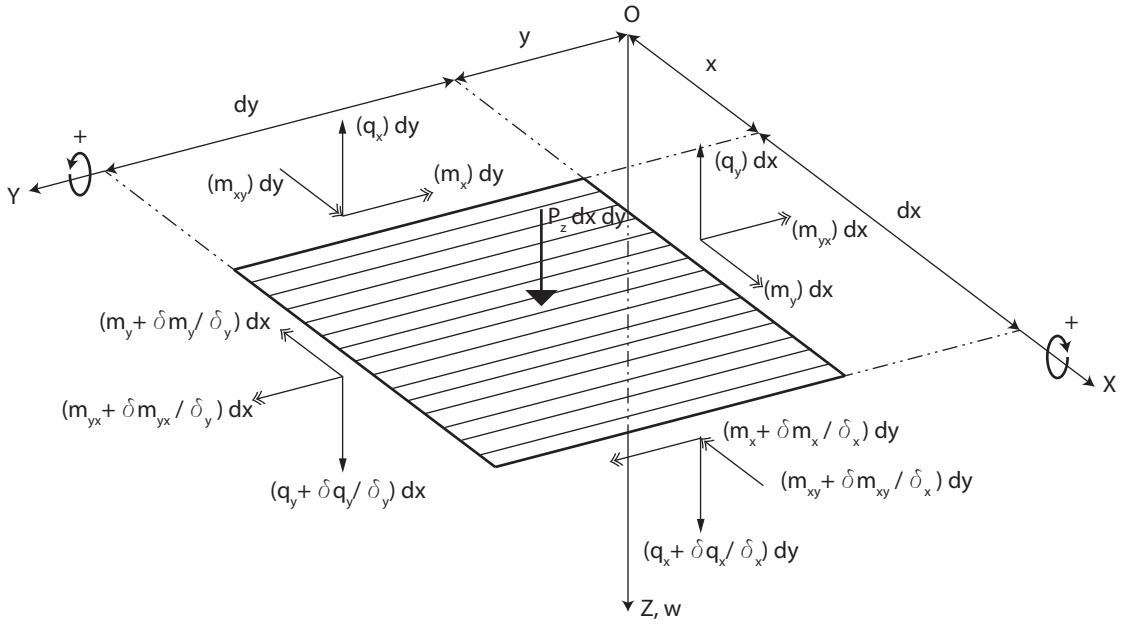

Figure 2.1.1: *Principles for establishing plate equilibrium equations.*

Moment equilibrium around y and midpoint gives, see figure **??**.

$$(m_x + \frac{\partial m_x}{\partial x}dx)dy - m_x \cdot dy + (m_{yx} + \frac{\partial m_{yx}}{\partial y}dy)dx - m_{yx} \cdot dx - q_x \cdot dy\frac{dx}{2} - (q_x + \frac{\partial q_x}{\partial x}dx)dy\frac{dx}{2} = 0 \quad (2.1.1)$$

$$dx^2 \longrightarrow 0 \text{ in relation to } dx$$

$$\frac{\partial m_x}{\partial x}dx \cdot dy + \frac{\partial m_{yx}}{\partial y}dy \cdot dx - q_x \cdot dy \cdot dx = 0 \quad (2.1.2)$$

$$\frac{\partial m_x}{\partial x} + \frac{\partial m_{yx}}{\partial y} = q_x \quad (2.1.3)$$

The same principle but instead moment equilibrium around x gives:

$$\frac{\partial m_y}{\partial y} + \frac{\partial m_{xy}}{\partial x} = q_y \quad (2.1.4)$$

Summation of forces in z-direction:

$$q_x \cdot dy - (q_x + \frac{\partial q_x}{\partial x}dx)dy + q_y \cdot dx - (q_y + \frac{\partial q_y}{\partial y}dy)dx - P_z \cdot dx \cdot dy = 0 \quad (2.1.5)$$

$$\frac{\partial q_x}{\partial x} + \frac{\partial q_y}{\partial y} = -P_z \quad (2.1.6)$$

Inserting equation (2.1.3) and (2.1.4) into (2.1.6) gives:

$$\frac{\partial(\frac{\partial m_x}{\partial x} + \frac{\partial m_{yx}}{\partial y})}{\partial x} + \frac{\partial(\frac{\partial m_y}{\partial y} + \frac{\partial m_{xy}}{\partial x})}{\partial y} = -P_z \quad (2.1.7)$$

$$\frac{\partial^2 m_x}{\partial x^2} + \frac{\partial^2 m_{yx}}{\partial y \partial x} + \frac{\partial^2 m_y}{\partial y^2} + \frac{\partial^2 m_{xy}}{\partial x \partial y} = -P_z \quad (2.1.8)$$

Note that: $m_{xy} = m_{yx}$ has to be true to keep equilibrium.

$$\frac{\partial^2 m_x}{\partial x^2} + 2\frac{\partial^2 m_{xy}}{\partial x \partial y} + \frac{\partial^2 m_y}{\partial y^2} = -P_z \tag{2.1.9}$$

Stress-strain relations for an isotropic plate governed by Hooke's law are given in equations (2.1.10a-b)

$$\sigma_x = E \cdot \varepsilon_x + \nu \cdot \sigma_y \tag{2.1.10a}$$
$$\sigma_y = E \cdot \varepsilon_y + \nu \cdot \sigma_x \tag{2.1.10b}$$

Combining equations (2.1.10a-b) results in:

$$\sigma_x = E \cdot \varepsilon_x + \nu(E \cdot \varepsilon_y + \nu \cdot \sigma_x) \tag{2.1.11}$$

$$\sigma_x - \nu^2 \cdot \sigma_x = E \cdot \varepsilon_x + \nu \cdot E \cdot \varepsilon_y \tag{2.1.12}$$

This leads to the final Hookean stress-strain relationship in (2.1.13a-c):

$$\sigma_x = \frac{E(\varepsilon_x + \nu \cdot \varepsilon_y)}{1 - \nu^2} \tag{2.1.13a}$$
$$\sigma_y = \frac{E(\varepsilon_y + \nu \cdot \varepsilon_x)}{1 - \nu^2} \tag{2.1.13b}$$
$$\tau_{xy} = \frac{E}{2(1+\nu)}\gamma_{xy} \tag{2.1.13c}$$

If a small section of the plate is studied during bending, the angle ϑ is the sections rotation in relation to the normal going through the undeflected cross section. The angle of rotation for the section dx away from ϑ can be characterized as:

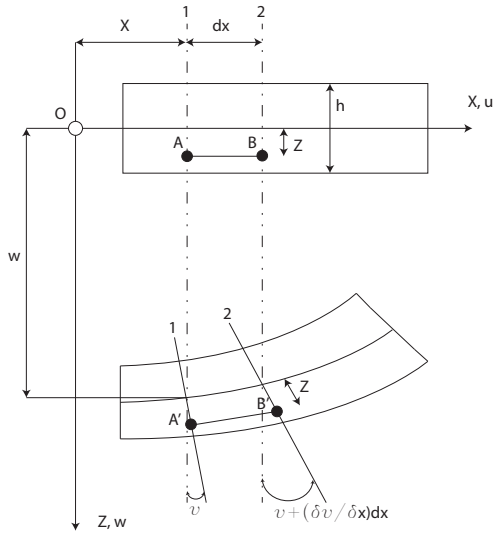

Figure 2.1.2: *Deflection of the section, before/after.*

$$\vartheta = \vartheta + \frac{\partial \vartheta}{\partial x}dx \tag{2.1.14}$$

$$\vartheta = -\frac{\partial \omega}{\partial x} \tag{2.1.15}$$

Where ω is the deflection of the plate.
The strain in a fiber with distance z from the neutral layer is obtained by:

$$\varepsilon_x = z\frac{\partial \vartheta}{\partial x} \tag{2.1.16}$$

Combining equation (2.1.15) with (2.1.16), the strain-deflection relationship is obtained:

$$\varepsilon_x = -z\frac{\partial^2 \omega}{\partial x^2} \tag{2.1.17a}$$

$$\varepsilon_y = -z\frac{\partial^2 \omega}{\partial y^2} \tag{2.1.17b}$$

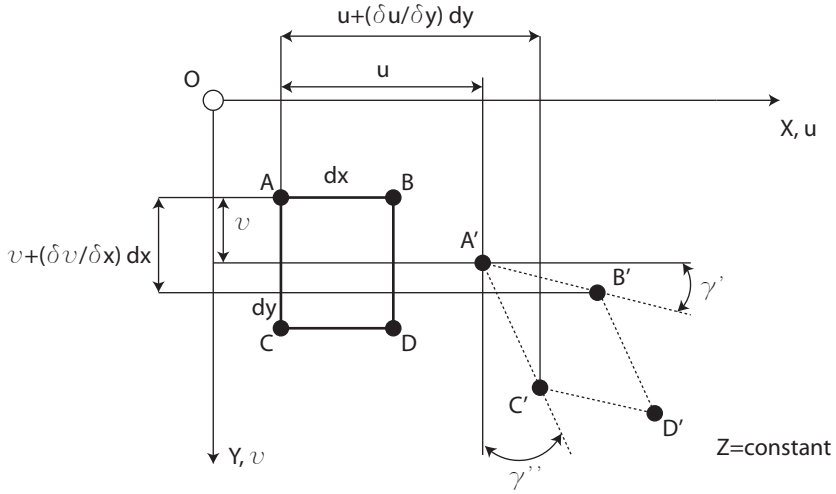

Figure 2.1.3: *Angels of distortion.*

The angular distortion can be obtained by studying figure 2.1.3.

$$\gamma' = \frac{\partial v}{\partial x} \tag{2.1.18a}$$

$$\gamma'' = \frac{\partial u}{\partial y} \tag{2.1.18b}$$

$$u = -\frac{\partial \omega}{\partial x} \tag{2.1.18c}$$

$$v = -\frac{\partial \omega}{\partial y} \tag{2.1.18d}$$

$$\gamma_{xy} = \gamma' + \gamma'' \tag{2.1.19}$$

Combine equations (2.1.18a-d) with (2.1.19) to obtain the strain-deflection relationship γ_{xy} (shear strain):

$$\gamma_{xy} = -2z\frac{\partial^2 \omega}{\partial x \partial y} \tag{2.1.20}$$

$$\kappa_x = -\frac{\partial^2 \omega}{\partial x^2} \tag{2.1.21a}$$

$$\kappa_y = -\frac{\partial^2 \omega}{\partial y^2} \tag{2.1.21b}$$

$$\chi = -\frac{\partial^2 \omega}{\partial x \partial y} \tag{2.1.21c}$$

The moment per unit length is obtained by multiplying the stress over the cross-section with its level on z and integrating over the height of the cross-section:

$$m_x = \int_{-h/2}^{h/2} \sigma_x z \cdot dz \tag{2.1.22}$$

Using the Hookean relationship from equations (2.1.13a-c) and expressing ε_x, ε_y and γ_{xy} according to (2.1.17a-b) and (2.1.20), the integral becomes:

$$m_x = -\int_{-h/2}^{h/2} \frac{E \cdot z^2}{1-\nu^2}\left(\frac{\partial^2 \omega}{\partial x^2} + \nu \frac{\partial^2 \omega}{\partial y^2}\right) dz \tag{2.1.23}$$

Performing the integration gives:

$$m_x = -\frac{E \cdot h^3}{12(1-\nu^2)}\left(\frac{\partial^2 \omega}{\partial x^2} + \nu \frac{\partial^2 \omega}{\partial y^2}\right) \tag{2.1.24}$$

Set:

$$D = \frac{E \cdot h^3}{12(1-\nu^2)} \tag{2.1.25}$$

Which leads to the final expression of the moment per length m_x and m_y, on compressed form, where D is the bending stiffness of the system:

$$m_x = D(\kappa_x + \nu \cdot \kappa_y) \tag{2.1.26a}$$

$$m_y = D(\kappa_y + \nu \cdot \kappa_x) \tag{2.1.26b}$$

The shear moment is calculated in a similar way:

$$m_{xy} = \int_{-h/2}^{h/2} \tau_{xy} z \cdot dz \tag{2.1.27}$$

$$m_{xy} = -\int_{-h/2}^{h/2} \frac{E \cdot z^2}{2(1+\nu)} \cdot 2\frac{\partial^2 \omega}{\partial x \partial y} \cdot dz \tag{2.1.28}$$

Performing the integral produces:

$$m_{xy} = -\frac{E \cdot h^3}{12(1+\nu)} \frac{\partial^2 \omega}{\partial x \partial y} \tag{2.1.29}$$

By expansion with $(1-\nu)$ the difference of two squares can be used to express the moment in terms of the general bending stiffness D:

$$m_{xy} = -\frac{E \cdot h^3 \cdot (1-\nu)}{12(1+\nu) \cdot (1-\nu)} \cdot \frac{\partial^2 \omega}{\partial x \partial y} \tag{2.1.30}$$

$$m_{xy} = D(1-\nu) \cdot \chi \tag{2.1.31}$$

By inserting the obtained expression for the moments into the original equilibrium equation (2.1.8), the governing bending equation for isotropic plates is established:

$$\frac{\partial^2 (D(-\frac{\partial^2 \omega}{\partial x^2} - \nu \frac{\partial^2 \omega}{\partial y^2}))}{\partial x^2} + 2 \cdot \frac{\partial^2 (D(1-\nu)(-\frac{\partial^2 \omega}{\partial x \partial y}))}{\partial x \partial y} + \frac{\partial^2 (D(-\frac{\partial^2 \omega}{\partial y^2} - \nu \frac{\partial^2 \omega}{\partial x^2}))}{\partial y^2} = P_z(x,y) \tag{2.1.32}$$

$$D\left(\frac{\partial^4 \omega}{\partial x^4} - \nu \frac{\partial^4 \omega}{\partial x^2 \partial y^2}\right) + 2 \cdot D(1-\nu)\left(-\frac{\partial^4 \omega}{\partial x^2 \partial y^2}\right) + D\left(-\frac{\partial^4 \omega}{\partial y^4} - \nu \frac{\partial^4 \omega}{\partial x^2 \partial y^2}\right) = P_z(x,y) \tag{2.1.33}$$

The final expression for the governing differential equation for isotropic plates reads:

$$\boxed{\frac{\partial^4 \omega}{\partial x^4} + 2\frac{\partial^4 \omega}{\partial x^2 \partial y^2} + \frac{\partial^4 \omega}{\partial y^4} = \frac{P_z(x,y)}{D}} \tag{2.1.34}$$

2.2 Orthotropic plates

Ortotropic plates can have different stiffnesses and/or strengths in all directions. This behavior could be due to orthotrophy of the material itself or that the plate has irregular geometry such as stiffeners, ribs or other stiffness altering features. The derivation of the governing equation for bending follows the same procedure as for isotropic plates found in the previous chapter, but with some small additions added to the stress-strain relation and the in plane shear modulus.

2.2.1 Assumptions

The assumptions for orthotropic Kirchoff-Love plates are the same as for the isotropic version, see chapter 2.1.1.

2.2.2 Governing differential equation for bending in Cartesian coordinate system

The stress-strain relationship for orthotropic plates reads (Szilard 2004):

$$\varepsilon_x = \frac{\sigma_x}{E_x} - \nu_y \frac{\sigma_y}{E_y} \tag{2.2.1a}$$

$$\varepsilon_y = \frac{\sigma_y}{E_y} - \nu_x \frac{\sigma_x}{E_x} \tag{2.2.1b}$$

$$\gamma_{xy} = \frac{\tau_{xy}}{G} \tag{2.2.1c}$$

$$G = \frac{\sqrt{E_x E_y}}{2(1+\sqrt{\nu_x \nu_y})} \tag{2.2.1d}$$

Combine equation (2.2.1a) with (2.2.1b) and solve for σ_x and σ_y:

$$\sigma_x = \frac{E_x(\varepsilon_x + \nu_y \varepsilon_y)}{(1-\nu_x \nu_y)} \tag{2.2.2a}$$

$$\sigma_y = \frac{E_y(\varepsilon_y + \nu_x \varepsilon_x)}{(1-\nu_x \nu_y)} \tag{2.2.2b}$$

$$\tau_{xy} = G \cdot \gamma_{xy} \tag{2.2.2c}$$

Introduce equations (2.1.17a-b) and (2.1.20) into the orthotropic strain-stress relashionships (2.2.2a-c) gives:

$$\sigma_x = -\frac{E_x}{(1-\nu_x \nu_y)} \cdot (\frac{\partial^2 \omega}{\partial x^2} + \nu_y \frac{\partial^2 \omega}{\partial y^2}) \cdot z \tag{2.2.3a}$$

$$\sigma_y = -\frac{E_y}{(1-\nu_x \nu_y)} \cdot (\frac{\partial^2 \omega}{\partial y^2} + \nu_x \frac{\partial^2 \omega}{\partial x^2}) \cdot z \tag{2.2.3b}$$

The moments per unit length are calculated in the same manner as for the isotropic plate (2.1.22):

$$m_x = \int_{-h/2}^{h/2} \sigma_x z \cdot dz = -\int_{-h/2}^{h/2} \frac{E_x}{(1-\nu_x \nu_y)} \cdot (\frac{\partial^2 \omega}{\partial x^2} + \nu_y \frac{\partial^2 \omega}{\partial y^2}) z^2 \cdot dz \tag{2.2.4a}$$

$$m_y = \int_{-h/2}^{h/2} \sigma_y z \cdot dz = -\int_{-h/2}^{h/2} \frac{E_y}{(1-\nu_x \nu_y)} \cdot (\frac{\partial^2 \omega}{\partial y^2} + \nu_x \frac{\partial^2 \omega}{\partial x^2}) z^2 \cdot dz \tag{2.2.4b}$$

$$m_{xy} = \int_{-h/2}^{h/2} \tau_{xy} z \cdot dz = -\int_{-h/2}^{h/2} \frac{\sqrt{E_x E_y}}{2(1+\sqrt{\nu_x \nu_y})} \cdot 2(\frac{\partial^2 \omega}{\partial x \partial y}) z^2 \cdot dz \tag{2.2.4c}$$

Performing the integration gives:

$$m_x = -\frac{E_x h^3}{12(1-\nu_x \nu_y)} \cdot (\frac{\partial^2 \omega}{\partial x^2} + \nu_y \frac{\partial^2 \omega}{\partial y^2}) \tag{2.2.5a}$$

$$m_y = -\frac{E_y h^3}{12(1-\nu_x \nu_y)} \cdot (\frac{\partial^2 \omega}{\partial y^2} + \nu_x \frac{\partial^2 \omega}{\partial x^2}) \tag{2.2.5b}$$

$$m_{xy} = -2G\frac{h^3}{12} \cdot \frac{\partial^2 \omega}{\partial x \partial y} \tag{2.2.5c}$$

The equations can be written on a more condensed form by introducing the constants D_x, D_{xy}, D_y, D_{yx} and D_s:

$$D_x = \frac{E_x h^3}{12(1-\nu_x \nu_y)} \qquad D_y = \frac{E_y h^3}{12(1-\nu_x \nu_y)} \tag{2.2.6a}$$

$$D_{xy} = \frac{E_x h^3 \nu_y}{12(1-\nu_x \nu_y)} \qquad D_{yx} = \frac{E_y h^3 \nu_x}{12(1-\nu_x \nu_y)} \tag{2.2.6b}$$

$$D_s = \frac{G h^3}{12} \tag{2.2.6c}$$

$$m_x = -(D_x \frac{\partial^2 \omega}{\partial x^2} + D_{xy} \frac{\partial^2 \omega}{\partial y^2}) \tag{2.2.7a}$$

$$m_y = -(D_y \frac{\partial^2 \omega}{\partial y^2} + D_{yx} \frac{\partial^2 \omega}{\partial x^2}) \tag{2.2.7b}$$

$$m_{xy} = -2D_s \frac{\partial^2 \omega}{\partial x \partial y} \tag{2.2.7c}$$

Note: $\frac{\nu_x}{E_x} = \frac{\nu_y}{E_y}$ which explains why $D_{xy} = D_{yx}$
Inserting equations (2.2.7a-c) into the general expression (2.1.3) and (2.1.4) gives:

$$-\frac{\partial(D_x \cdot \frac{\partial^2 \omega}{\partial x^2} + D_{xy} \cdot \frac{\partial^2 \omega}{\partial y^2})}{\partial x} - \frac{\partial(2D_s \frac{\partial^2 \omega}{\partial x \partial y})}{\partial y} = q_x \tag{2.2.8}$$

$$-\frac{\partial(D_x \cdot \frac{\partial^2 \omega}{\partial x^2} + D_{xy} \cdot \frac{\partial^2 \omega}{\partial y^2} + 2D_s \cdot \frac{\partial^2 \omega}{\partial y^2})}{\partial x} = q_y \tag{2.2.9}$$

Let:

$$H = D_{xy} + 2D_s \tag{2.2.10}$$

Which gives:

$$-\frac{\partial(D_x \cdot \frac{\partial^2 \omega}{\partial x^2} + H \cdot \frac{\partial^2 \omega}{\partial y^2})}{\partial x} = q_x \tag{2.2.11a}$$

$$-\frac{\partial(D_y \cdot \frac{\partial^2 \omega}{\partial y^2} + H \cdot \frac{\partial^2 \omega}{\partial x^2})}{\partial y} = q_y \tag{2.2.11b}$$

Use the derived expression (2.2.11a-b) in (2.1.6) to obtain the differential equation for bending of orthotropic plates:

$$\boxed{D_x \frac{\partial^4 \omega}{\partial x^4} + 2H \frac{\partial^4 \omega}{\partial x^2 \partial y^2} + D_y \frac{\partial^4 \omega}{\partial y^4} = P_z(x, y)} \tag{2.2.12}$$

2.3 Fourier expansion

The derived 4th order differential equations (2.1.34) and (2.2.12) can only be solved rigorously for a few specific cases, Szilard (2004). For higher number of supports (three or four) there is a need to implement an approximation of the function to be able to perform the integration. This can be done by Fourier expansion of the function $w(x, y)$ and $P_z(x, y)$ which is the deflection- and load-function respectively.

The Fourier expansion is built around the trigonometric functions cosine and sine. For a one dimensional equation the approximation reads:

$$f(x) = \frac{1}{2} A_0 + \sum_{n=1}^{\infty} A_n \cos(n\omega x) + \sum_{n=1}^{\infty} B_n \sin(n\omega x) \tag{2.3.1}$$

$$\text{for } n = 1, 2, 3 \ldots$$

As expressed in (2.3.1), the function is equal to the expansion when the number of summations approaches infinity. Where A_0, A_n and B_n are Fourier expansions coefficients obtained by (2.3.2a-c):

$$A_0 = \frac{2}{T} \int_0^T f(x) dx \tag{2.3.2a}$$

$$A_n = \frac{2}{T} \int_0^T f(x) \cos(n\omega x) dx \tag{2.3.2b}$$

$$B_n = \frac{2}{T} \int_0^T f(x) \sin(n\omega x) dx \tag{2.3.2c}$$

Where T is the period of the function. ω can be obtained by equation (2.3.3):

$$\omega = \frac{2\pi}{T} \tag{2.3.3}$$

2.3.1 Navier's approach

Navier's approach is a general solution of the 4th order governing differential equation for rectangular plates, valid for both the isotropic (2.1.34) and orthotropic (2.2.12). It is performed by approximating the deflection- and load-function by double Fourier sine series. The approach originally treated simply supported plates, but with the implement of superposition theorem it is possible to solve for other, more complex boundary and loading conditions. The following derivation is performed for a simply supported plate subjected to a distributed load.

The deflection $\omega(x, y)$ is approximated by:

$$\omega(x,y) = \sum_m^\infty \sum_n^\infty W_{mn} \sin(\frac{m\pi x}{a}) \sin(\frac{n\pi y}{b}) \tag{2.3.4}$$

The load function $P_z(x, y)$ is approximated in the same manner:

$$P_z(x,y) = \sum_m^\infty \sum_n^\infty P_{mn} \sin(\frac{m\pi x}{a}) \sin(\frac{n\pi y}{b}) \tag{2.3.5}$$

Inserting the Fourier expansions (2.3.4) and (2.3.5) into the governing differential equation for isotropic plates (2.1.34) gives:

$$\frac{\pi^4 W_{mn} m^4 \sin(\frac{m\pi x}{a}) \sin(\frac{n\pi y}{b})}{a^4} + \frac{\pi^4 W_{mn} n^4 \sin(\frac{m\pi x}{a}) \sin(\frac{n\pi y}{b})}{b^4} +$$

$$+ \frac{2\pi^4 W_{mn} m^2 n^2 \sin(\frac{m\pi x}{a}) \sin(\frac{n\pi y}{b})}{a^2 b^2} = \frac{P_{mn} \sin(\frac{m\pi x}{a}) \sin(\frac{n\pi y}{b})}{D} \tag{2.3.6}$$

Simplify and solve for W_{mn}:

$$\pi^4 W_{mn} (\frac{m^4}{a^4} + \frac{n^4}{b^4} + 2\frac{m^2 n^2}{a^2 b^2}) = \frac{P_{mn}}{D} \tag{2.3.7}$$

$$W_{mn} = \frac{P_{mn}}{D\pi^4 (\frac{m^2}{a^2} + \frac{n^2}{b^2})^2} \tag{2.3.8}$$

P_z is previously described in equation (2.3.5). Solve for P_{mn} by multiplying the expression with $\sin(\frac{k\pi y}{b})dy$ and integrating between 0 and b, do note that the following steps is only valid for an evenly distributed load:

$$\int_0^b P_z(x,y) \sin(\frac{k\pi y}{b}) dy = \sum_m^\infty \sum_n^\infty P_{mn} \sin(\frac{m\pi x}{a}) \int_0^b \sin(\frac{n\pi y}{b}) \sin(\frac{k\pi y}{b}) dy \tag{2.3.9}$$

Performing the right integral from the previous expression (2.3.9) gives:

$$\int_0^b \sin(\frac{m\pi y}{b}) \sin(\frac{k\pi y}{b}) dy =$$

$$= \frac{bk \sin(\pi n)(2\sin(\frac{\pi k}{2})^2 - 1) - bn \sin(\pi k)(2\sin(\frac{\pi n}{2})^2 - 1)}{\pi k^2 - \pi n^2} \tag{2.3.10}$$

There are two cases for the variables n and k, if $n \neq k$ and if $n = k$. Note that n and k are integers $n, k = 1, 2, 3 \ldots$
for $n \neq k$:

$$\frac{bk \sin(\pi n)(2\sin(\frac{\pi k}{2})^2 - 1) - bn \sin(\pi k)(2\sin(\frac{\pi n}{2})^2 - 1)}{\pi k^2 - \pi n^2} = 0 \tag{2.3.11}$$

This behavior can be explained by cancellation of the trigonometric function. By inserting $n \neq k$ a phase shift is introduced in between the different sine-functions.

Because of the denominator of expression (2.3.10), the case for $n = k$ must be characterized as a limit:

$$\lim_{n=k}\left(\frac{bk\sin(\pi n)(2\sin(\frac{\pi k}{2})^2-1)-bn\sin(\pi k)(2\sin(\frac{\pi n}{2})^2-1)}{\pi k^2-\pi n^2}\right) \tag{2.3.12}$$

Carrying out the limit gives:

$$\frac{b}{2}-\frac{b\sin(2\pi k)}{4\pi k}=\frac{b}{2} \tag{2.3.13}$$

Where $\sin(2\pi k)$ for $k = 1, 2, 3\ldots$ are even rotations and always equal to zero. The expression (2.3.9) now reads:

$$\int_0^b P_z(x,y)\sin(\frac{k\pi y}{b})dy=\frac{b}{2}\sum_m^\infty\sum_n^\infty P_{mn}\sin(\frac{m\pi x}{a}) \tag{2.3.14}$$

By performing the same procedure but instead multiplying with $\sin(\frac{m\pi x}{a})dx$ and integrating between 0 and a gives an expression that can be solved for P_{mn}, this procedure is only valid for a plate which is simply supported on all four edges:

$$P_{mn}\frac{a}{2}\frac{b}{2}=\int_0^a\int_0^b P_z(x,y)\sin(\frac{m\pi x}{a})\sin(\frac{n\pi y}{b})dxdy \tag{2.3.15}$$

$$P_{mn}=\frac{4}{ab}\int_0^a\int_0^b P_z(x,y)\sin(\frac{m\pi x}{a})\sin(\frac{n\pi y}{b})dxdy \tag{2.3.16}$$

Performing the integral with constant load $P_z(x, y) = P_0$ gives:

$$P_{mn}=\frac{4P_0}{ab}\frac{a}{m\pi}(-\cos(m\pi)-(-1))\cdot\frac{b}{n\pi}(-\cos(n\pi)-(-1)) \tag{2.3.17}$$

$$-\cos(m\pi)-(-1)=\begin{cases}2 & \text{if } m \text{ is odd,}\\ 0 & \text{if } m \text{ is even.}\end{cases} \tag{2.3.18a}$$

$$-\cos(n\pi)-(-1)=\begin{cases}2 & \text{if } n \text{ is odd,}\\ 0 & \text{if } n \text{ is even.}\end{cases} \tag{2.3.18b}$$

It is also known that $m = n$ based on the previous condition (2.3.11), which leads to the final expression for P_{mn}:

$$P_{mn}=\begin{cases}\frac{16P_0}{\pi^2 mn} & \text{for odd } m \text{ and } n,\\ 0 & \text{for even } m \text{ and } n.\end{cases} \tag{2.3.19}$$

Combine equations (2.3.4), (2.3.8) and (2.3.19) to obtain the final expression for the deflection $\omega(x, y)$ of an isotropic plate subjected to a uniformly distributed load:

$$\boxed{\omega(x,y)=\frac{16P_0}{\pi^6 D}\sum_m^\infty\sum_n^\infty\frac{\sin(\frac{m\pi x}{a})\sin(\frac{n\pi y}{b})}{(\frac{m^2}{a^2}+\frac{n^2}{b^2})^2 mn},\ \text{for } m,n=1,3,5,7\ldots} \tag{2.3.20}$$

By inserting the expression for the deflection $\omega(x, y)$ into (2.1.26a-b) and (2.1.31) it is possible to characterize the moment per unit length on a solvable first order form:

$$m_x=\frac{16P_0}{\pi^4}\sum_m^\infty\sum_n^\infty[(\frac{m}{a})^2+\nu(\frac{n}{b})^2]\frac{\sin(\frac{m\pi x}{a})\sin(\frac{n\pi y}{b})}{((\frac{m^2}{a^2})+(\frac{n^2}{b^2}))^2 mn} \tag{2.3.21a}$$

$$m_y=\frac{16P_0}{\pi^4}\sum_m^\infty\sum_n^\infty[(\frac{n}{b})^2+\nu(\frac{m}{a})^2]\frac{\sin(\frac{m\pi x}{a})\sin(\frac{n\pi y}{b})}{((\frac{m^2}{a^2})+(\frac{n^2}{b^2}))^2 mn} \tag{2.3.21b}$$

$$m_{xy}=-\frac{16P_0}{\pi^4}(1-\nu)\sum_m^\infty\sum_n^\infty\frac{\cos(\frac{m\pi x}{a})\cos(\frac{n\pi y}{b})}{ab((\frac{m^2}{a^2})+(\frac{n^2}{b^2}))^2} \tag{2.3.21c}$$

The stress is obtained in a similar manner by introducing the expression of the deflection $\omega(x,y)$ into equations (2.1.13a-c) combined with (2.1.17) and (2.1.20):

$$\sigma_x = -\frac{192P_0}{h^3\pi^4} z \sum_m^\infty \sum_n^\infty [(\frac{m}{a})^2 + \nu(\frac{n}{b})^2] \frac{\sin(\frac{m\pi x}{a})\sin(\frac{n\pi y}{b})}{((\frac{m^2}{a^2}) + (\frac{n^2}{b^2}))^2 mn} \tag{2.3.22a}$$

$$\sigma_y = -\frac{192P_0}{h^3\pi^4} z \sum_m^\infty \sum_n^\infty [(\frac{n}{b})^2 + \nu(\frac{m}{a})^2] \frac{\sin(\frac{m\pi x}{a})\sin(\frac{n\pi y}{b})}{((\frac{m^2}{a^2}) + (\frac{n^2}{b^2}))^2 mn} \tag{2.3.22b}$$

$$\tau_{xy} = -\frac{192P_0}{h^3\pi^4} z(1-\nu) \sum_m^\infty \sum_n^\infty \frac{\cos(\frac{m\pi x}{a})\cos(\frac{n\pi y}{b})}{ab((\frac{m^2}{a^2}) + (\frac{n^2}{b^2}))^2} \tag{2.3.22c}$$

The derivation for orthotropic plates is performed in a similar manner. The Fourier approximation of $\omega(x,y)$ (2.3.4) and P_z (2.3.5) still holds true, but the coefficients W_{mn} and P_{mn} needs to be reevaluated:

$$D_x \frac{m^4\pi^4 W_{mn}\sin(\frac{m\pi x}{a})\sin(\frac{n\pi y}{b})}{a^4} + 2H\frac{W_{mn}m^2n^2\pi^4\sin(\frac{m\pi x}{a})\sin(\frac{n\pi x}{b})}{a^2b^2} +$$

$$+D_y \frac{n^4\pi^4 W_{mn}\sin(\frac{m\pi x}{a})\sin(\frac{n\pi y}{b})}{b^4} = P_{mn}\sin(\frac{m\pi x}{a})\sin(\frac{n\pi y}{b}) \tag{2.3.23}$$

Solve for W_{mn}:

$$W_{mn} = \frac{P_{mn}}{\pi^4(D_x\frac{m^4}{a^4} + 2H\frac{m^2n^2}{a^2b^2} + D_y\frac{n^4}{b^4})} \tag{2.3.24}$$

P_{mn} for an orthotropic plate subjected to a uniformly distributed load is solved by multiplying with $\sin(\frac{k\pi y}{b})dy$ and $\sin(\frac{k\pi x}{a})dx$ and integrating between 0 to a and 0 to b, same method as for the isotropic plate:

$$\int_0^b P_z(x,y)\sin(\frac{k\pi y}{b})dy = \sum_m^\infty \sum_n^\infty P_{mn}\int_0^b \sin(\frac{m\pi x}{a})\sin(\frac{n\pi y}{b})dy \tag{2.3.25}$$

$$P_{mn} = \begin{cases} \frac{16P_0}{\pi^2 mn} & \text{for odd } m \text{ and } n, \\ 0 & \text{for even } m \text{ and } n. \end{cases} \tag{2.3.26}$$

Insert equation (2.3.24) and (2.3.26) in the original expression for the deflection $\omega(x,y)$ (2.3.4) and get the full expression of the deflection for an orthotropic plate:

$$\omega(x,y) = \frac{16P_0}{\pi^6}\sum_m^\infty\sum_n^\infty \frac{\sin(\frac{m\pi x}{a})\sin(\frac{n\pi y}{b})}{mn(D_x\frac{m^4}{a^4} + 2H\frac{m^2n^2}{a^2b^2} + D_y\frac{n^4}{b^4})}, \text{ for } m,n = 1,3,5,7\ldots \tag{2.3.27}$$

Inserting (2.3.27) into equations (2.2.7a-c) to obtain the moment per length for a orthotropic plate subjected to a uniformly distributed load:

$$m_x = \frac{16P_0}{\pi^4}\sum_m^\infty\sum_n^\infty (D_x \frac{m\sin(\frac{m\pi x}{a})\sin(\frac{n\pi y}{b})}{a^2 n(D_x\frac{m^4}{a^4} + 2H\frac{m^2n^2}{a^2b^2} + D_y\frac{n^4}{b^4})} +$$

$$+D_{xy}\frac{n\sin(\frac{m\pi x}{a})\sin(\frac{n\pi y}{b})}{mb^2(D_x\frac{m^4}{a^4} + 2H\frac{m^2n^2}{a^2b^2} + D_y\frac{n^4}{b^4})}) \tag{2.3.28}$$

$$m_y = \frac{16P_0}{\pi^4}\sum_m^\infty\sum_n^\infty (D_y \frac{n\sin(\frac{m\pi x}{a})\sin(\frac{n\pi y}{b})}{b^2 m(D_x\frac{m^4}{a^4} + 2H\frac{m^2n^2}{a^2b^2} + D_y\frac{n^4}{b^4})}$$

$$+D_{xy}\frac{m\sin(\frac{m\pi x}{a})\sin(\frac{n\pi y}{b})}{na^2(D_x\frac{m^4}{a^4} + 2H\frac{m^2n^2}{a^2b^2} + D_y\frac{n^4}{b^4})}) \tag{2.3.29}$$

$$m_{xy} = -G\frac{h^3}{12}\frac{16P_0}{\pi^4}\sum_m^\infty\sum_n^\infty \frac{\cos(\frac{m\pi x}{a})\cos(\frac{n\pi y}{b})}{ab(D_x\frac{m^4}{a^4} + 2H\frac{m^2n^2}{a^2b^2} + D_y\frac{n^4}{b^4})} \tag{2.3.30}$$

The stress for an orthotropic plate subjected to an uniformly distributed load is obtained by inserting equation (2.3.27) into the combined equations (2.1.17a-b) and (2.2.2a-c):

$$\sigma_x = -\frac{16P_0E_x}{(1-\nu_x\nu_y)\pi^4}z\sum_m^\infty\sum_n^\infty\Big(\frac{m\sin\left(\frac{m\pi x}{a}\right)\sin\left(\frac{n\pi y}{b}\right)}{a^2n(D_x\frac{m^4}{a^4}+2H\frac{m^2n^2}{a^2b^2}+D_y\frac{n^4}{b^4})}+$$

$$+\nu_y\frac{n\sin\left(\frac{m\pi x}{a}\right)\sin\left(\frac{n\pi y}{b}\right)}{mb^2(D_x\frac{m^4}{a^4}+2H\frac{m^2n^2}{a^2b^2}+D_y\frac{n^4}{b^4})}\Big) \tag{2.3.31}$$

$$\sigma_y = -\frac{16P_0E_y}{(1-\nu_x\nu_y)\pi^4}z\sum_m^\infty\sum_n^\infty\Big(\frac{n\sin\left(\frac{m\pi x}{a}\right)\sin\left(\frac{n\pi y}{b}\right)}{b^2m(D_x\frac{m^4}{a^4}+2H\frac{m^2n^2}{a^2b^2}+D_y\frac{n^4}{b^4})}$$

$$+\nu_x\frac{m\sin\left(\frac{m\pi x}{a}\right)\sin\left(\frac{n\pi y}{b}\right)}{na^2(D_x\frac{m^4}{a^4}+2H\frac{m^2n^2}{a^2b^2}+D_y\frac{n^4}{b^4})}\Big) \tag{2.3.32}$$

$$\tau_{xy} = -\frac{\sqrt{E_xE_y}}{(1+\sqrt{\nu_x\nu_y})}\frac{16P_0}{\pi^4}z\sum_m^\infty\sum_n^\infty\frac{\cos\left(\frac{m\pi x}{a}\right)\cos\left(\frac{n\pi y}{b}\right)}{ab(D_x\frac{m^4}{a^4}+2H\frac{m^2n^2}{a^2b^2}+D_y\frac{n^4}{b^4})} \tag{2.3.33}$$

3 Equivalent Plate Transformation

The reason for transforming a sandwich structure to an equivalent homogeneous orthotropic layer is to be able to perform a parametric study with a limited amount of indata parameters. This will give a more reliable result with useful ratios and relations because of the manageable number of parameters that affect the result. However, when deriving the transformation some assumptions have to be introduced which may be a source of inaccuracy if the margin of error for the transformed plate compared to the original plate is too big. This has to be examined by verifying the transformed plate in several steps for different indata to ensure a good and meaningful conversion.

The transformation is executed in two steps, see figure 3.0.1. The first step transforms the sandwich structure to a three layered plate and the second part translates the three layers into one layer. The first transformation is mainly done by loading the structure in different ways and measuring displacements in Abaqus CAE. The equivalent stiffnesses of the core are then obtained from simple formulas that treat shear and bending deflection. The second transformation, however, is derived analytically from assumptions regarding the behavior and equilibrium of a three layered sandwich plate.

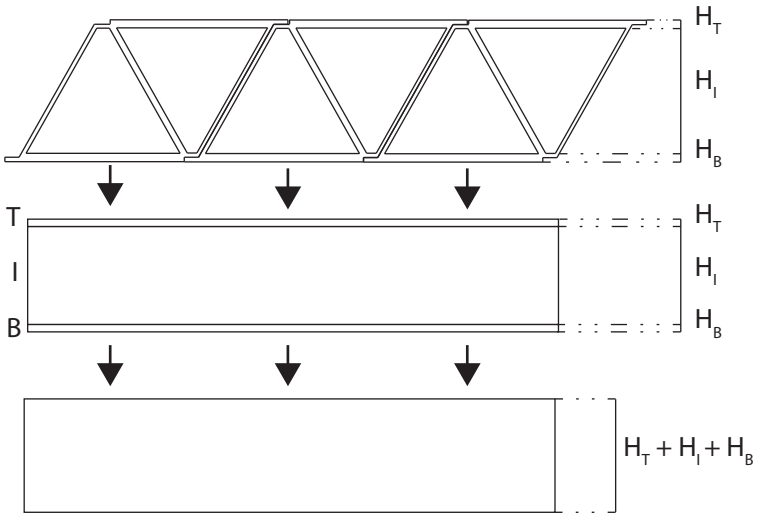

Figure 3.0.1: *Illustration of the two steps in the transformation between a structured sandwich plate to an equivalent one layered plate.*

3.1 Derivations of equivalent properties of a three layered sandwich structure

The transformation is performed for nine different elastic parameters, three Young's modulus, three shear modulus and three Poisson's ratio. No interaction between the different parameters is assumed. There are two different investigated approaches when transforming the elastic moduli E_{11} and E_{22}, see figure 3.1.1, either assume a constant modulus based on axial loaded deformation TALD, Zhou (2002), or constant flexural rigidity TCFR. It is not apparent which of these base assumptions simulate the reality best, consequently both variations have to be investigated further in an extensive verification.

The assumptions regarding the transformation of the elastic modulus in z-direction is only compression because of the low height to length ratio. This means that there is no bending in this direction, thus the transformation is only based on the assumption of axial loaded deformation for both methods.

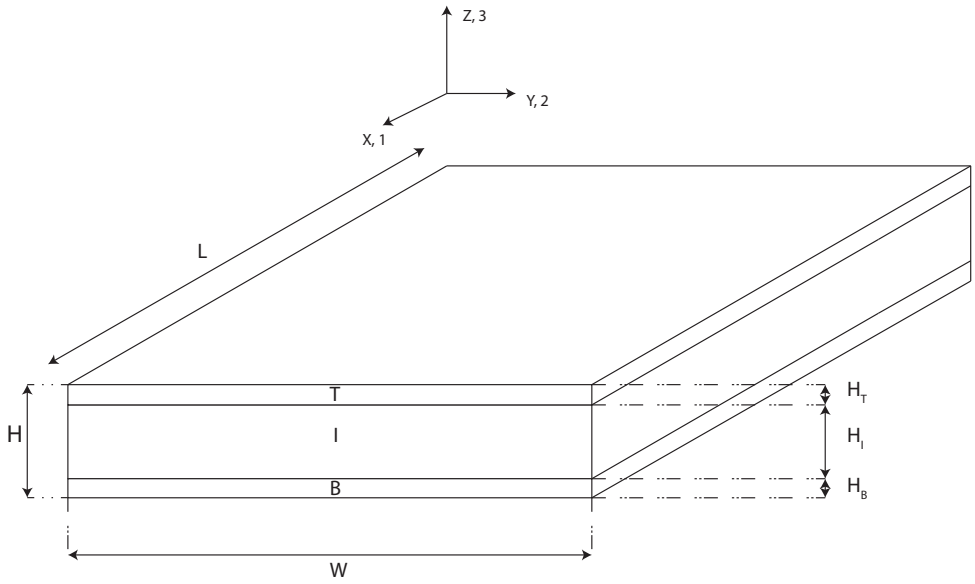

Figure 3.1.1: *The concerned sandwich plate with labeling of geometric dimensions.*

3.1.1 Equivalent Young's modulus - TALD

For determining the in-plane Young's moduli of E_{11} and E_{22}, the following setup of the plate and loading is to be used, see figure 3.1.2. The equivalent moduli computation is based on Aixi Zhou's work, Zhou (2002).

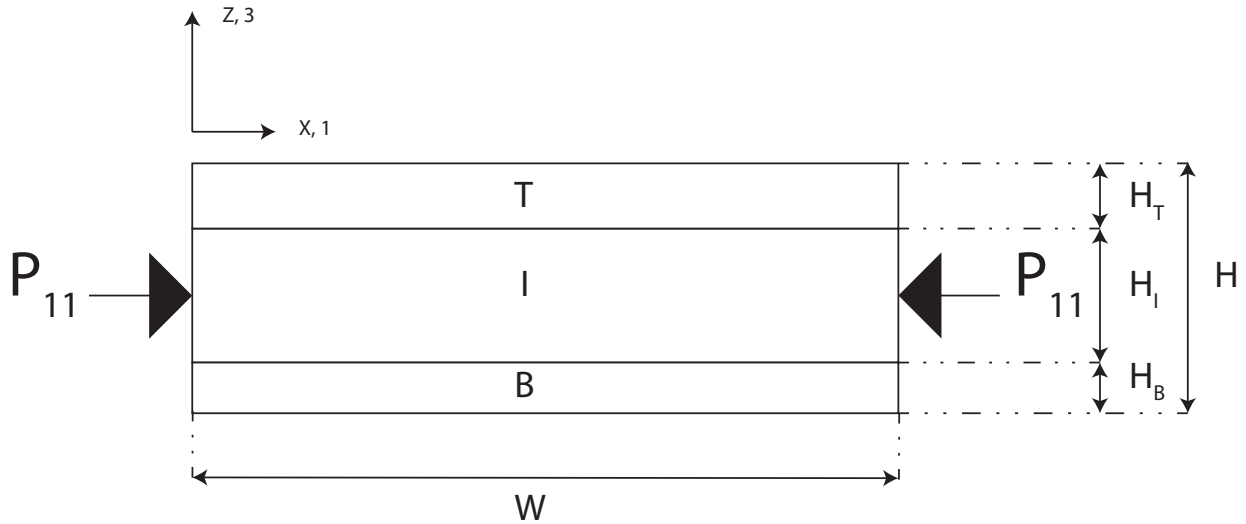

Figure 3.1.2: *Assumed load in x- and y-direction for transformation based on axial loaded deformation, TALD. Note that the force shown in the figure is the resultant force and should be distributed over all layers.*

Assume loading of the plate in x-direction (direction 1) and that the load is divided to all layers, see figure 3.1.2, where T - top layer, I - interface layer, B - bottom layer:

$$P_{11} = P_{11}^T + P_{11}^I + P_{11}^B \tag{3.1.1}$$

Which is the same as:

$$\sigma_{11} \cdot A_{11} = \sigma_{11}^T \cdot A_{11}^T + \sigma_{11}^I \cdot A_{11}^I + \sigma_{11}^B \cdot A_{11}^B \tag{3.1.2}$$

Rewrite to:

$$\sigma_{11} = \sigma_{11}^{T} \cdot \frac{A_{11}^{T}}{A_{11}} + \sigma_{11}^{I} \cdot \frac{A_{11}^{I}}{A_{11}} + \sigma_{11}^{B} \cdot \frac{A_{11}^{B}}{A_{11}} \tag{3.1.3}$$

With:

$$A_{11} = H \cdot W \tag{3.1.4a}$$
$$A_{11}^{T} = H^{T} \cdot W \tag{3.1.4b}$$
$$A_{11}^{I} = H^{I} \cdot W \tag{3.1.4c}$$
$$A_{11}^{B} = H^{B} \cdot W \tag{3.1.4d}$$

Let:

$$\alpha_T = \frac{H_T}{H} \tag{3.1.5a}$$
$$\alpha_I = \frac{H^I}{H} \tag{3.1.5b}$$
$$\alpha_B = \frac{H^B}{H} \tag{3.1.5c}$$

Substitute (3.1.5a-c) and (3.1.4a-d) into (3.1.3), simplify and recieve:

$$\sigma_{11} = \sigma_{11}^{T} \cdot \alpha_T + \sigma_{11}^{I} \cdot \alpha_B + \sigma_{11}^{B} \cdot \alpha_B \tag{3.1.6}$$

Divide (3.1.6) by ϵ_{11}:

$$\frac{\sigma_{11}}{\epsilon_{11}} = \frac{\sigma_{11}^{T}}{\epsilon_{11}} \cdot \alpha_T + \frac{\sigma_{11}^{I}}{\epsilon_{11}} \cdot \alpha_I + \frac{\sigma_{11}^{B}}{\epsilon_{11}} \cdot \alpha_B \tag{3.1.7}$$

Which gives the transformation of E_{11} based on axial loaded deformation (TALD):

$$\boxed{E_{11} = E_{11}^{T} \cdot \alpha_T + E_{11}^{I} \cdot \alpha_I + E_{11}^{I} \cdot \alpha_B} \tag{3.1.8}$$

The same procedure can be used to determine E_{22}

$$\boxed{E_{22} = E_{22}^{T} \cdot \alpha_T + E_{22}^{I} \cdot \alpha_I + E_{22}^{I} \cdot \alpha_B} \tag{3.1.9}$$

3.1.2 Equivalent Young's modulus - TCFR

The computation of the equivalent moduli of E_{11} and E_{22} for the TCFR method is based on bending stiffness. The following procedure is based on the setup, which can be seen in figure (3.1.3). The bending stiffness of the plate is treated as a beam, which simplifies the computation a little. This method is fully developed by the authors of the thesis.

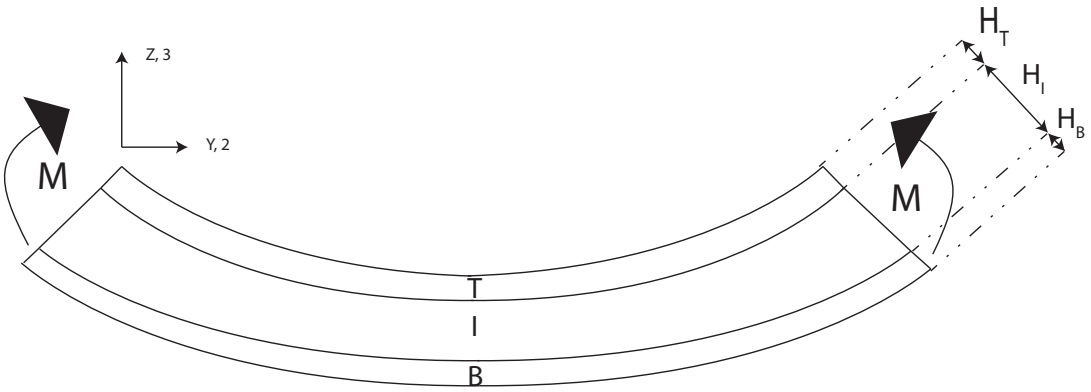

Figure 3.1.3: *Assumed load and deflection for the transformation based on constant flexural rigidity, TCFR.*

Consider a three layered sandwich structure, see figure 3.1.3. In order to calculate at what level the neutral axis will be situated, the following procedure has to be performed.

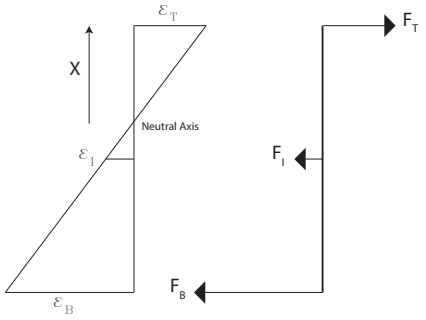

Figure 3.1.4: *Strain and force equilibrium*

Establish the relation between the different strains of the three layers, where H is the total height of the sandwich plate and W is the width:

$$\frac{\epsilon_T}{x - \frac{h_T}{2}} = \frac{\epsilon_B}{x - H + \frac{H_B}{2}} \tag{3.1.10}$$

$$\epsilon_B = \frac{\epsilon_T (x - H + \frac{H_B}{2})}{x - \frac{H_T}{2}} \tag{3.1.11}$$

In the same manner for ϵ_I

$$\epsilon_I = \frac{\epsilon_T (x - \frac{H}{2})}{x - \frac{H_T}{2}} \tag{3.1.12}$$

Establish the global equilibrium and rewriting:

$$F_T + F_I + F_B = 0 \tag{3.1.13}$$

$$(\epsilon \cdot E \cdot A)_T + (\epsilon \cdot E \cdot A)_I + (\epsilon \cdot E \cdot A)_B = 0 \tag{3.1.14}$$

Insert equations (3.1.11) and (3.1.12) into (3.1.14) gives:

$$\epsilon_T \cdot E_T \cdot A_T + \frac{\epsilon_T (x - \frac{H}{2})}{x - \frac{H_T}{2}} \cdot E_I \cdot A_I + \frac{\epsilon_T (x - H + \frac{H_B}{2})}{x - \frac{H_T}{2}} \cdot E_B \cdot A_B = 0 \tag{3.1.15}$$

Solve this expression for x and receive:

$$x = \frac{-E_B\,{H_B}^2 + 2\,E_B\,H\,H_B + E_T\,{H_T}^2 + E_I\,H\,H_I}{2\,(E_B\,H_B + E_I\,H_I + E_T\,H_T)} \tag{3.1.16}$$

Assuming that the flexural rigidity of the plate will stay constant yields following expression:

$$D = D_T + D_I + D_B \tag{3.1.17}$$

With D_T, D_I and D_B as:

$$D_T = E_{11}^T \cdot \frac{I_{11}^T}{W} \tag{3.1.18}$$

$$I_{11}^T = W \cdot \frac{H_T^3}{12} + W \cdot H_T \cdot x^2 \tag{3.1.19}$$

$$D_T = E_{11}^T(\frac{H_T^3}{12} + H_T \cdot x^2) \tag{3.1.20a}$$

$$D_I = E_{11}^I(\frac{H_I^3}{12} + H_I(x - \frac{H_T}{2} - \frac{H_I}{2})^2) \tag{3.1.20b}$$

$$D_B = E_{11}^B(\frac{H_B^3}{12} + H_B(H - x)^2) \tag{3.1.20c}$$

The single layer stiffness D is:

$$D = E_{EQ} \cdot \frac{H^3}{12} \tag{3.1.21}$$

Using equations (3.1.16), (3.1.20a-c) and (3.1.21) in (3.1.17) the equivalent elastic modulus (E_{eq}) based on constant flexural rigidity can be expressed:

$$\begin{aligned} E_{eq} = {} & \frac{12\,E_T\left(\frac{{H_T}^3}{12} + \frac{H_T\left(-E_B\,{H_B}^2 + 2\,E_B\,H\,H_B + E_T\,{H_T}^2 + E_I\,H\,H_I\right)^2}{4\,(E_B\,H_B + E_I\,H_I + E_T\,H_T)^2}\right)}{H^3} + \\ & + \frac{12\,E_B\left(\frac{{H_B}^3}{12} + H_B\left(H - \frac{-E_B\,{H_B}^2 + 2\,E_B\,H\,H_B + E_T\,{H_T}^2 + E_I\,H\,H_I}{2\,E_B\,H_B + 2\,E_I\,H_I + 2\,E_T\,H_T}\right)^2\right)}{H^3} + \\ & + \frac{12\,E_I\left(\frac{{H_I}^3}{12} + H_I\left(\frac{H_I}{2} + \frac{H_T}{2} - \frac{-E_B\,{H_B}^2 + 2\,E_B\,H\,H_B + E_T\,{H_T}^2 + E_I\,H\,H_I}{2\,E_B\,H_B + 2\,E_I\,H_I + 2\,E_T\,H_T}\right)^2\right)}{H^3} \end{aligned} \tag{3.1.22}$$

Equation (3.1.22) can be used to express both E_{11} and E_{22}.

3.1.3 Equivalent Young's modulus in z-direction

The equivalent Young's modulus in z-direction can be described as compression of the plate over its thickness. This process is also used in both transformational methods, TALD and TCFR. The method is derived from Aixi Zhou's work, Zhou (2002).

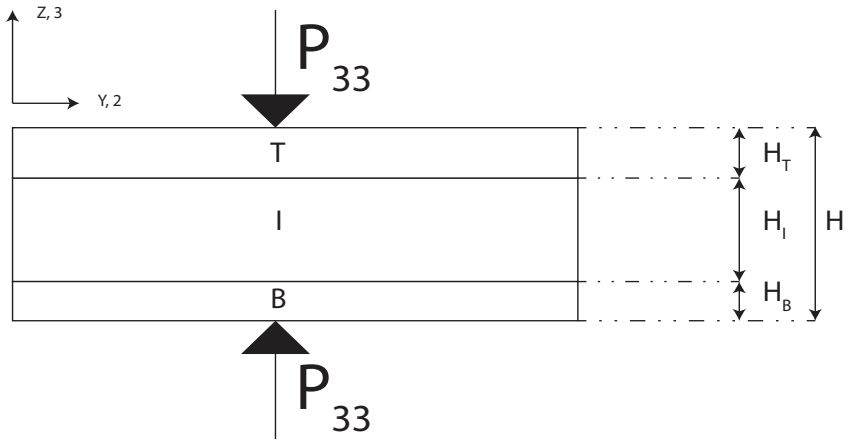

Figure 3.1.5: *Assumed load in z-direction evenly distributed over the face sheet.*

Assume load in z-direction (direction 3), see figure 3.1.5. The force P_{33} is distributed over the whole bottom and top face sheets:

$$\sigma_{33} = \frac{P_{33}}{A_{33}} \tag{3.1.23}$$

All stresses must be transformed to all layers of the plate, which leads to:

$$\sigma_{33} = \sigma_{33}^T = \sigma_{33}^I = \sigma_{33}^B \tag{3.1.24}$$

The strains of each layer can be expressed as:

$$\epsilon_{33}^T = \frac{\sigma_{33}^T}{E_{33}^T} \tag{3.1.25a}$$

$$\epsilon_{33}^I = \frac{\sigma_{33}^I}{E_{33}^I} \tag{3.1.25b}$$

$$\epsilon_{33}^B = \frac{\sigma_{33}^B}{E_{33}^B} \tag{3.1.25c}$$

The total displacement can be expressed by the sum of the contribution from all layers:

$$\delta_{33} = \delta_{33}^T + \delta_{33}^I + \delta_{33}^B = \epsilon_{33}^T \cdot H^T + \epsilon_{33}^I \cdot H^I + \epsilon_{33}^B \cdot H^B \tag{3.1.26}$$

The total strain for the deck is:

$$\epsilon_{33} = \frac{\delta_{33}}{H} = \frac{\epsilon_{33}^T \cdot H^T}{H} + \frac{\epsilon_{33}^I \cdot H^I}{H} + \frac{\epsilon_{33}^B \cdot H^B}{H} \tag{3.1.27}$$

Divide (3.1.27) by σ_{33} and aquire and applicate (3.1.5a-c):

$$\frac{\epsilon_{33}}{\sigma_{33}} = \frac{\epsilon_{33}^T}{\sigma_{33}} \cdot \alpha^T + \frac{\epsilon_{33}^I}{\sigma_{33}} \cdot \alpha^I + \frac{\epsilon_{33}^B}{\sigma_{33}} \cdot \alpha^B \tag{3.1.28}$$

Solve for E_{33} to get the equation for the transformation of the elastic modulus in z-direction:

$$\frac{1}{E_{33}} = \frac{\alpha^T}{E_{33}^T} + \frac{\alpha^I}{E_{33}^I} + \frac{\alpha^B}{E_{33}^B} \tag{3.1.29}$$

$$\boxed{E_{33} = \frac{1}{\frac{\alpha^T}{E_{33}^T} + \frac{\alpha^I}{E_{33}^I} + \frac{\alpha^B}{E_{33}^B}}} \tag{3.1.30}$$

3.1.4 Equivalent shear moduli

This section treats the calculation of the equivalent shear moduli, Zhou (2002). The obtained expressions are used both for the TALD and TCFR method.

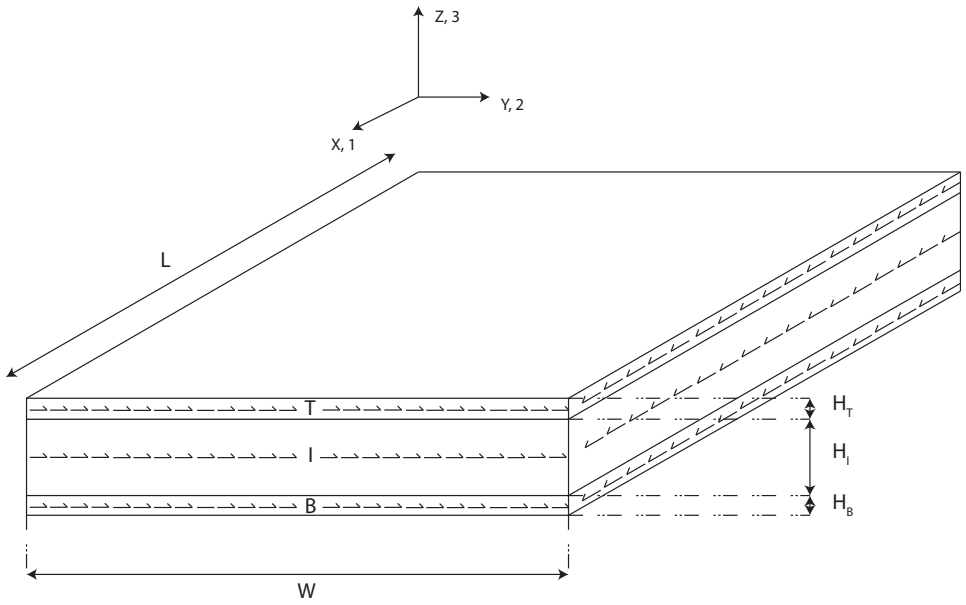

Figure 3.1.6: *Assumed shear load for G_{12}. Note that the shear force is distributed over all layers.*

The shear stiffness G_{12} is obtained by summation of the stiffness of the individual, see figure 3.1.6, layers in the same manner as for E_{11} calculated from axial loaded deflection (TALD) found in section 3.1.1. The equation for the transformation will therefore become:

$$\boxed{G_{12} = \alpha^T \cdot G_{12}^T + \alpha^I \cdot G_{12}^I + \alpha^B \cdot G_{12}^B} \tag{3.1.31}$$

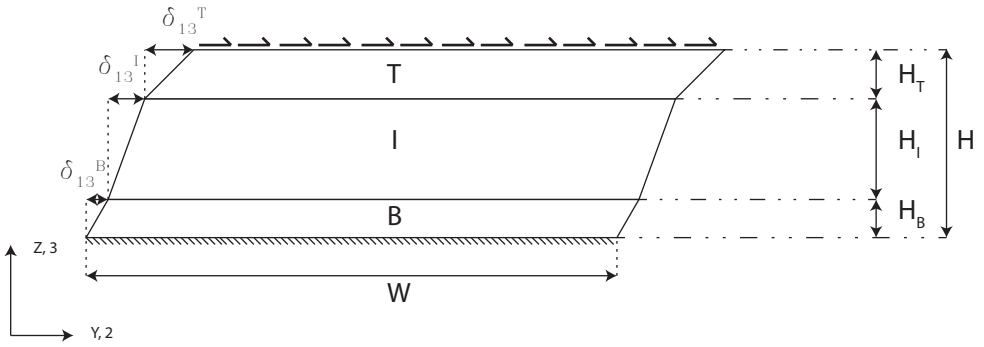

Figure 3.1.7: *Assumed shear load for the modulus of G_{13} and G_{23}. The load is evenly distributed over the top sheet and fixed at the bottom.*

Expressing the shear strain and displacement for all layers according to figure 3.1.7:

$$\delta_{13}^T = \gamma_{13}^T \cdot H_T \ \ , \ \ \delta_{13}^I = \gamma_{13}^I \cdot H_I \ \ , \ \ \delta_{13}^B = \gamma_{13}^B \cdot H_B \tag{3.1.32}$$

$$\delta_{13} = \delta_{13}^T + \delta_{13}^I + \delta_{13}^B = \gamma_{13}^T \cdot H_T + \gamma_{13}^I \cdot H_I + \gamma_{13}^B \cdot H_B \tag{3.1.33}$$

Combining (3.1.32) and (3.1.33) gives:

$$\gamma_{13} = \frac{\delta_{13}}{H} = \gamma_{13}^{T} \cdot \frac{H_T}{H} + \gamma_{13}^{I} \cdot \frac{H_I}{H} + \gamma_{13}^{B} \cdot \frac{H_B}{H} \tag{3.1.34}$$

$$\gamma_{13} = \alpha_T \cdot \gamma_{13}^{T} + \alpha_I \cdot \gamma_{13}^{B} + \alpha_T \cdot \gamma_{13}^{B} \tag{3.1.35}$$

Dividing all terms by τ_{13} gives:

$$\frac{\gamma_{13}}{\tau_{13}} = \alpha_T \cdot \frac{\gamma_{13}^{T}}{\tau_{13}} + \alpha_I \cdot \frac{\gamma_{13}^{I}}{\tau_{13}} + \alpha_B \cdot \frac{\gamma_{13}^{B}}{\tau_{13}} \tag{3.1.36}$$

$$\frac{1}{G_{13}} = \frac{\alpha_T}{G_{13}^{T}} + \frac{\alpha_I}{G_{13}^{B}} + \frac{\alpha_T}{G_{13}^{B}} \tag{3.1.37}$$

Which gives the transformation equation for G_{13} and G_{23}:

$$\boxed{G_{13} = \frac{1}{\frac{\alpha^T}{G_{13}^{T}} + \frac{\alpha^I}{G_{13}^{I}} + \frac{\alpha^B}{G_{13}^{B}}}} \tag{3.1.38}$$

$$\boxed{G_{23} = \frac{1}{\frac{\alpha^T}{G_{23}^{T}} + \frac{\alpha^I}{G_{23}^{I}} + \frac{\alpha^B}{G_{23}^{B}}}} \tag{3.1.39}$$

3.1.5 Poisson's ratios

Poisson's ratio is a measure of how much an object expands/contracts transversely during axial loading. A positive value Poisson's ratio gives contraction, which is the normal case, and a negative one gives expansion. The following procedure is used to obtain values for both transformation methods, TALD and TCFR, Zhou (2002).
Assume loading of σ_{11} in direction 1, each component will then have a displacement in direction 2 that can be expressed as:

$$\delta_2^{T} = -\nu_{12}^{T} \cdot \epsilon_{11}^{T} \cdot W \ , \ \delta_2^{I} = -\nu_{12}^{I} \cdot \epsilon_{11}^{I} \cdot W \ , \ \delta_2^{B} = -\nu_{12}^{B} \cdot \epsilon_{11}^{B} \cdot W \tag{3.1.40}$$

The total displacement in direction 2 can be obtained by following relationship:

$$\delta_2 = \alpha_T \cdot \delta_2^{T} + \alpha_I \cdot \delta_2^{I} + \alpha_B \cdot \delta_2^{B} \tag{3.1.41}$$

Combine (3.1.41) with (3.1.40) and obtain the following expression:

$$\delta_2 = -\alpha_T \cdot \nu_{12}^{T} \cdot \epsilon_{11} \cdot W - \alpha_I \cdot \nu_{12}^{I} \cdot \epsilon_{11} \cdot W - \alpha_B \cdot \nu_{12}^{B} \cdot \epsilon_{11} \cdot W \tag{3.1.42}$$

Total displacement for the 2-direction can also be expressed as $\delta_2 = -\nu_{12} \cdot \epsilon_{11} \cdot W$, which in turn gives:

$$-\nu_{12} \cdot \epsilon_{11} \cdot W = -\alpha_T \cdot \nu_{12}^{T} \cdot \epsilon_{11}^{T} \cdot W - \alpha_I \cdot \nu_{12}^{I} \cdot \epsilon_{11}^{I} \cdot W - \alpha_B \cdot \nu_{12}^{B} \cdot \epsilon_{11}^{B} \cdot W \tag{3.1.43}$$

Divide both sides of expression (3.1.43) with $-\epsilon_{11} \cdot W$ gives:

$$\nu_{12} = \alpha_T \cdot \nu_{12}^{T} \cdot \frac{\epsilon_{11}^{T}}{\epsilon_{11}} + \alpha_I \cdot \nu_{12}^{I} \cdot \frac{\epsilon_{11}^{I}}{\epsilon_{11}} + \alpha_B \cdot \nu_{12}^{B} \cdot \frac{\epsilon_{11}^{B}}{\epsilon_{11}} \tag{3.1.44}$$

Using the relation that all members suffer the same strain of ϵ_{11}, i.e.:
$\epsilon_{11}^{T} = \epsilon_{11}$, $\epsilon_{11}^{I} = \epsilon_{11}$, $\epsilon_{11}^{B} = \epsilon_{11}$, into (3.1.44) gives following expression:

$$\boxed{\nu_{12} = \alpha_T \cdot \nu_{12}^{T} + \alpha_I \cdot \nu_{12}^{I} + \alpha_B \cdot \nu_{12}^{B}} \tag{3.1.45}$$

Considering ν_{13} instead under the stress σ_{11} which is defined as: $\nu_{13} = -\frac{\epsilon_{33}}{\epsilon_{11}}$
Displacements for the 3-direction can be established as:

$$\delta_3^{T} = -\nu_{13}^{T} \cdot \epsilon_{11}^{T} \cdot H_T \ , \ \delta_3^{I} = -\nu_{13}^{I} \cdot \epsilon_{11}^{I} \cdot H_I \ , \ \delta_3^{B} = -\nu_{13}^{B} \cdot \epsilon_{11}^{B} \cdot H_B \tag{3.1.46}$$

The total deformation for the 3-direction can then be obtained by summation of the individual deformation of the layers.

$$\delta_3 = \delta_3^T + \delta_3^I + \delta_3^B = -\nu_{13}^T \cdot \epsilon_{11}^T \cdot H_T - \nu_{13}^I \cdot \epsilon_{11}^I \cdot H_I - \nu_{13}^B \cdot \epsilon_{11}^B \cdot H_B \tag{3.1.47}$$

Rewriting (3.1.47) by $\delta_3 = -\nu_{13} \cdot \epsilon_{11} \cdot H$

$$-\nu_{13} \cdot \epsilon_{11} \cdot H = -\nu_{13}^T \cdot \epsilon_{11}^T \cdot H_T - \nu_{13}^I \cdot \epsilon_{11}^I \cdot H_I - \nu_{13}^B \cdot \epsilon_{11}^B \cdot H_B \tag{3.1.48}$$

Which is the same as:

$$\nu_{13} = \nu_{13}^T \cdot \frac{\epsilon_{11}^T \cdot H_T}{\epsilon_{11} \cdot H} + \nu_{13}^I \cdot \frac{\epsilon_{11}^I \cdot H_I}{\epsilon_{11} \cdot H} + \nu_{13}^B \cdot \frac{\epsilon_{11}^B \cdot H_B}{\epsilon_{11} \cdot H} \tag{3.1.49}$$

Recall (3.1.5a-c) and the last step for deriving ν_{12},

$$\boxed{\nu_{13} = \alpha_T \cdot \nu_{13}^T + \alpha_I \cdot \nu_{13}^I + \alpha_B \cdot \nu_{13}^B} \tag{3.1.50}$$

In the same manner as for ν_{13}, ν_{23} can be derived, which gives:

$$\boxed{\nu_{23} = \alpha_T \cdot \nu_{23}^T + \alpha_I \cdot \nu_{23}^I + \alpha_B \cdot \nu_{23}^B} \tag{3.1.51}$$

3.2 Transformation between three-layered sandwich plate to one equivalent layer - Summary

Table 3.2.1: Transformation algorithm for the two different transformation assumptions; transformation from axial loaded deflection (TALD) and transformation based on constant flexural rigidity (TCFR). The equation number is found in the table.

Transformation	E_{11}	E_{22}	E_{33}	G_{12}	G_{13}	G_{23}	ν_{12}	ν_{13}	ν_{23}
TALD	(3.1.8)	(3.1.9)	(3.1.30)	(3.1.31)	(3.1.38)	(3.1.39)	(3.1.45)	(3.1.50)	(3.1.51)
TCFR	(3.1.22)	(3.1.22)	(3.1.30)	(3.1.31)	(3.1.38)	(3.1.39)	(3.1.45)	(3.1.50)	(3.1.51)

4 FE-Simulation

The two transformation methods derived in chapter 3 are to be evaluated for comparison and possible improvements. This verification is done for two different cases; the plate resting on four supports and the plate working in a full scale bridge, where it is resting on two primary girders. This bridge model is later to be the subject of the parametric study.

Both the verification and the parametric study are performed by a finite element simulation (FE). The full bridge is modeled in Abaqus CAE which is a commercial FEA-software. The strength of Abaqus CAE is that it is a general program which can handle a wide variety of different analysis and simulations. However, in the case of the verification and the parametric study, a simple linear analysis will suffice.

Do note, results are presented in both local and global coordinates. Local coordinates refers to the sandwich structure alone, where the direction of the core studs generally is in x-direction and cross studs are y-direction. The x-direction (local coordinate) translates to the global y-direction and the y-direction (local coordinate) translates to the global x-direction. This can be explained by the direction of the sandwich plate in the total bridge structure, illustrated in figure 4.1.1. If nothing else is stated, assume global coordinates.

4.1 Geometric properties of the full bridge model

The bridge consists of two primary girders in the main direction of the bridge, where the sandwich plates are placed on top of the girders perpendicular to the main direction. The bridge's length is set to 15 meters, which should be sufficient to span a normal highway's width. The width of the bridge deck is set to 8 meters, in order to have wide lanes which grants high speed and still space left for side walks and guard rails. The primary girders are placed at a c/c-distance 5 meters apart and 1.5 meters in from the edge of the deck, see figure 4.1.1. Vertical bracing elements for the steel beams are placed in the middle of the span and at the supports. A transverse beam based on the standard beam UPE300 is also fastened between the middle stiffeners in order to decrease twisting for the main girders, see figure 4.1.2. The composite sandwich bridge deck has the total height of 275 millimeters, and consists of a lower face sheet of 10 millimeters, a core of 250 millimeters and an upper face sheet of 15 millimeter.

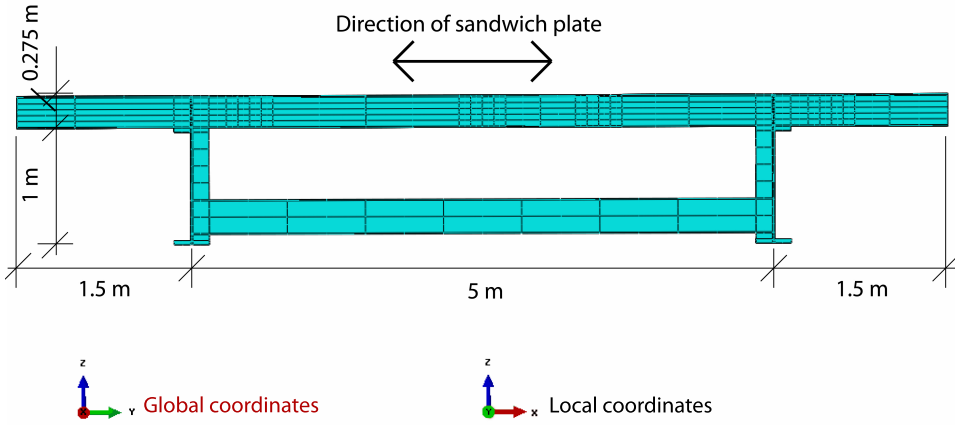

Figure 4.1.1: *Geometric dimensions of the bridge model. The arrows show the direction of the sandwich structure which is placed between the two main girders.*

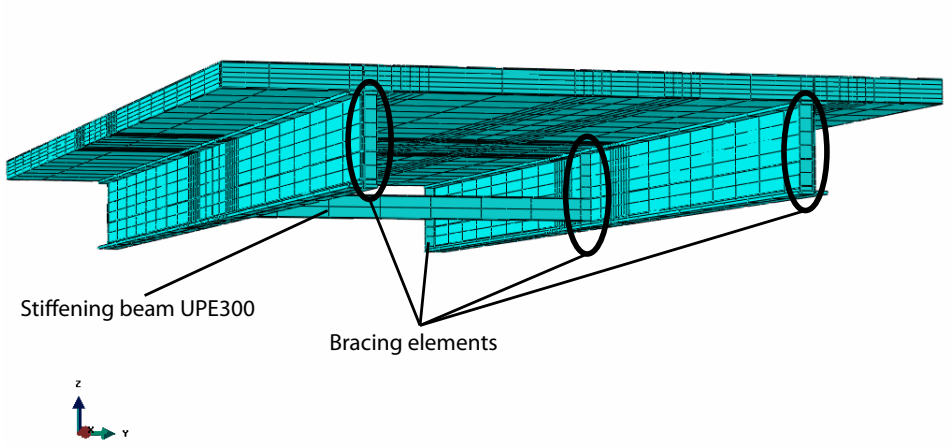

Figure 4.1.2: *The bridge model with the bracing and stiffening elements highlighted.*

It is important to have a reasonable relationship in stiffness between the sandwich element and the underlying longitudinal beams in order to obtain a realistic global behavior and also so that the deflection ratios between the two parts fit. The steel beams are therefore designed by a rough calculation made by hand, see appendix 10.1. The calculations are performed in accordance with *EUROPEAN STANDARD EN 1991-2:2003* (2003). The chosen load case for the bridge is taken as Load Model 1 (LM1) which is used to calculate the general behavior of bridges subjected to normal traffic pattern. When the design moment affecting the main girders is known, a beam is chosen from a table with I-beams of standard sizes. The beams are chosen to be a bit undersized in order to account for the increase of stiffness the sandwich structure contributes to the global frame system. In this case HEB1000 girders were chosen and they were simplified as having non rounded shapes. For dimensions of the different standardized beams used see table 4.1.1 and figure 4.1.3. The total height of the complete bridge system becomes 1275 millimeters.

Table 4.1.1: Geometric properties of the standardized girders used [mm]

Profile	h	b	t	d	R
HEB 1000	1000	300	36.0	19.0*	30*
UPE 300**	300	10	10	15*	4.5*

* *Rounded corners are not modeled.*
** *This is a customized version of UPE300 with different values of b and t.*

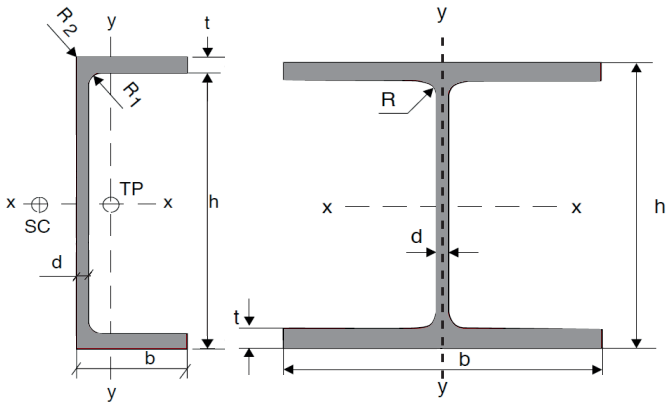

Figure 4.1.3: *UPE-profile (left) and HEB-profile (right).*

4.2 Mesh and model remarks for the full bridge model

The bridge structure is modeled with solid elements with a mesh constructed by 20-node brick elements (C3D20R). Solid elements are chosen to be able to obtain values of out of plane shear stresses and strains. However, this presents problems when constructing the mesh. Because of the geometric properties of the bridge, the automated mesh constructor is unable to create a mesh consisting of brick elements without distorting and warping some of them. It is possible to find a good mesh with tetrahedrons instead of brick elements, though these types of elements are not good when dealing with shear stresses. This can be explained by the geometry of the element where shear loads are received by truss action in the individual elements which will lead to an overestimation of the stiffness. Instead approximately 40 partitions are created in order to regulate and control the mesh to be able to use brick elements. These partitions will help the automated mesh constructor to find a suitable and structured mesh without any warped elements.

All components of the bridge are assembled with full interaction between them. This also applies to the layers of the composite sandwich structure. This means that the sandwich structure will work both as a plate resting on two supports and as an upper flange for the global beam frame system.

The boundaries are situated at the lower flange of both the steel girders on each end of the bridge. The boundary conditions are assigned to a small area of $0.1 \cdot 0.3m^2$ to get a good transfer of the reaction force to the structure and to avoid local discontinuities which a line boundary condition may bring. The bridge is simply supported with all displacements locked on once side and x-direction free to move on the other side, see figure 4.2.1. No rotations are prescribed.

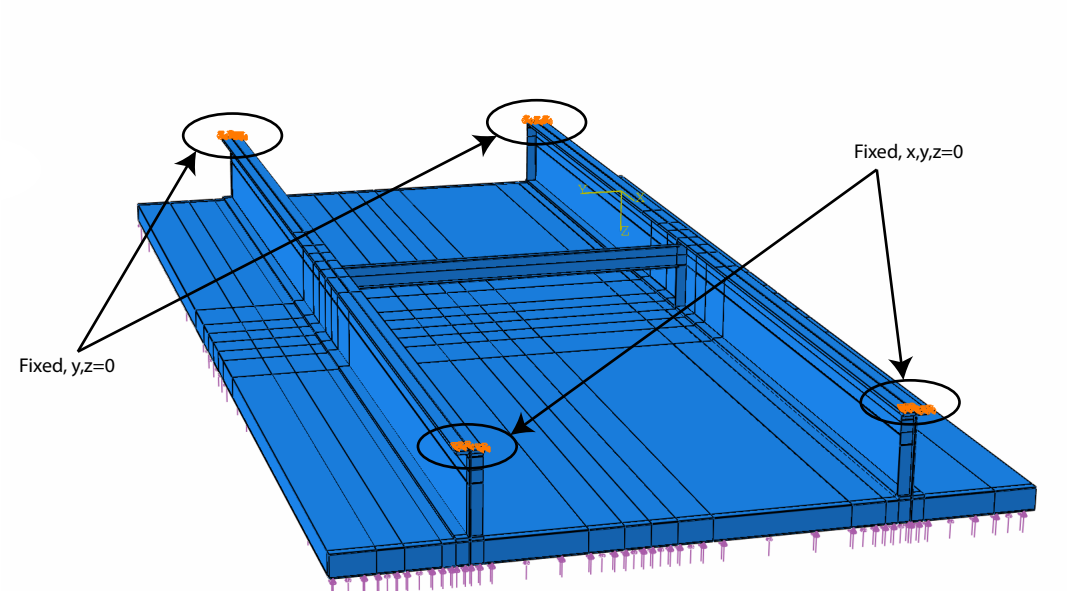

Figure 4.2.1: *The bridge model upside down with the set boundaries marked.*

4.3 Convergence study

When performing a FE-analysis, a good mesh is critical to obtain accurate results and behavior. The verification of the results from chapter 3.1 is done in two steps, first a comparison when the plates are resting on four supports and secondly, when the plate systems are resting on the two longitudinal steel beams in the main bridge model presented in section 4.1. There is no need for an extensive convergence study in verification one. This is due to the simple geometrics of the plate system and the ease which the mesh can reach an adequate resolution. The second verification, however, is a more complex structure with geometric properties which will cause problems to the automated mesh constructor to create a mesh with good resolution. There is a need to introduce partitions and manually adjust and increase the local seeding with regard to

the mesh density. This is done to ensure a good and structured mesh without the risk of inaccurate integration interpolation, which can be obtained when the elements in the mesh are warped or distorted in some way.

When constructing the mesh seeding manually, there are a few rules of thumb that are followed; at least five elements in z-direction for elements subjected to bending, localized finer mesh seeding in the areas where point loads are applied and adequate number of elements in warped parts, for example the steel beam flanges. Hence, a local seeding of the height is inserted for both the two I-beams and for the plate system, and the automated mesh is examined in problem areas to ensure a good and structured mesh.

To validate the mesh for verification two, a convergence study is performed by changing the global seeding in steps from 0.8 to 0.2 which will result in meshes with approximately 7.000 to 40.000 elements. This is compared with a change of local seeds around the area where the point loads are applied. The local seeds are changed in three steps; 0.15, 0.1 and 0.08 and are represented by red dots in the graphs below. If the local seeds are effective, the points should move closer towards the calculated value for 40.000 elements compared to the same increase of elements on a global scale. The local seeding of the height of the beams and sandwich layers are not investigated further in the convergence study and are assumed to be satisfactory.

The deflection is measured and compared at five points; in between the point loads in the heavy lane (point one), at the edge by the heavy lane (point two), at the inner side of the lower flange for the beam under the heavy lane (point three), at the middle part of the lower flange for the beam under the heavy lane (point four) and finally at the outer part of the lower flange for the beam under the heavy lane (point five). These measure points are shown in figure 4.3.1 and 4.3.2 along with the loading conditions according to Eurocode LM1. For specific values of the different applied loads, see appendix 10.1.These points are chosen to measure both the local maximum deflection, obtained either in the edge or in between the point loads (point one and two), and the global behavior of the beam obtained from the lower flange (point three to five).

The obtained values and comparison can be found in graphs 4.3.3 to 4.3.7.

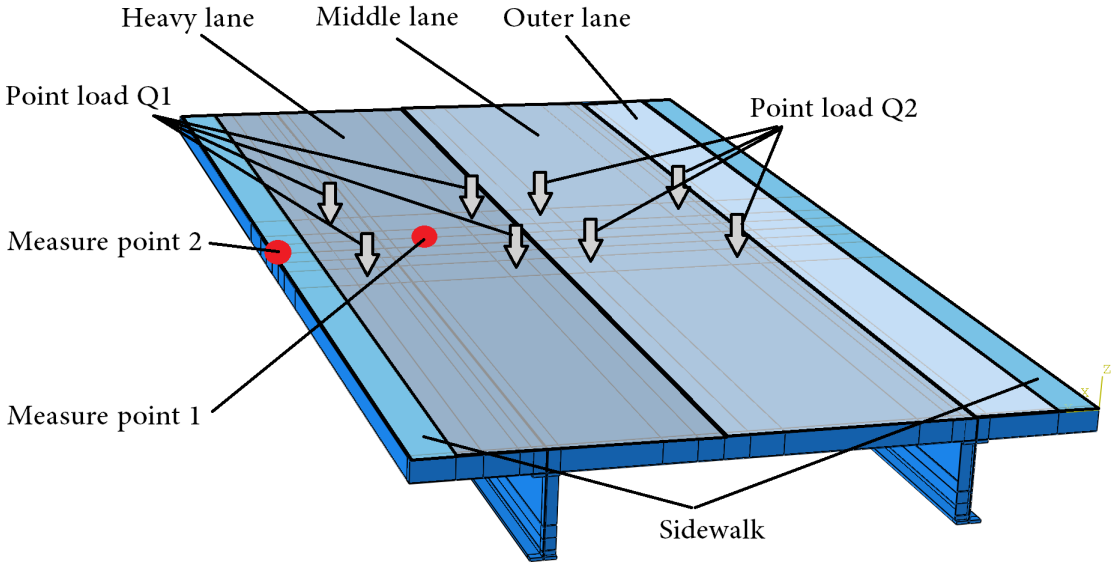

Figure 4.3.1: *Loading conditions for the convergence study. Measure points one and two are marked with red circles.*

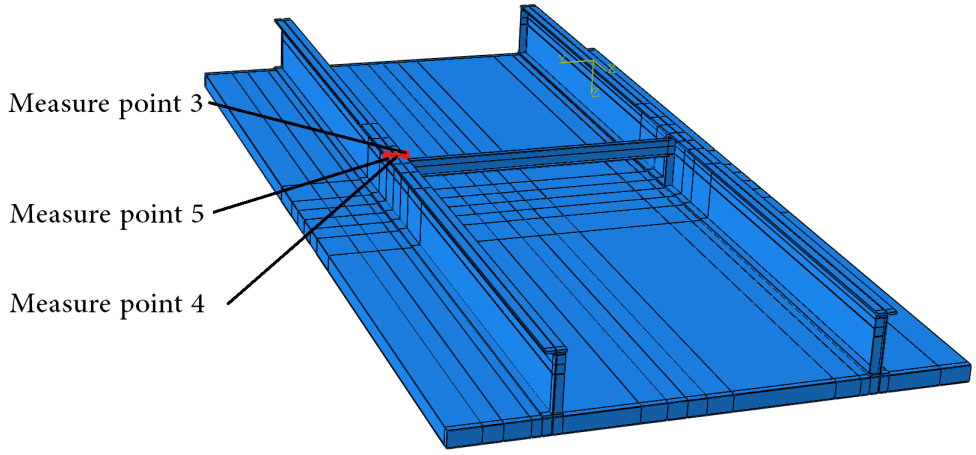

Figure 4.3.2: *Measure points three, four and five are marked with red circles. The readings are taken at the beam below the heavy lane.*

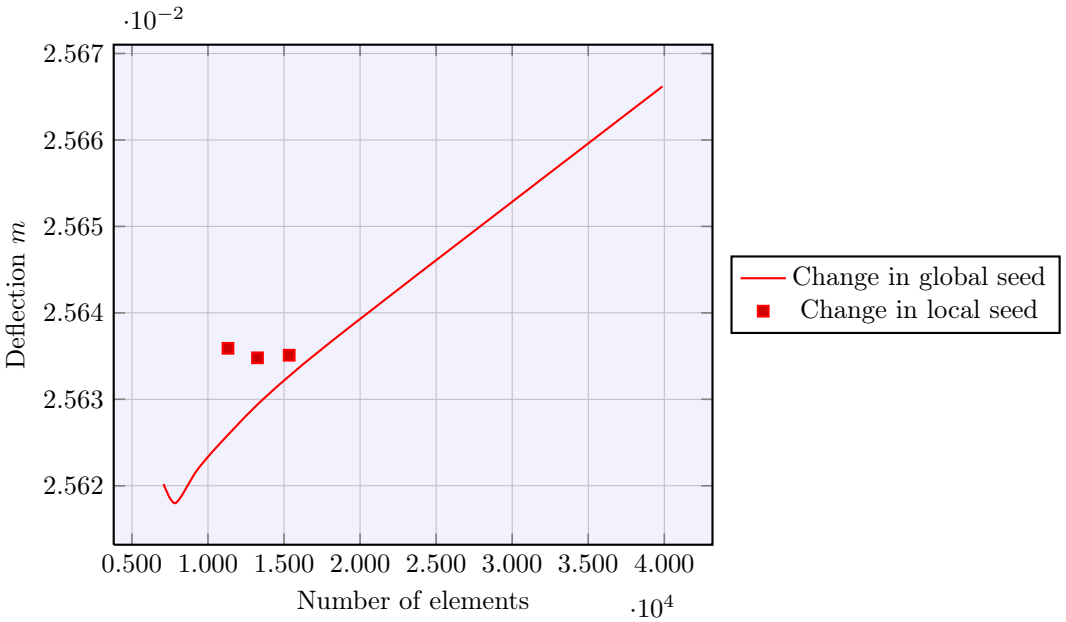

Figure 4.3.3: *Deflection between the point loads in the heavy lane.*

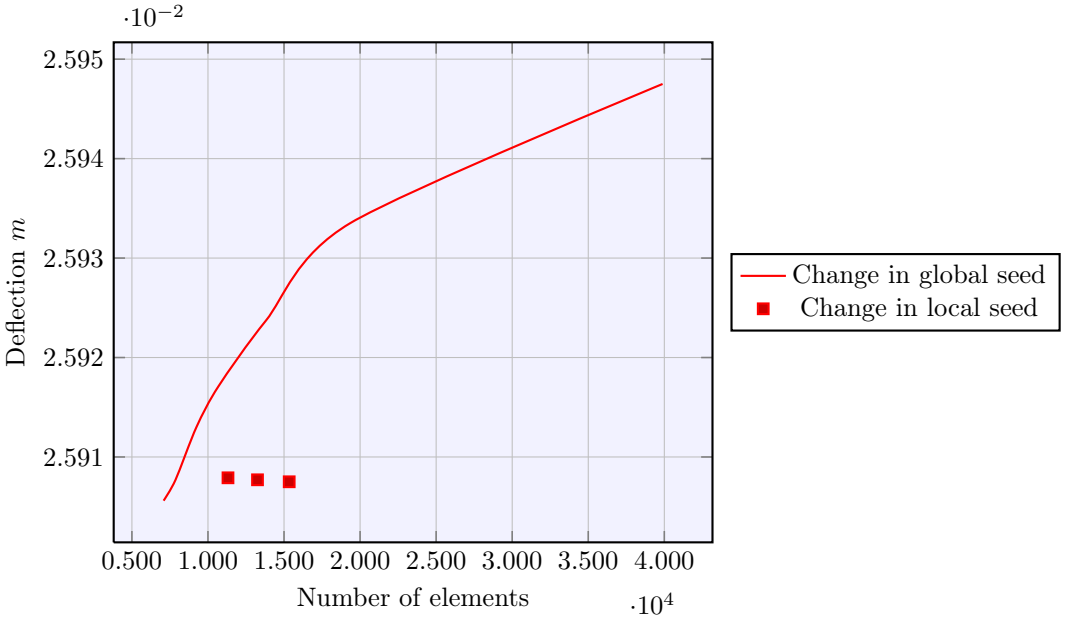

Figure 4.3.4: *Deflection at the edge by the heavy lane.*

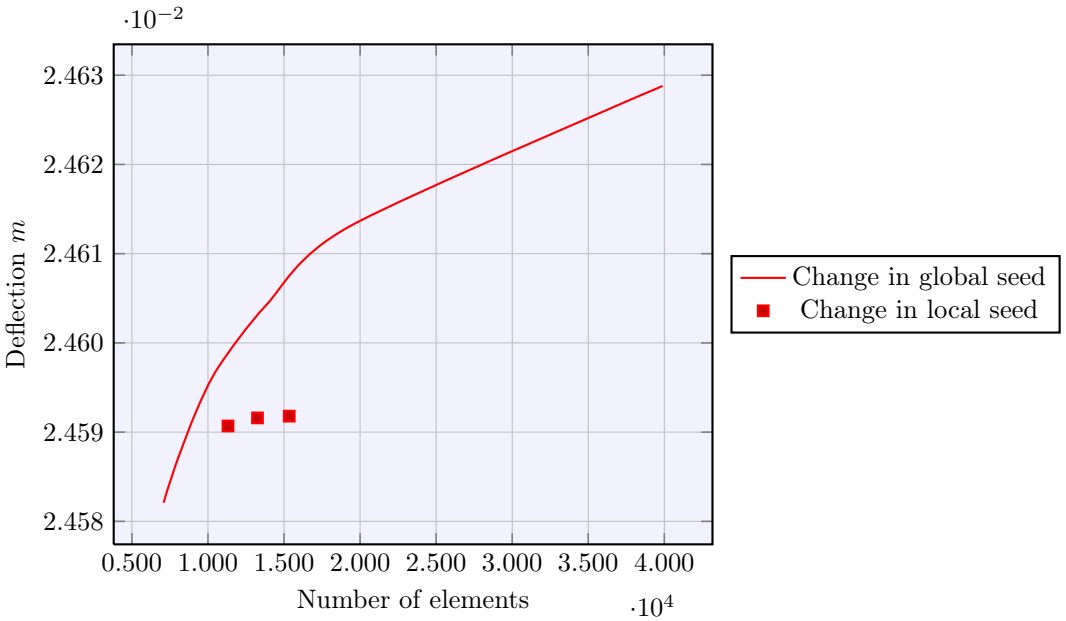

Figure 4.3.5: *Deflection at the inner side of the lower flange for the beam under the heavy lane.*

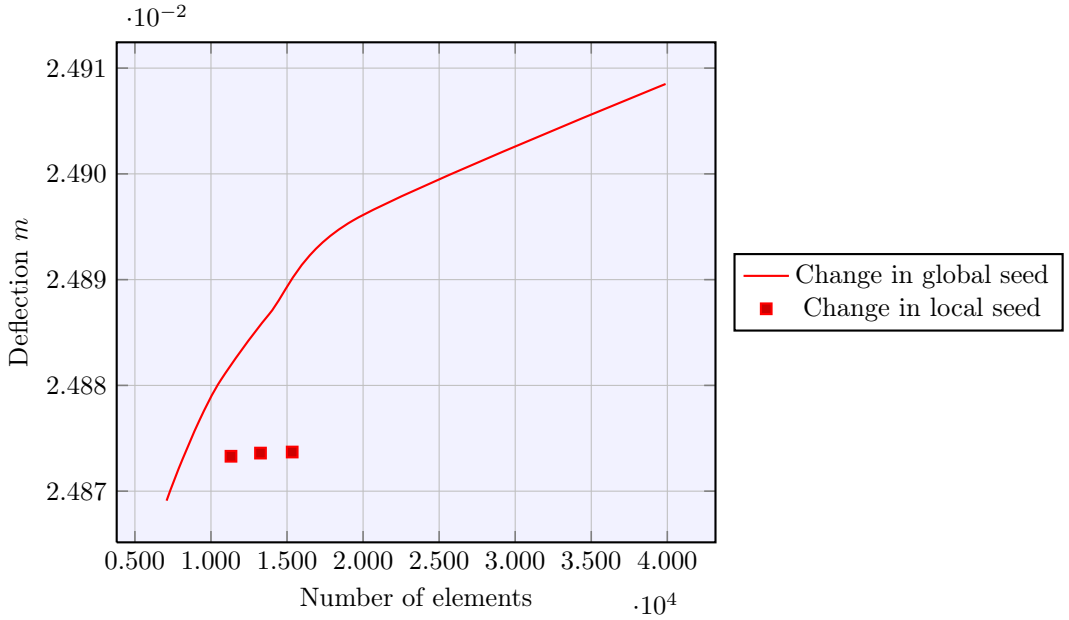

Figure 4.3.6: *Deflection of the middle part of the lower flange for the beam under the heavy lane.*

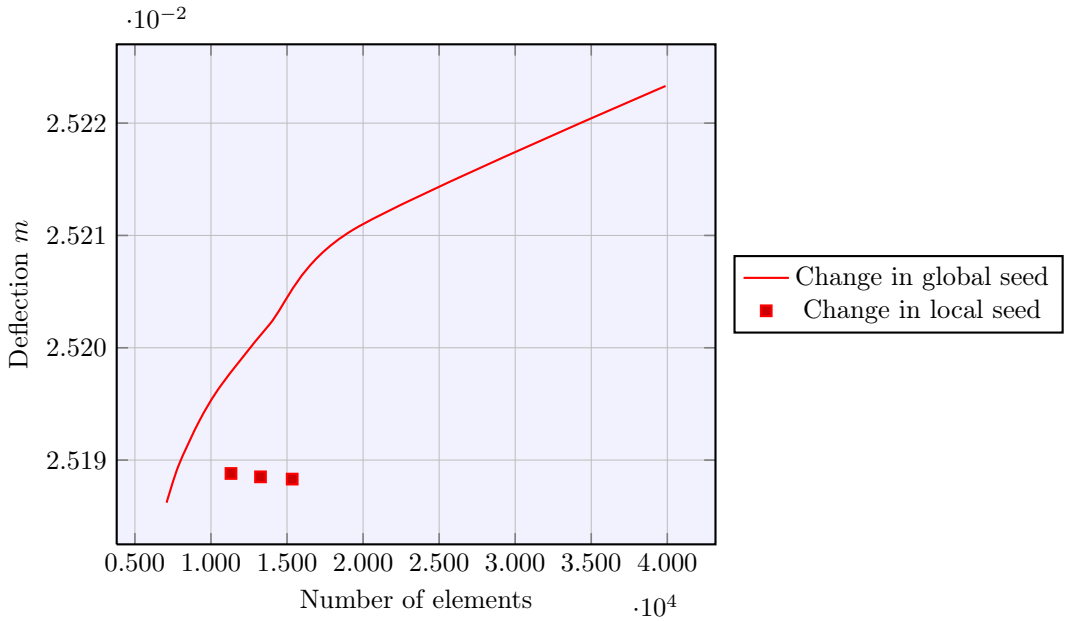

Figure 4.3.7: *Deflection of the outer part of the lower flange for the beam under the heavy lane.*

The difference between the results are one hundredth of a millimeter which means that the obtained result for the coarser mesh has already converged enough. Due to the geometry of the structure, a lot of partitions needed to be created to obtain a structured and good mesh with as few as possible mesh inconsistencies. Because of these partitions, it is impossible to get a very coarse mesh which means that a full scale convergence study cannot be performed. Though, there are some things that can be noted;

The global behavior is not changed by introducing a finer local seed around the area where the point loads are applied, see figure 4.3.4, 4.3.5, 4.3.6 and 4.3.7 Hence, this is not an effective way of increasing the number of elements in regard to the global behavior. Though, this has a positive effect on the result of the maximum local value obtained in between the two point loads in the heavy lane, see figure 4.3.3.

The conclusion of this convergence study is to use a coarse global seed with a small increase in mesh density around areas where the point loads are applied for verification two. The created partitions gives a structured mesh with reliable results.

4.4 Verification 1 of TALD and TCFR

The verification of the transformation models for an equivalent plate is performed to distinguish the difference between the two transformation methods and to try to approximate the error for different sets of parameter inputs. This is done by comparing the result from different FE-analysis performed in Abaqus CAE. First a reference plate is created containing three layers where all layers have orthotropic behavior. This is compared with the two corresponding equivalent plates created containing one layer with the orthotropic material properties obtained from the transformation algorithm (TALD and TCFR). The plates are modeled with both solid and shell elements separately.

The material properties are inserted as engineering constants with three Young's moduli, three Poisson's ratios and three shear moduli. These parameters are chosen as random as possible but still in the same magnitude as a real material. A total of seven material property sets with different parameters are created. To ensure that the chosen materials have a realistic behavior, a check of the ratio between Poisson's ratio and Young's modulus is performed in the algorithm. In general, the top and bottom face sheets are assigned stiffer properties compared to the core. Although, the last two material sets have a stiffer core compared to the face sheets. This is not a realistic case and is chosen only on the basis to study and understand the behavior of the different transformations better.

The length of the plates are set to 5 m, the width to 3 m and the height to 0.27 m. They are subjected to a uniformly distributed load (3 kN/m^2) and are simply supported on four edges. The plates are free to expand/retract in x- and y-direction along two sides. The boundary condition is assigned a width of 5 centimeters when using solid elements to ensure a good transfer of the support force to the three layers without the risk of local distortion corrupting the result. A linear boundary condition is used for the shell elements. A full list of boundary conditions can be found in table 4.4.1.

Table 4.4.1: Boundary conditions used in the verification 1

Edge	$U1$	$U2$	$U3$	$UR1$	$UR2$	$UR3$
Short side 1	free	0	0	free	free	free
Long side 1	0	free	0	free	free	free
Short side 2	free	free	0	free	free	free
Long side 2	free	free	0	free	free	free

The reference plate is modeled with solid elements constructed by three separate layers, each layer with unique input data. These layers are merged together to create the full plate, see figure 4.4.1. Full interaction between the layers is assumed, no additional slip or friction is modeled. When modeling the plate with transformed equivalent stiffness, a solid part with the same height as the reference plate is created and assigned its transformed material properties. The mesh for both the reference plate and the equivalent plates is constructed by 3D stress linear 8-node brick elements (C3D8R), approximately 20.000 elements. The obtained deflection is measured along x-direction on both top and bottom side to be able to track the compression of the different parts of the plates.

The thickness of the plate constructed with shell elements is assigned in the section property module. This is done in two different ways for the reference plate and the equivalent plate. The 3-layered reference plate is assigned a composite section property, which contains both thickness and the three orthotropic material properties. The equivalent plate is assigned a section with the same total thickness as the reference plate and consisting of a homogeneous material. These sections are assigned to the shells from the bottom up to ensure that the boundary conditions end up at the bottom edges and not in the middle of the plate. Standard linear elements (S4R) are used. Three integration points are used in the flanges and five points in the core material for the reference plate. Six points are used for the equivalent plates. The mesh consists of 1500 elements, see figure 4.4.2.

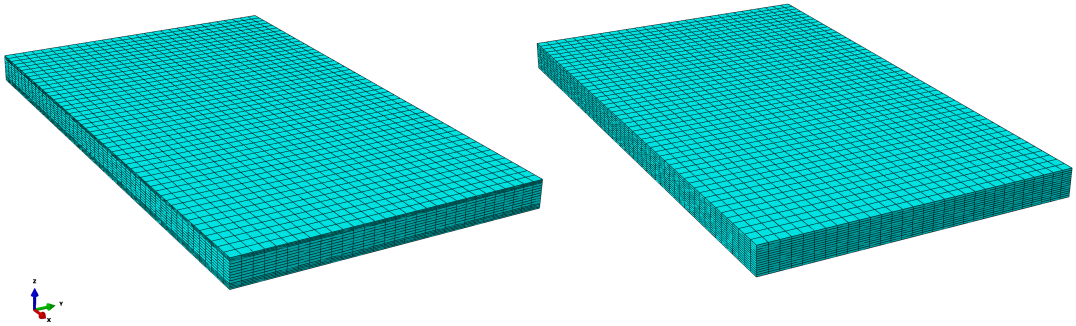

Figure 4.4.1: *Abaqus model for verification one, solid elements. Three layered reference plate (left) equivalent one layered plate (right)*

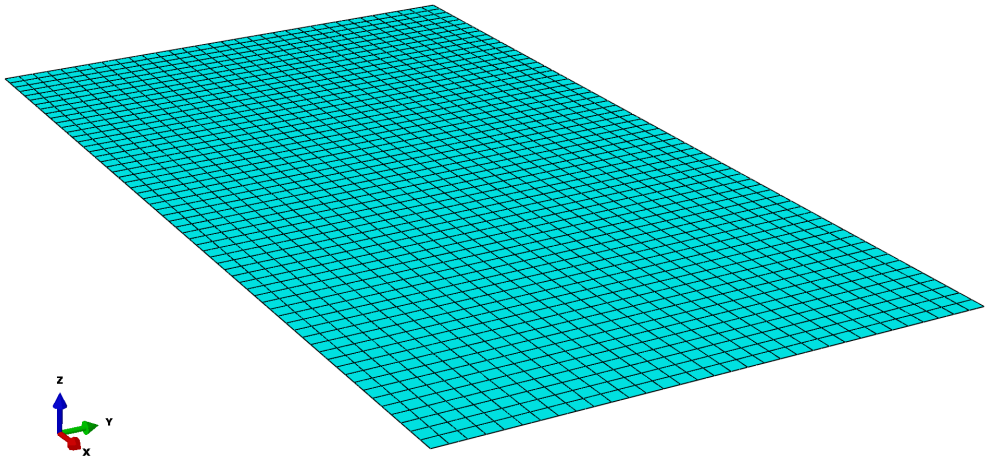

Figure 4.4.2: *Abaqus model for verification one, shell elements.*

4.4.1 Material parameters set 1

Table 4.4.2: Material parameters set 1. Initial values, stiffness parameters in $[Pa]$.

Layer	E_{xx}	E_{yy}	E_{zz}	ν_{xx}	ν_{yy}	ν_{zz}	G_{12}	G_{13}	G_{23}	h $[m]$
TOP	16.6e9	9.58e9	9.58e9	0.31	0.31	0.29	5.12e9	4.87e9	3.72e9	0.03
CORE	6.55e9	0.17e9	5.52e9	0.33	0.33	0.1	0.483e9	5.45e9	0.345e9	0.19
BOT	12.4e9	6.21e9	6.21e9	0.31	0.31	0.29	3.6e9	3.38e9	2.41e9	0.05

Table 4.4.3: Equivalent material parameters set 1 (Transformation based on constant flexural rigidity (TCFR), Transformation based on axial loaded deformation (TALD)), stiffness parameters in $[Pa]$.

Model	E_{xx}	E_{yy}	E_{zz}	ν_{xx}	ν_{yy}	ν_{zz}	G_{12}	G_{13}	G_{23}	h $[m]$
TCFR	15.4e9	6.77e9	5.93e9	0.324	0.324	0.156	1.58e9	4.84e9	0.466e9	0.27
TALD	8.75e9	2.33e9	5.93e9	0.324	0.324	0.156	1.58e9	4.84e9	0.466e9	0.27

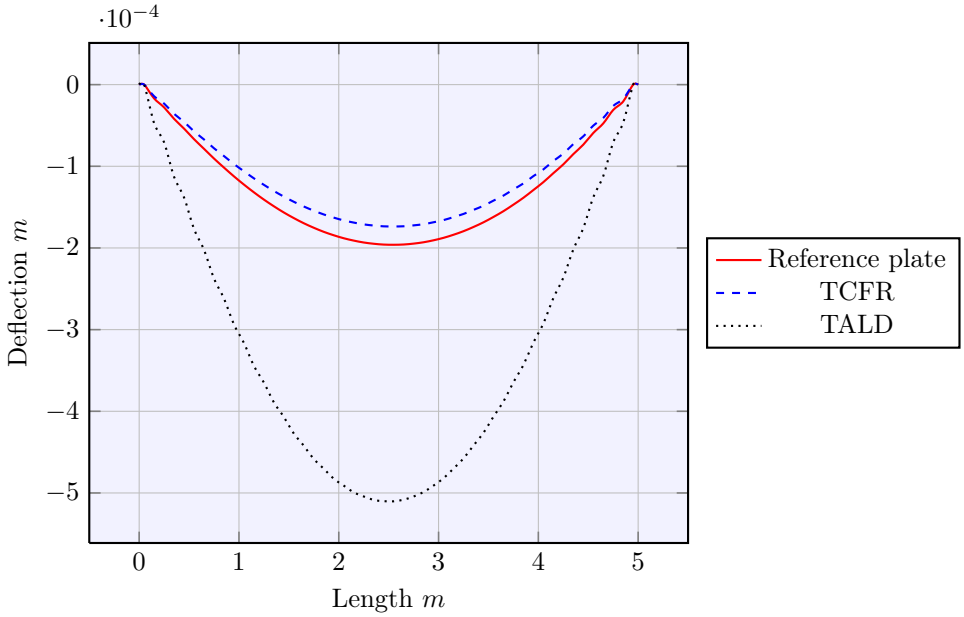

Figure 4.4.3: *Deflection U3 along x-direction for parameter set 1, solid elements.*

As seen in figure 4.4.3, the TCFR shows much better correlation with the reference plate than the TALD. TCFR shows a small overestimation of stiffness and TALD a large underestimation.

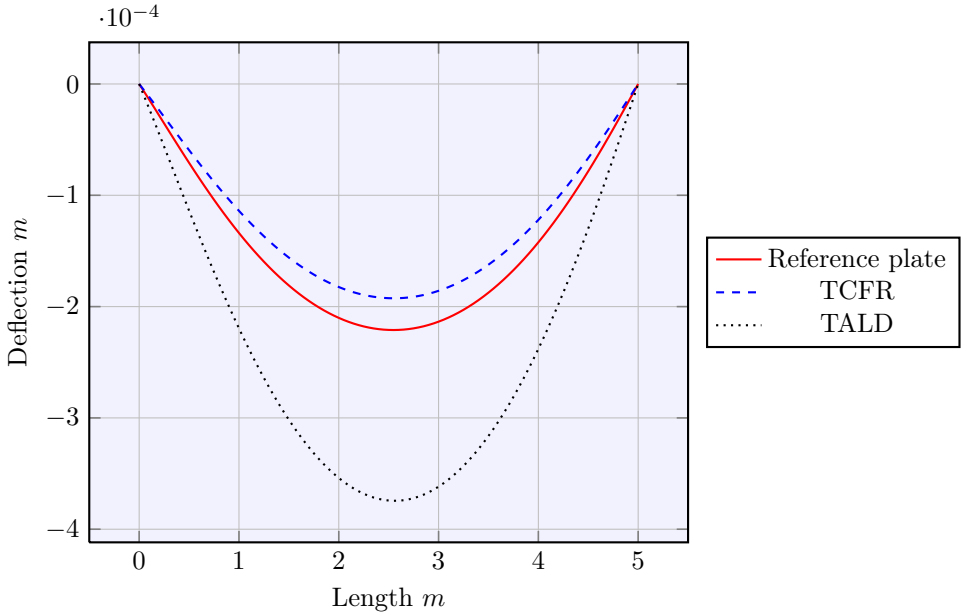

Figure 4.4.4: *Deflection U3 along x-direction for parameter set 1, shell elements.*

For the case with shell elements, the TCFR overestimates the stiffness and the TALD underestimates it compared to the reference.

Table 4.4.4: Comparison of deflection for the transformed plates in relation to the reference plate, parameter set 1.

Model	$U3$ solid, TOP	% diff	$U3$ solid, BOT	% diff	$U3$ shell	% diff
REF	-196.287E-06	0%	-196.093E-06	0%	-220.958E-06	0%
TCFR	-174E-06	-11.4%	-173.673E-06	-11.4%	-192.437E-06	-12.9%
TALD	-510.728E-06	160%	-510.238E-06	161%	-374.214E-06	69.4%

4.4.2 Material parameters set 2

Table 4.4.5: Material parameters, set 2. Initial values, stiffness parameters in $[Pa]$.

Layer	E_{xx}	E_{yy}	E_{zz}	ν_{xx}	ν_{yy}	ν_{zz}	G_{12}	G_{13}	G_{23}	h $[m]$
TOP	210e9	210e9	210e9	0.3	0.3	0.3	80.7e9	80.7e9	80.7e9	0.03
CORE	0.36e9	0.36e9	0.36e9	0.08	0.08	0.08	0.097e9	0.097e9	0.097e9	0.19
BOT	210e9	210e9	210e9	0.3	0.3	0.3	80.7e9	80.7e9	80.7e9	0.05

Table 4.4.6: Equivalent material parameters set 2 (Transformation based on constant flexural rigidity (TCFR), Transformation based on axial loaded deformation (TALD), stiffness parameters in $[Pa]$.

Model	E_{xx}	E_{yy}	E_{zz}	ν_{xx}	ν_{yy}	ν_{zz}	G_{12}	G_{13}	G_{23}	h $[m]$
TCFR	178e9	178e9	0.511e9	0.145	0.145	0.145	24.0e9	0.138e9	0.138e9	0.27
TALD	62.5e9	62.5e9	0.511e9	0.145	0.145	0.145	24.0e9	0.138e9	0.138e9	0.27

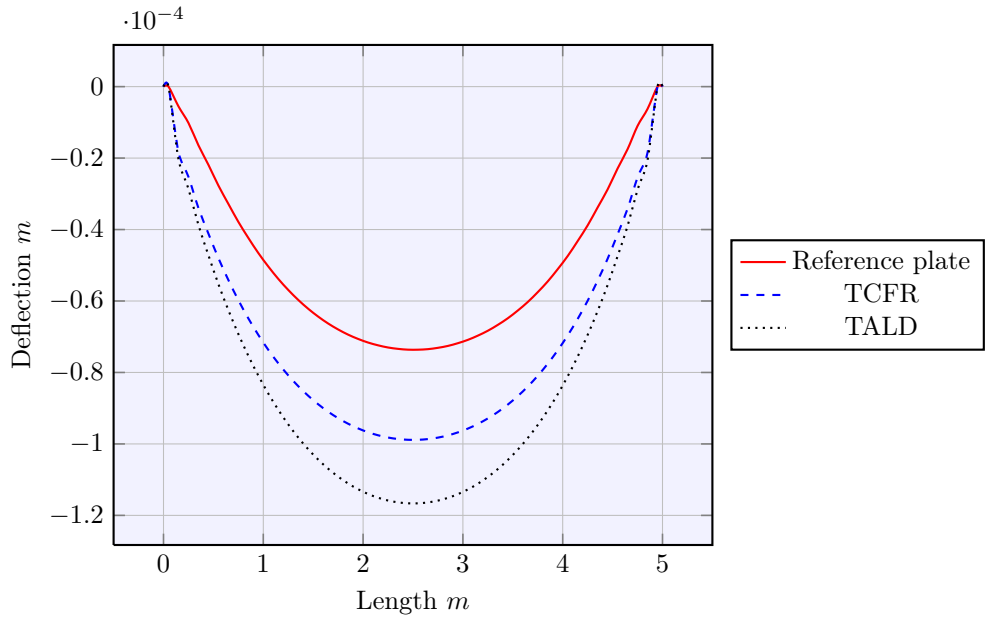

Figure 4.4.5: *Deflection U3 along x-direction for parameter set 2, solid elements.*

For solid elements, both methods underestimates the bending stiffness compared to the reference.

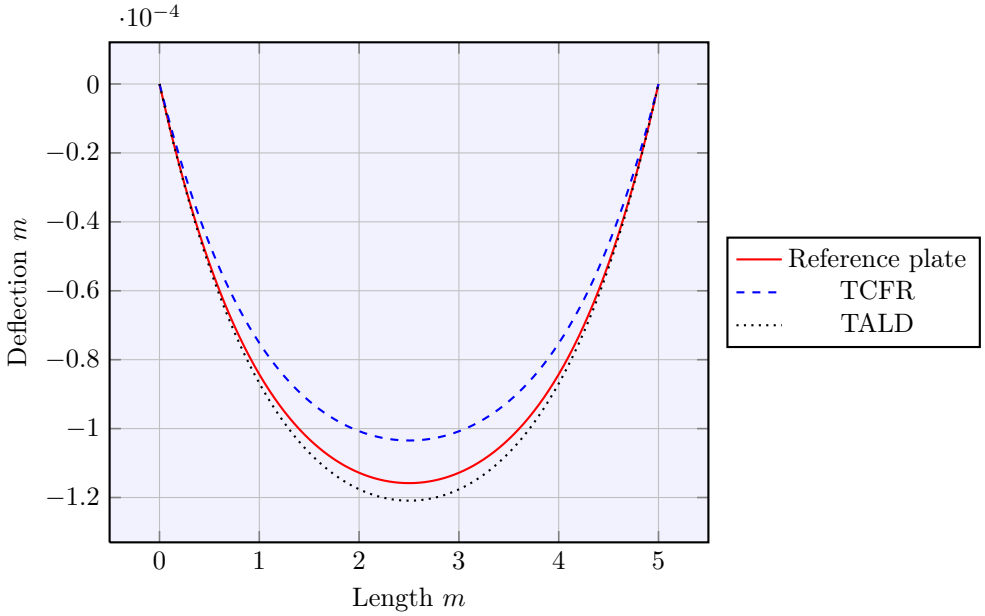

Figure 4.4.6: *Deflection U3 along x-direction for parameter set 2, shell elements.*

Shell elements in this case shows overestimation of stiffness for TCFR and underestimation for TALD, compared to the reference.

Table 4.4.7: Comparison of deflection for the transformed plates in relation to the reference plate, parameter set 2.

Model	$U3$ solid, TOP	% diff	$U3$ solid, BOT	% diff	$U3$ shell	% diff
REF	-74.471E-06	0%	-73.625E-06	0%	-115.823E-06	0%
TCFR	-99.648E-06	33.8%	-98.845E-06	34.3%	-103.455E-06	-10.7%
TALD	-117.446E-06	57.7%	-116.623E-06	58.4%	-120.917E-06	4.4%

4.4.3 Material parameters set 3

Table 4.4.8: Material parameters set 3. Initial values, stiffness parameters in $[Pa]$.

Layer	E_{xx}	E_{yy}	E_{zz}	ν_{xx}	ν_{yy}	ν_{zz}	G_{12}	G_{13}	G_{23}	h $[m]$
TOP	100e9	20e9	20e9	0.2	0.3	0.1	5e9	10e9	7e9	0.03
CORE	2e9	0.2e9	5e9	0.1	0.2	0.1	0.1e9	0.5e9	0.3e9	0.19
BOT	20e9	100e9	30e9	0.3	0.31	0.29	10e9	5e9	7e9	0.05

Table 4.4.9: Equivalent material parameters set 3 (Transformation based on constant flexural rigidity (TCFR), Transformation based on axial loaded deformation (TALD), stiffness parameters in $[Pa]$.

Model	E_{xx}	E_{yy}	E_{zz}	ν_{xx}	ν_{yy}	ν_{zz}	G_{12}	G_{13}	G_{23}	h $[m]$
TCFR	34.8e9	26.4e9	6.56e9	0.148	0.232	0.135	2.48e9	0.687e9	0.419e9	0.27
TALD	16.2e9	20.9e9	6.56e9	0.148	0.232	0.135	2.48e9	0.687e9	0.419e9	0.27

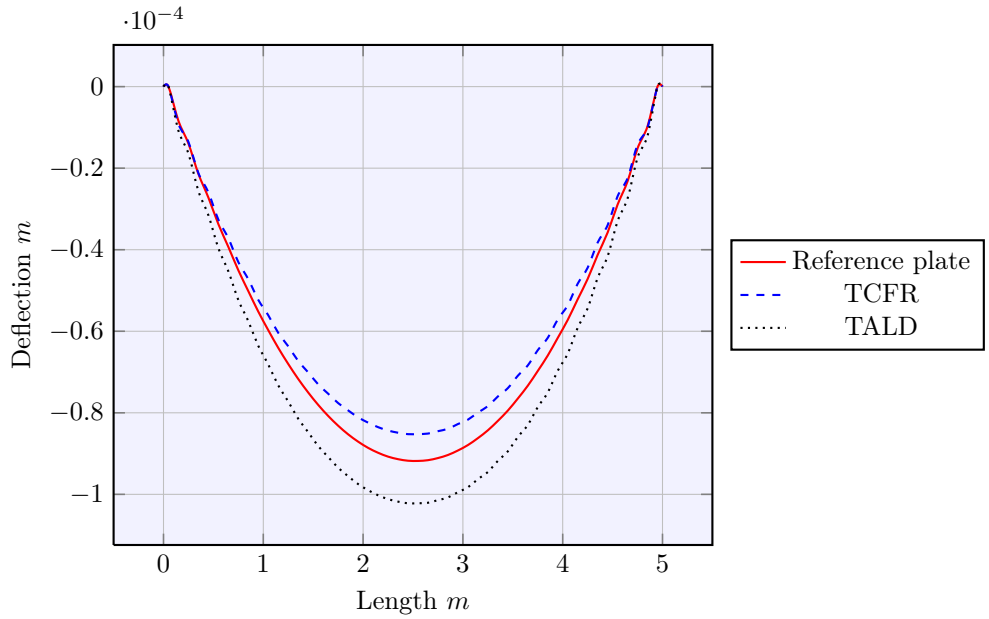

Figure 4.4.7: *Deflection U3 along x-direction for parameter set 3, solid elements.*

In this case the TCFR overestimates the bending stiffness and TALD underestimates it, compared to the reference. However, the deviation for them is not that large compared to the actual reference value.

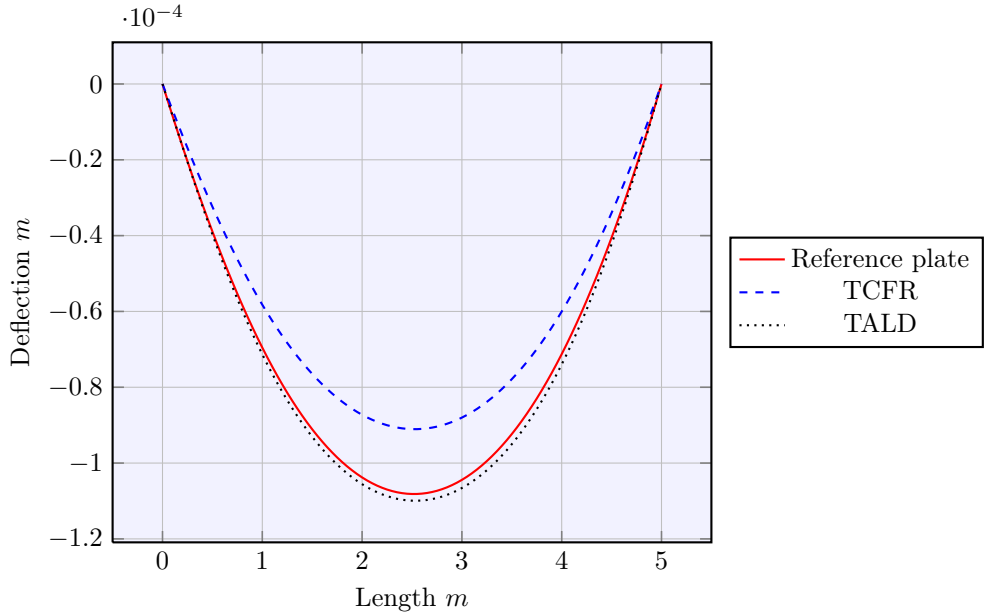

Figure 4.4.8: *Deflection U3 along x-direction for parameter set 3, shell elements.*

With shell elements, the result is quite similar as for the solid elements. In this case though, the TALD is almost totally accurate compared to the reference.

Table 4.4.10: Comparison of deflection for the transformed plates in relation to the reference plate, parameter set 3.

Model	$U3$ solid, TOP	% diff	$U3$ solid, BOT	% diff	$U3$ shell	% diff
REF	-91.803E-06	0%	-91.806E-06	0%	-108.155E-06	0%
TCFR	-85.387E-06	-7.0%	-85.216E-06	-7.2%	-91.046E-06	-15.8%
TALD	-102.382E-06	11.5%	-102.201E-06	11.3%	-109.92E-06	1.6%

4.4.4 Material parameters set 4

Table 4.4.11: Material parameters set 4. Initial values, stiffness parameters in $[Pa]$.

Layer	E_{xx}	E_{yy}	E_{zz}	ν_{xx}	ν_{yy}	ν_{zz}	G_{12}	G_{13}	G_{23}	h $[m]$
TOP	2000e9	1000e9	500e9	0.05	0.06	0.05	200e9	100e9	400e9	0.03
CORE	0.02e9	0.04e9	0.5e9	0.1	0.1	0.05	0.5e9	0.9e9	1e9	0.19
BOT	400e9	200e9	40e9	0.1	0.1	0.1	50e9	53e9	71e9	0.05

Table 4.4.12: Equivalent material parameters set 4 (Transformation based on constant flexural rigidity (TCFR), Transformation based on axial loaded deformation (TALD), stiffness parameters in $[Pa]$.

Model	E_{xx}	E_{yy}	E_{zz}	ν_{xx}	ν_{yy}	ν_{zz}	G_{12}	G_{13}	G_{23}	h $[m]$
TCFR	673e9	337e9	0.708e9	0.094	0.096	0.078	31.8e9	1.27e9	1.42e9	0.27
TALD	296e9	148e9	0.708e9	0.094	0.096	0.078	31.8e9	1.27e9	1.42e9	0.27

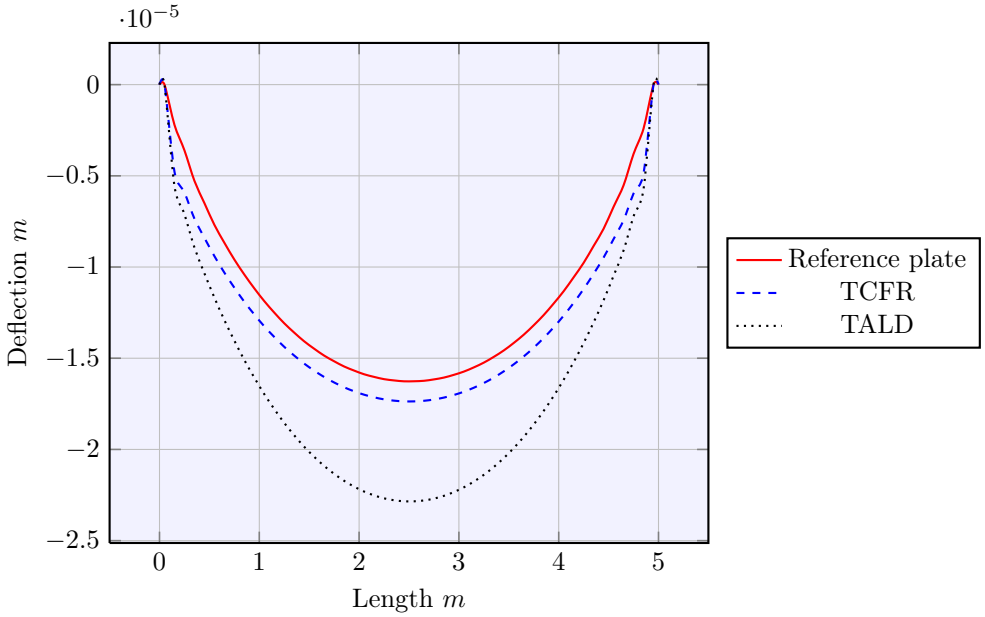

Figure 4.4.9: *Deflection U3 along x-direction for parameter set 4, solid elements.*

In this case both methods underestimates the bending stiffness. TCFR is though much closer to the actual reference value.

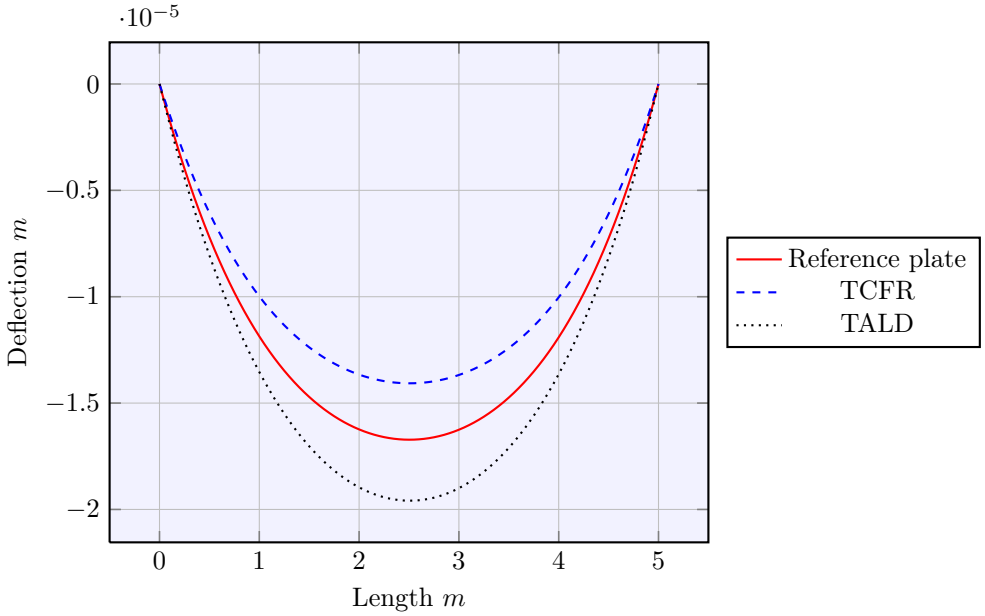

Figure 4.4.10: *Deflection U3 along x-direction for parameter set 4, shell elements.*

For shell elements, TCFR overestimates stiffness and TALD underestimates. They are approximately at the same distance, on opposite sides, of the reference.

Table 4.4.13: Comparison of deflection for the transformed plates in relation to the reference plate, parameter set 4.

Model	$U3$ solid, TOP	% diff	$U3$ solid, BOT	% diff	$U3$ shell	% diff
REF	-16.689E-06	0%	-16.262E-06	0%	-16.721E-06	0%
TCFR	-17.920E-06	7.4%	-17.365E-06	6.8%	-14.07E-06	-15.9%
TALD	-23.414E-06	40.3%	-22.844E-06	40.5%	-19.588E-06	17.1%

4.4.5 Material parameters set 5

Table 4.4.14: Material parameters set 5. Initial values, stiffness parameters in $[Pa]$.

Layer	E_{xx}	E_{yy}	E_{zz}	ν_{xx}	ν_{yy}	ν_{zz}	G_{12}	G_{13}	G_{23}	h $[m]$
TOP	20e9	2e9	50e9	0.15	0.26	0.12	5e9	3e9	1e9	0.03
CORE	0.02e9	0.046e9	0.2e9	0.13	0.22	0.09	0.4e9	0.09e9	0.1e9	0.19
BOT	15e9	40e9	1e9	0.15	0.11	0.15	2e9	3e9	24e9	0.05

Table 4.4.15: Equivalent material parameters set 5 (Transformation based on constant flexural rigidity (TCFR), Transformation based on axial loaded deformation (TALD)), stiffness parameters in $[Pa]$.

Model	E_{xx}	E_{yy}	E_{zz}	ν_{xx}	ν_{yy}	ν_{zz}	G_{12}	G_{13}	G_{23}	h $[m]$
TCFR	15.0e9	3.69e9	0.270e9	0.136	0.204	0.104	1.21e9	0.126e9	0.140e9	0.27
TALD	5.01e9	7.66e9	0.270e9	0.136	0.204	0.104	1.21e9	0.126e9	0.140e9	0.27

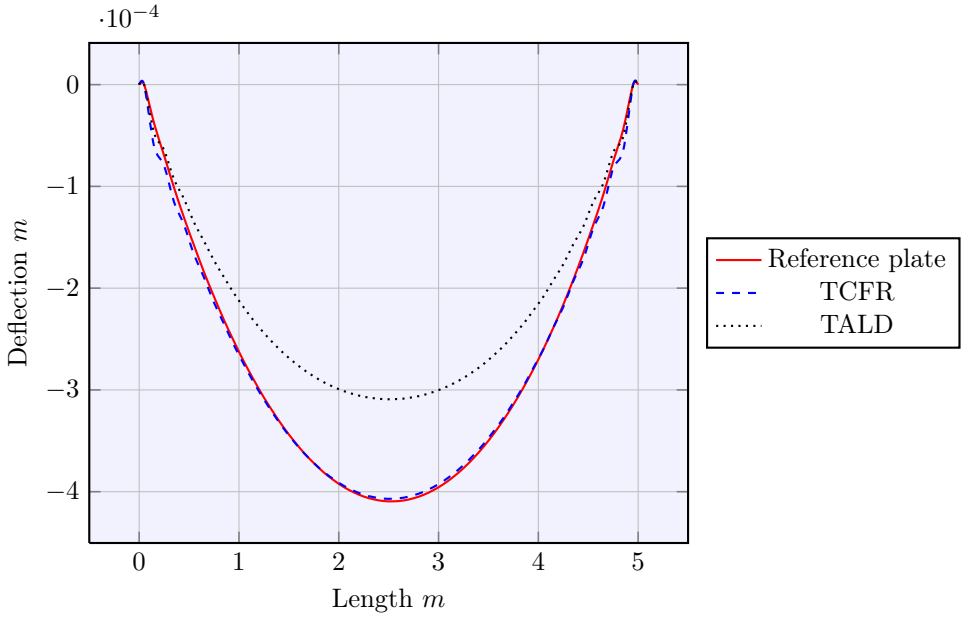

Figure 4.4.11: *Deflection U3 along x-direction for parameter set 5, solid elements.*

In this case the TCFR hits the reference very accurate and the TALD greatly overestimates the stiffness.

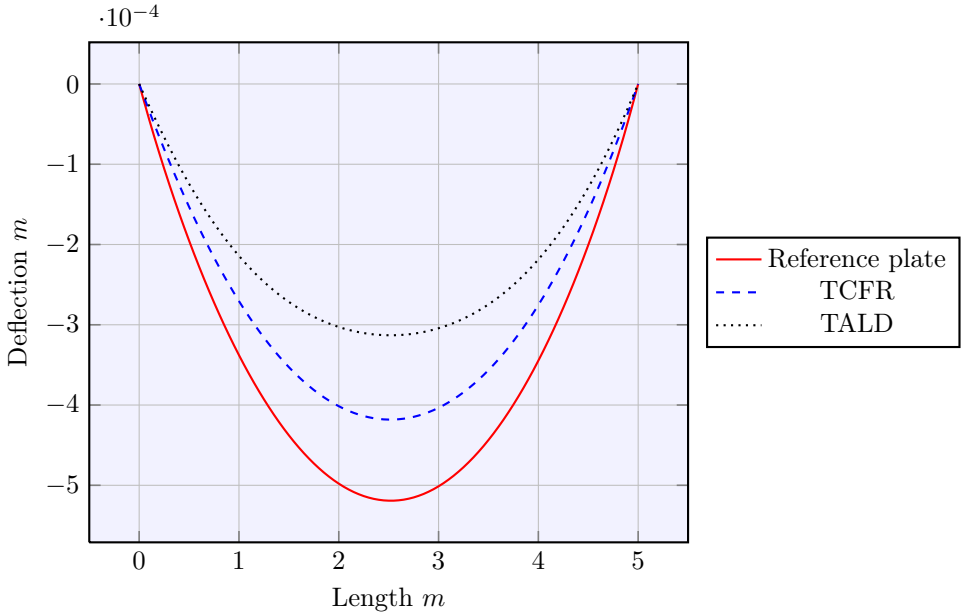

Figure 4.4.12: *Deflection U3 along x-direction for parameter set 5, shell elements.*

However for shell elements, both methods overestimates the bending stiffness compared to the reference.

Table 4.4.16: Comparison of deflection for the transformed plates in relation to the reference plate, parameter set 5.

Model	$U3$ solid, TOP	% diff	$U3$ solid, BOT	% diff	$U3$ shell	% diff
REF	-408.718E-06	0%	-409.47E-06	0%	-519.153E-06	0%
TCFR	-408.978E-06	0.06%	-406.832E-06	-0.6%	-418.128E-06	-19.5%
TALD	-310.929E-06	-23.9%	-309.096E-06	-24.5%	-313.077E-06	-39.7%

4.4.6 Material parameters set 6

Table 4.4.17: Material parameters set 6. Initial values, stiffness parameters in $[Pa]$.

Layer	E_{xx}	E_{yy}	E_{zz}	ν_{xx}	ν_{yy}	ν_{zz}	G_{12}	G_{13}	G_{23}	h $[m]$
TOP	2e9	5e9	10e9	0.2	0.1	0.3	0.5e9	0.3e9	0.1e9	0.03
CORE	200e9	100e9	300e9	0.23	0.12	0.3	10e9	0.5e9	2e9	0.19
BOT	10e9	20e9	2e9	0.12	0.15	0.2	5e9	1e9	5e9	0.05

Table 4.4.18: Equivalent material parameters set 6 (Transformation based on constant flexural rigidity (TCFR), Transformation based on axial loaded deformation (TALD)), stiffness parameters in $[Pa]$.

Model	E_{xx}	E_{yy}	E_{zz}	ν_{xx}	ν_{yy}	ν_{zz}	G_{12}	G_{13}	G_{23}	h $[m]$
TCFR	91.8e9	57.3e9	7.58e9	0.206	0.123	0.282	8.02e9	0.509e9	0.667e9	0.27
TALD	142e9	74.6e9	7.58e9	0.206	0.123	0.282	8.02e9	0.509e9	0.667e9	0.27

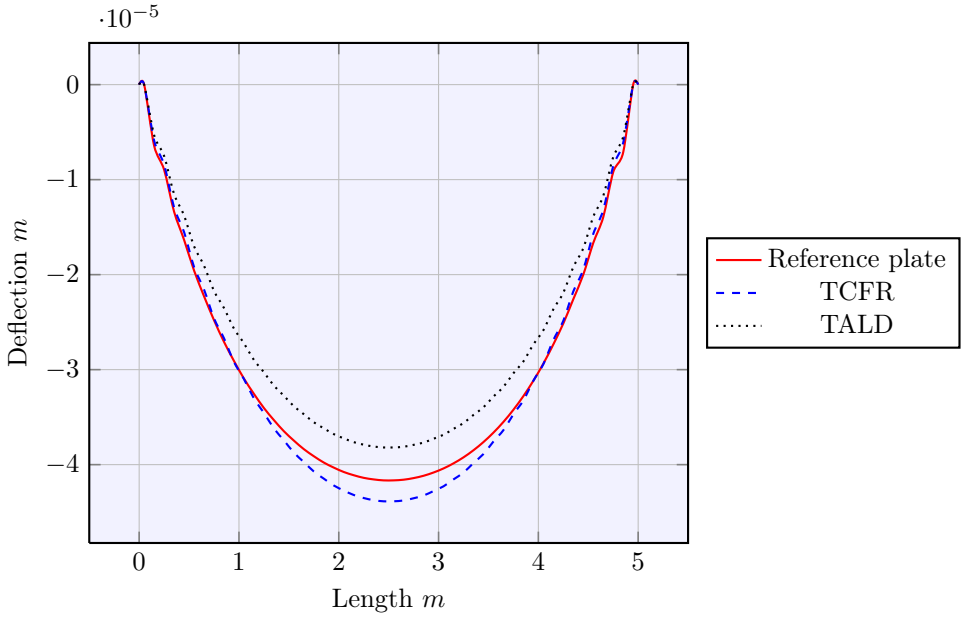

Figure 4.4.13: *Deflection U3 along x-direction for parameter set 6, solid elements.*

In this parameter set, both methods shows good correlation. TCFR underestimates the bending stiffness and TALD overestimates it compared to the reference.

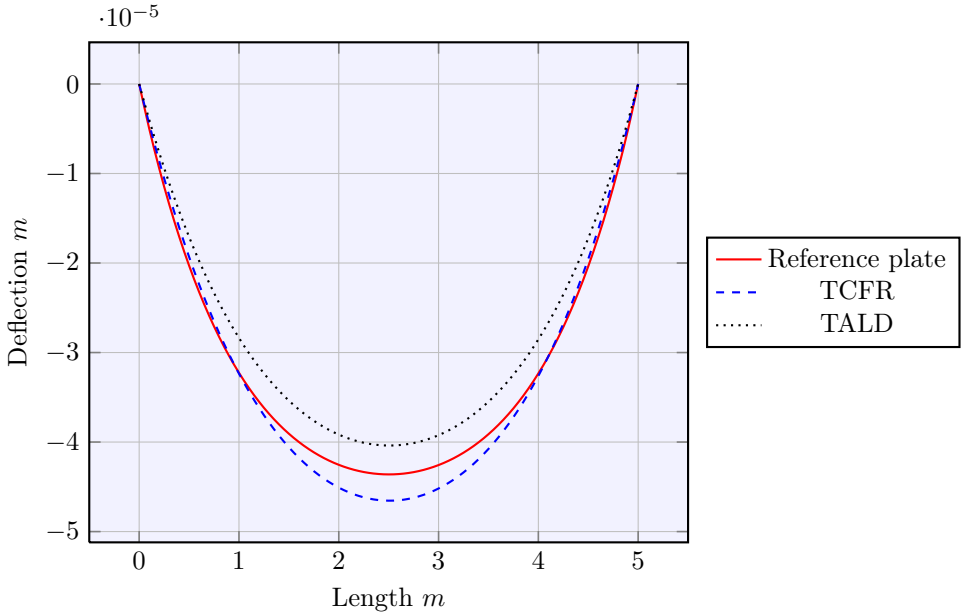

Figure 4.4.14: *Deflection U3 along x-direction for parameter set 6, shell elements.*

Also for shell elements, the two methods shows good correlation of the same order as for solid elements.

Table 4.4.19: Comparison of deflection for the transformed plates in relation to the reference plate, parameter set 6.

Model	$U3$ solid, TOP	% diff	$U3$ solid, BOT	% diff	$U3$ shell	% diff
REF	-41.690E-06	0%	-41.657E-06	0%	-43.614E-06	0%
TCFR	-43.952E-06	5.4%	-43.859E-06	5.3%	-46.549E-06	6.7%
TALD	-38.275E-06	-8.2%	-38.190E-06	-8.3%	-40.388E-06	-7.4%

4.4.7 Material parameters set 7

Table 4.4.20: Material parameters set 7. Initial values, stiffness parameters in $[Pa]$.

Layer	E_{xx}	E_{yy}	E_{zz}	ν_{xx}	ν_{yy}	ν_{zz}	G_{12}	G_{13}	G_{23}	h $[m]$
TOP	0.2e9	5e9	0.3e9	0.12	0.11	0.23	0.05e9	0.03e9	0.01e9	0.03
CORE	200e9	1000e9	600e9	0.15	0.22	0.23	100e9	6e9	10e9	0.19
BOT	1e9	2e9	22e9	0.17	0.14	0.15	0.5e9	10e9	1e9	0.05

Table 4.4.21: Equivalent material parameters set 7 (Transformation based on constant flexural rigidity (TCFR), Transformation based on axial loaded deformation (TALD), stiffness parameters in $[Pa]$.

Model	E_{xx}	E_{yy}	E_{zz}	ν_{xx}	ν_{yy}	ν_{zz}	G_{12}	G_{13}	G_{23}	h $[m]$
TCFR	84.9e9	423e9	2.63e9	0.150	0.193	0.215	70.5e9	0.260e9	0.088e9	0.27
TALD	141e9	705e9	2.63e9	0.150	0.193	0.215	70.5e9	0.260e9	0.088e9	0.27

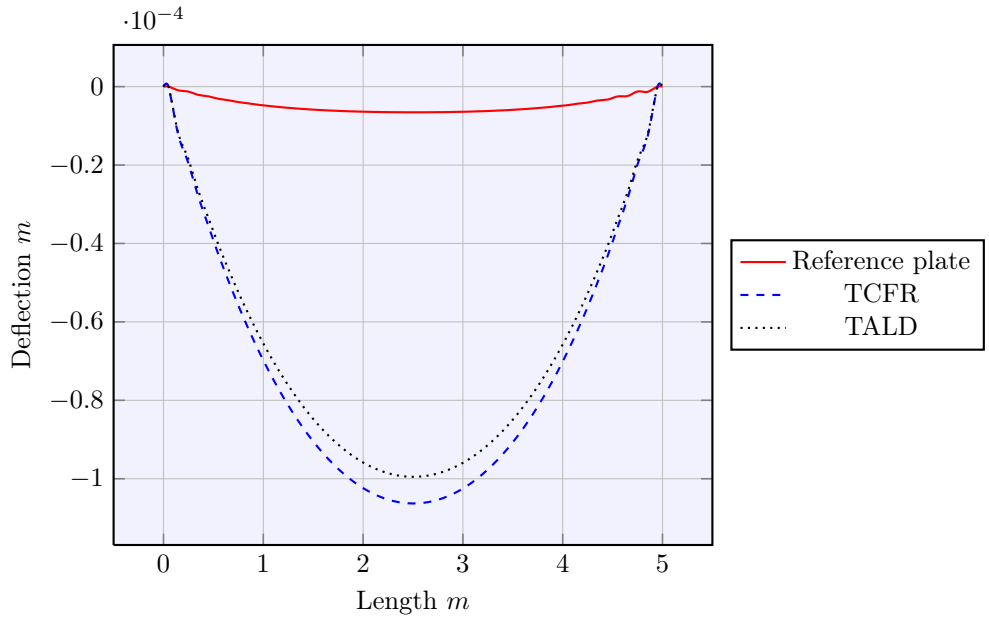

Figure 4.4.15: *Deflection U3 along x-direction for parameter set 7, solid elements.*

In this case, TALD and TCFR show very bad correlation with the reference. Both methods are heavily underestimating the bending stiffness compared to the reference.

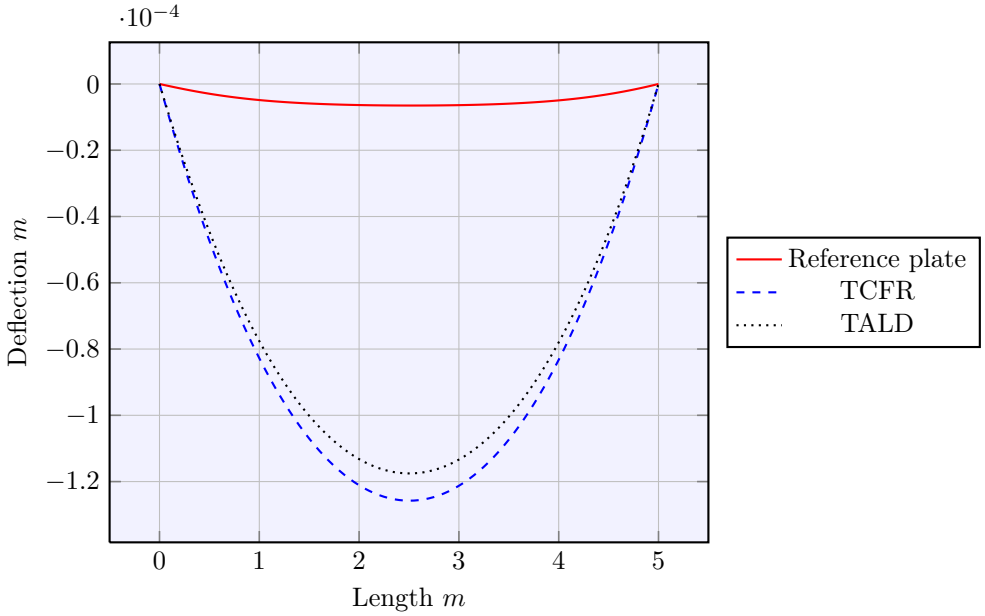

Figure 4.4.16: *Deflection U3 along x-direction for parameter set 7, shell elements.*

The same, as for solid elements, applies also to shell elements where non of the methods even are close to the reference's deflection.

Table 4.4.22: Comparison of deflection for the transformed plates in relation to the reference plate, parameter set 7.

Model	$U3$ solid, TOP	% diff	$U3$ solid, BOT	% diff	$U3$ shell	% diff
REF	-6.8343E-06	0%	-6.5438E-06	0%	-6.506E-06	0%
TCFR	-106.431E-06	1457%	-106.27E-06	1524%	-125.764E-06	1833%
TALD	-99.637E-06	1358%	-99.478E-06	1420%	-117.54E-06	1707%

4.4.8 Comment on the results from verification one

(I) Overall the transformation based on constant flexural rigidity (TCFR) seems to have better correlation compared to the transformation based on axial deformation (TALD).

(II) The transformation based on constant flexural rigidity seems to be a more stable method and is not varying as much between the different parameter sets as the other transformation (TALD).

(III) The last material set gives a bad correlation. This may be a result from the large difference between the layers for material parameters G_{13} and G_{23}. The equation used for the transformation have very similar properties as an equation used to calculate the electric resistance of a parallel connection. This means that a very small value of the material parameter affects the transformed shear modulus to a large extent, similar as for an electric current slipping through the circuit where the resistance is the lowest. In other words, a low value, even though the thickness of the layer is small, has a very large negative impact on the stiffness of the calculated equivalent parameter. This might mean that the transformation is not valid when the variation between the input shear parameters is too large compared to each other. Further verification is needed to investigate this more comprehensively.

(IV) One of the base assumption for the TCFR-method did not hold true for parameter set 5. The neutral axis was found to not be inside the core material for this case, which could lead to inaccurate results. The problem was noted in the MATLAB-algorithm that computes the equivalent stiffness, which warns the user if any assumptions are not fulfilled. The reason why this problem arose, was due to a large difference of the stiffness between the flanges, see table 4.4.14. However this did not affect the result

much since the flanges are fairly thin, which only gives a very small error when computing the equivalent properties.

(V) The TCFR method base assumption is founded in a case of bending and should consequently give a more accurate result for verification one when the plate is resting on four supports subjected to a evenly distributed load, in other words mainly bending. The TALD method gives unacceptable bad correlation for some parameter sets. However, the real case is not pure bending or axial loading but a combination of them depending on the direction.

(VI) Shell elements does only take into account in-plane shear stresses. Thus, the out of plane strain is not handled in a correct way which can lead to errors in the result. This is the reason why the results differ between shell and solid elements for some parameter sets. Because of this problem, only solid elements are used in further verifications.

(VII) There is a need to verify and compare the two methods further in a verification that simulates the real case better, with combined bending and axial load.

4.5 Verification 2 of TALD and TCFR

Since the composite sandwich structure is to be used as a bridge deck on the steel beam frame system, the verification also has to be done for this case. This will compliment verification one and establish a more reliable evaluation of the two different transformation methods. The sandwich plate is working both like a plate resting on two supports and as an upper flange for the global beam frame system in verification two. The deflection between the two girders is close to pure bending which should favor the transformation based on constant flexural rigidity. In the other direction the loading is a combination of bending and axial loading, hence it is not apparent which of the two transformation methods that should be favored. The geometry and model information used in the second verification can be found in section 4.1.

If one of the transformations result in an overestimation and the other method an underestimation, it could be of value to combine these to get a better correlation to the reference plate. This would constitute a third method of transformation. The solution could theoretically be relevant due to the combined bending and axial load which is found in the main direction of the bridge. In order to decide the proportions to be used of the different transformations, the strains of the section has to be investigated.

Verification two is performed for the full bridge model and the deflection is measured in both x and y direction (global coordinates), where x is the main longitudinal direction of the bridge and y is along the width of the deck. The structure is subjected to a load in accordance with Eurocode load case LM1, see appendix 10.1. The graphs show the deflection plotted against the distance along (x-direction), or across (y-direction) the bridge. Because of the inaccuracy of shell elements, only solid elements are used in verification two.

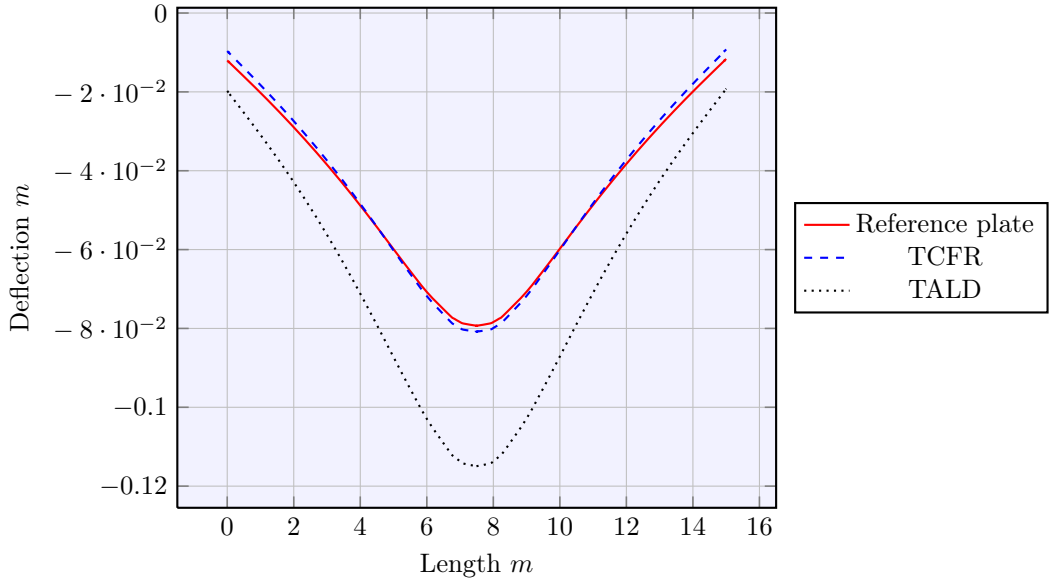

Figure 4.5.1: *Deflection U3 along x-direction for parameter set 1.*

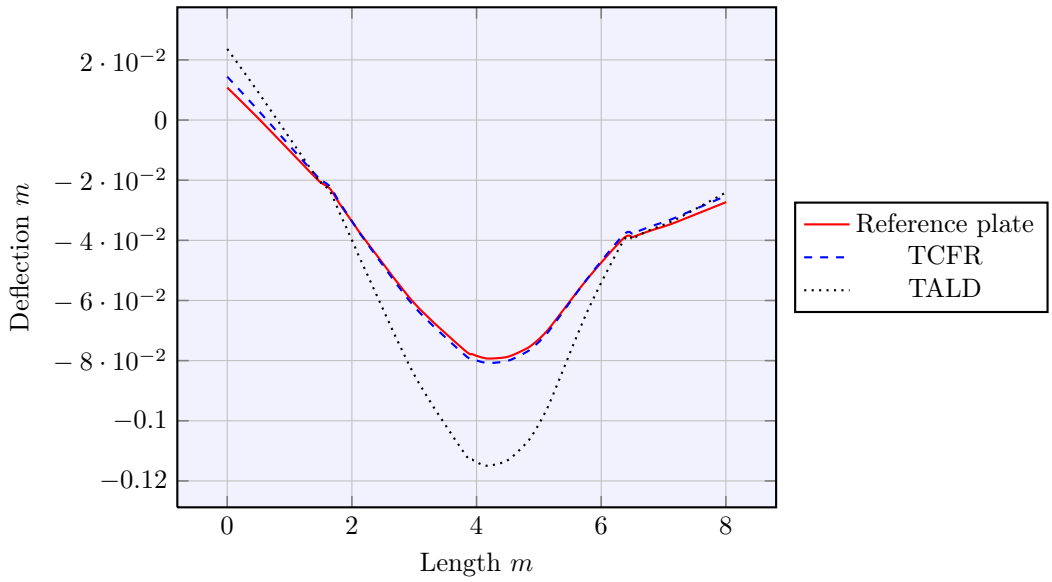

Figure 4.5.2: *Deflection U3 along y-direction for parameter set 1.*

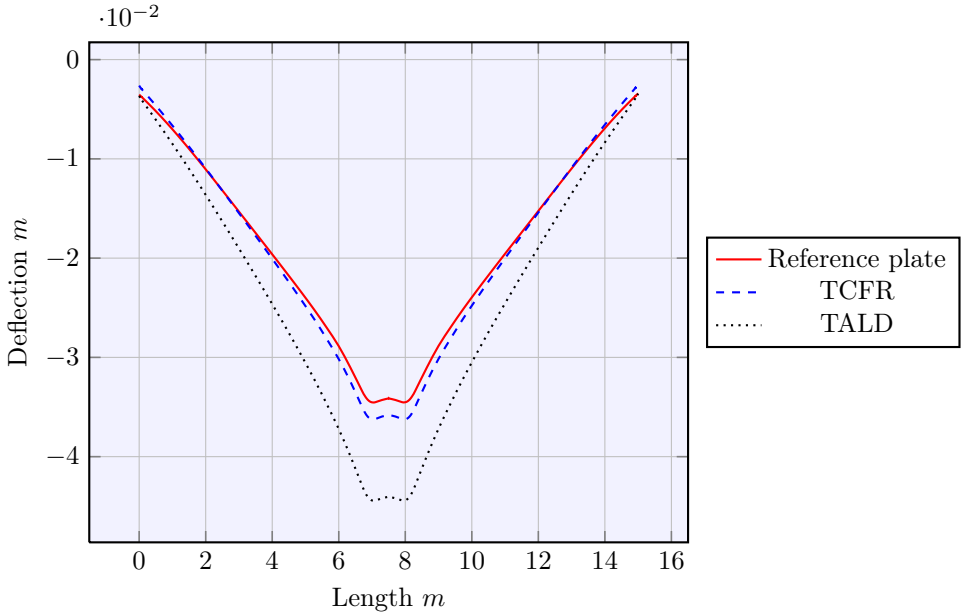

Figure 4.5.3: *Deflection U3 along x-direction for parameter set 2.*

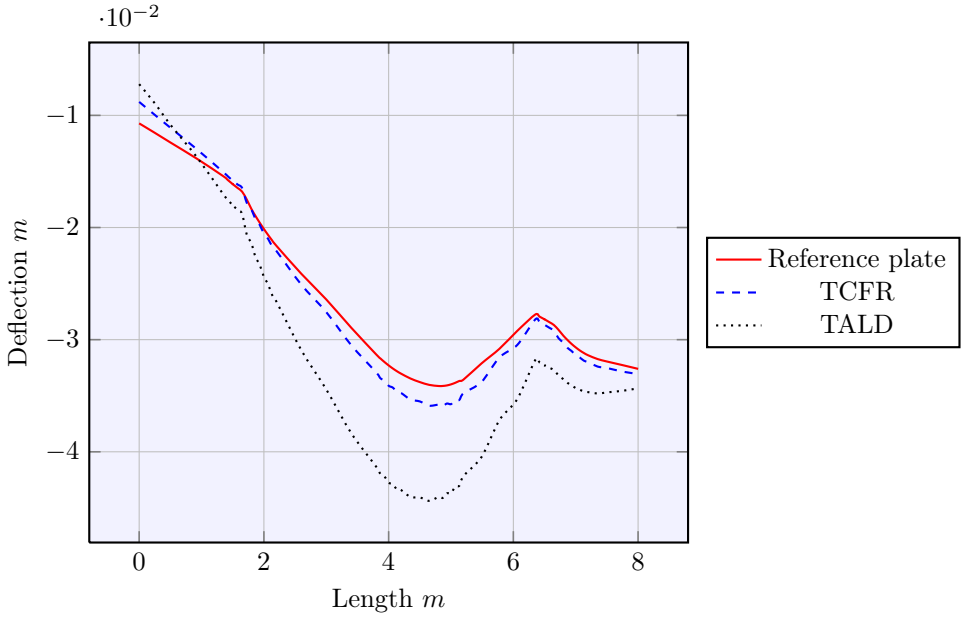

Figure 4.5.4: *Deflection U3 along y-direction for parameter set 2.*

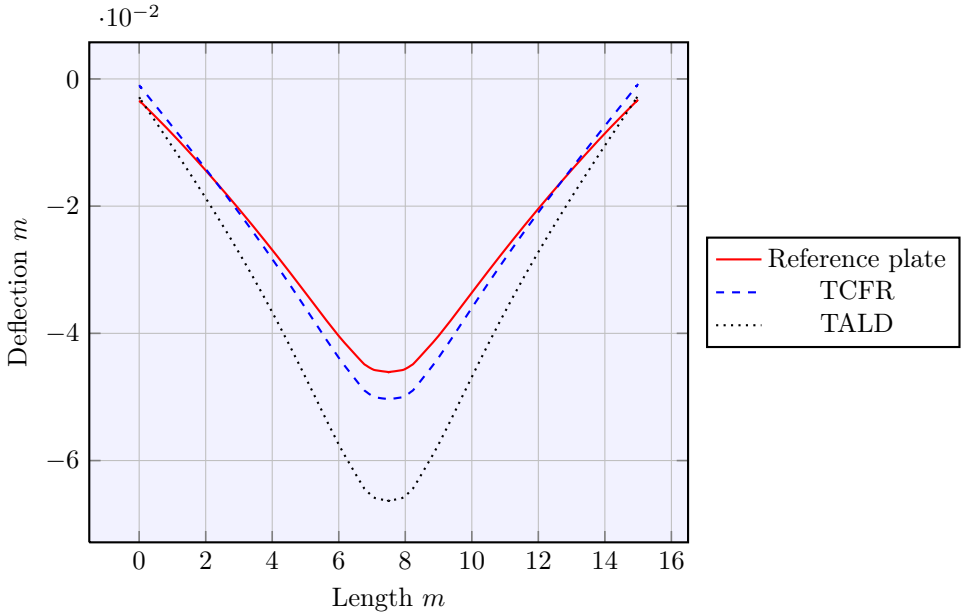

Figure 4.5.5: *Deflection U3 along x-direction for parameter set 3.*

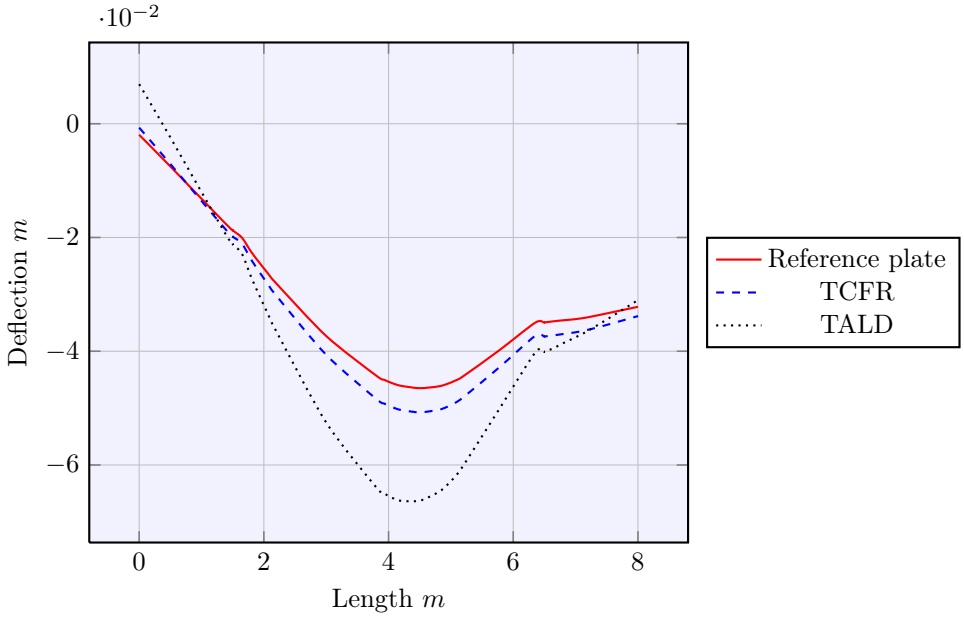

Figure 4.5.6: *Deflection U3 along y-direction for parameter set 3.*

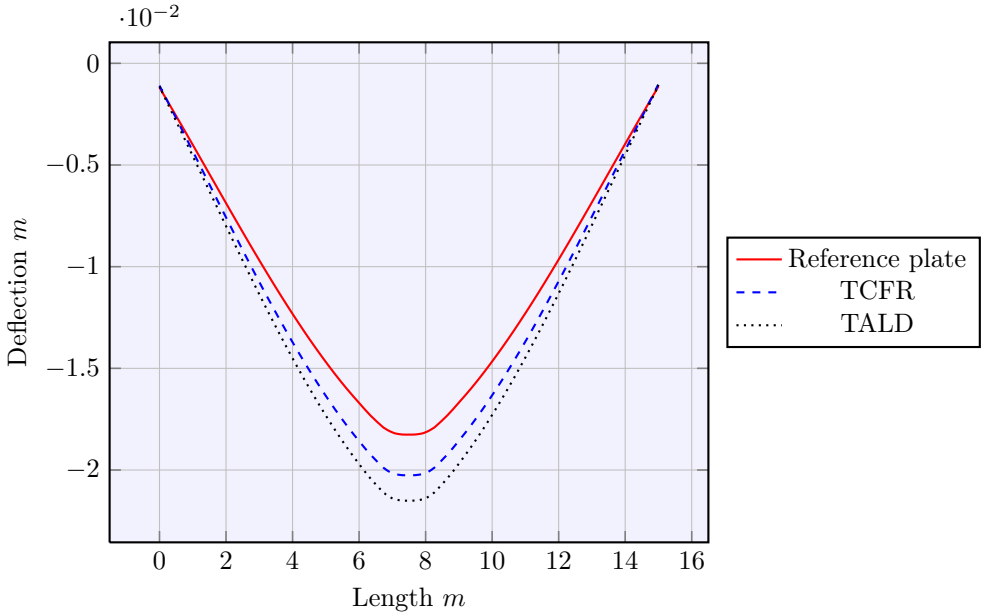

Figure 4.5.7: *Deflection U3 along x-direction for parameter set 4.*

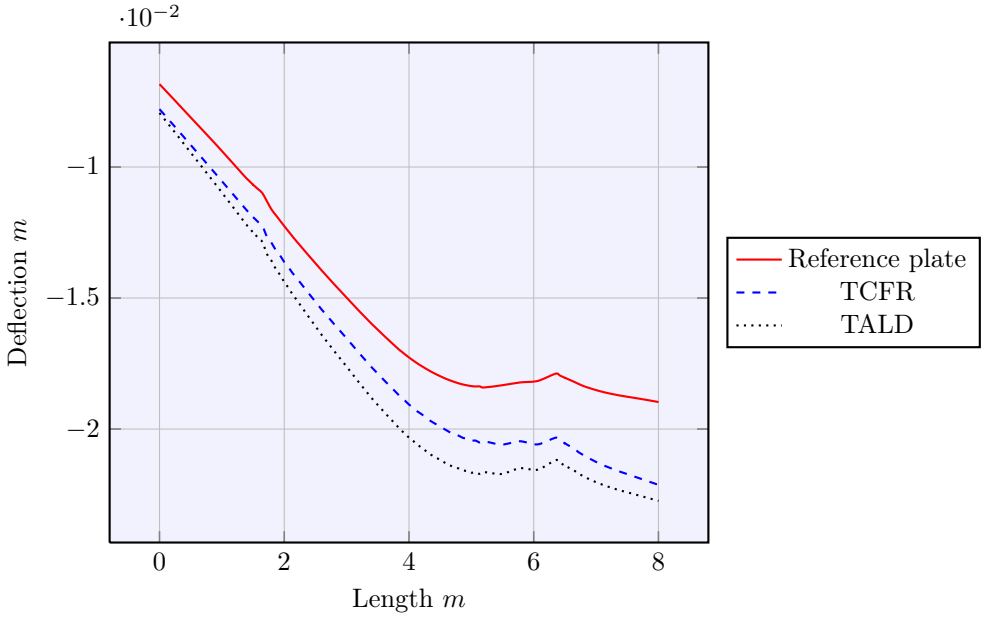

Figure 4.5.8: *Deflection U3 along y-direction for parameter set 4.*

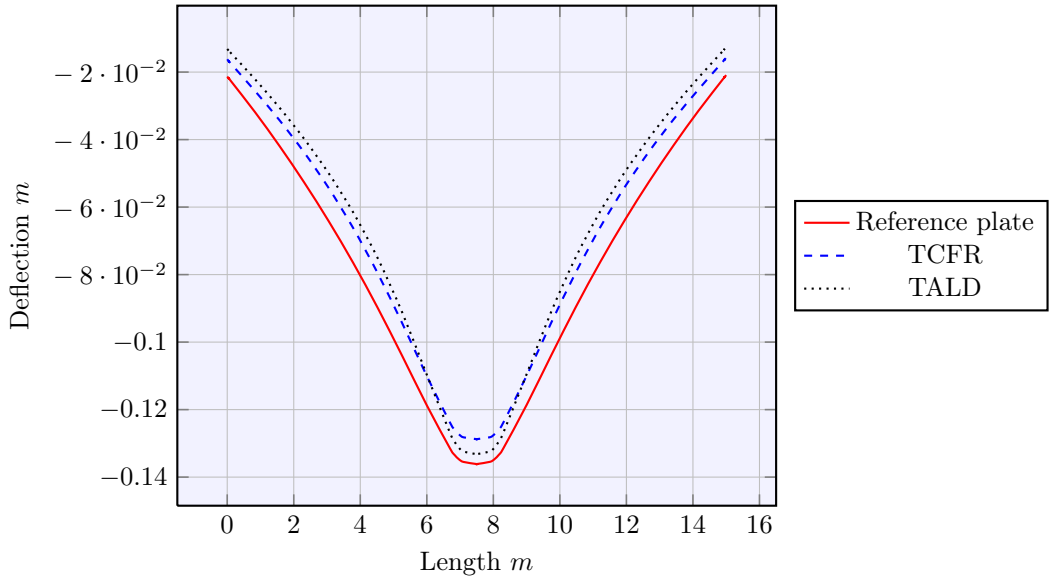

Figure 4.5.9: *Deflection U3 along x-direction for parameter set 5.*

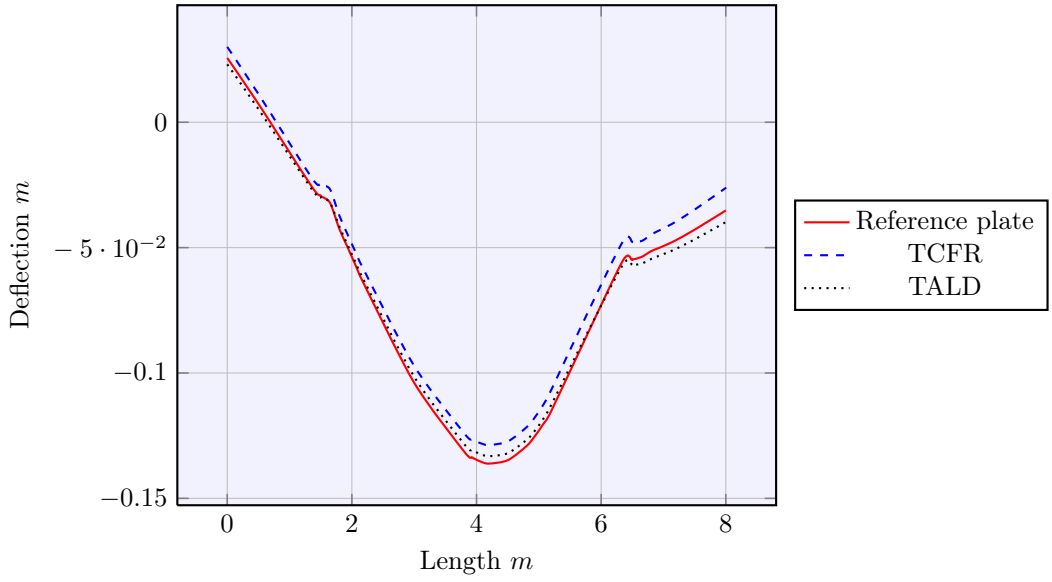

Figure 4.5.10: *Deflection U3 along y-direction for parameter set 5.*

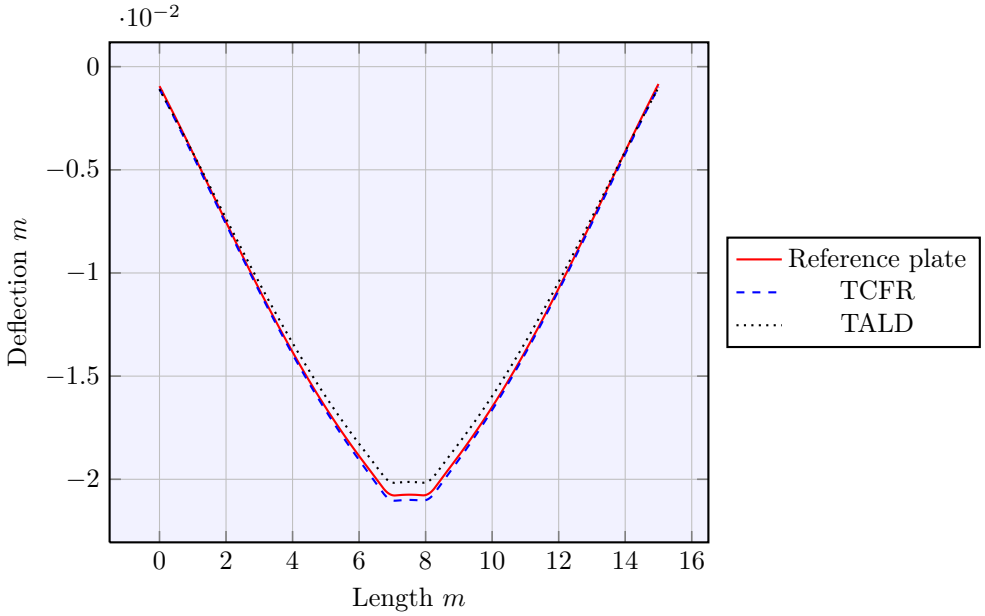

Figure 4.5.11: *Deflection U3 along x-direction for parameter set 6.*

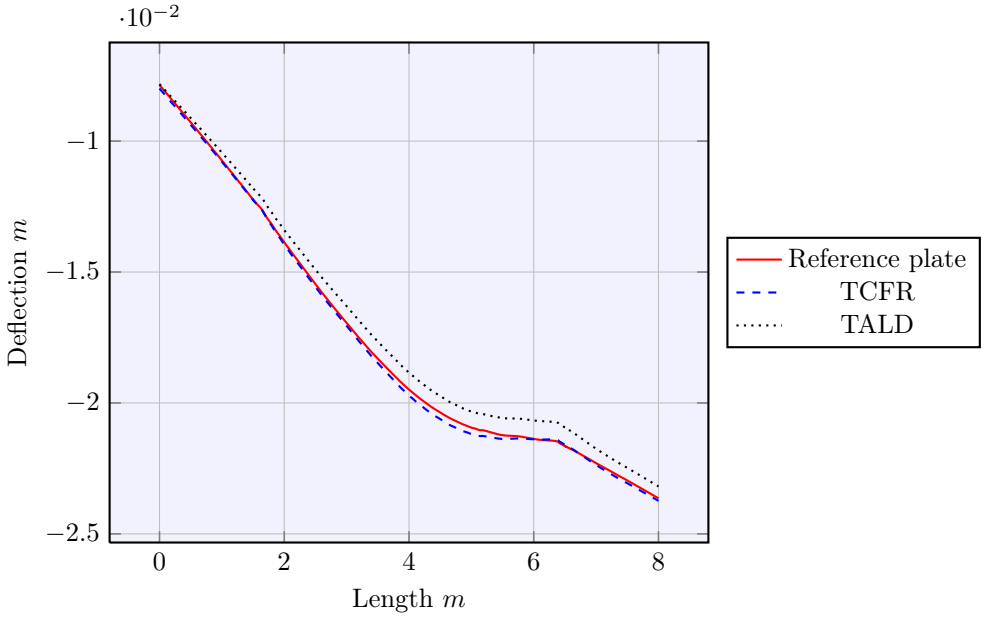

Figure 4.5.12: *Deflection U3 along y-direction for parameter set 6.*

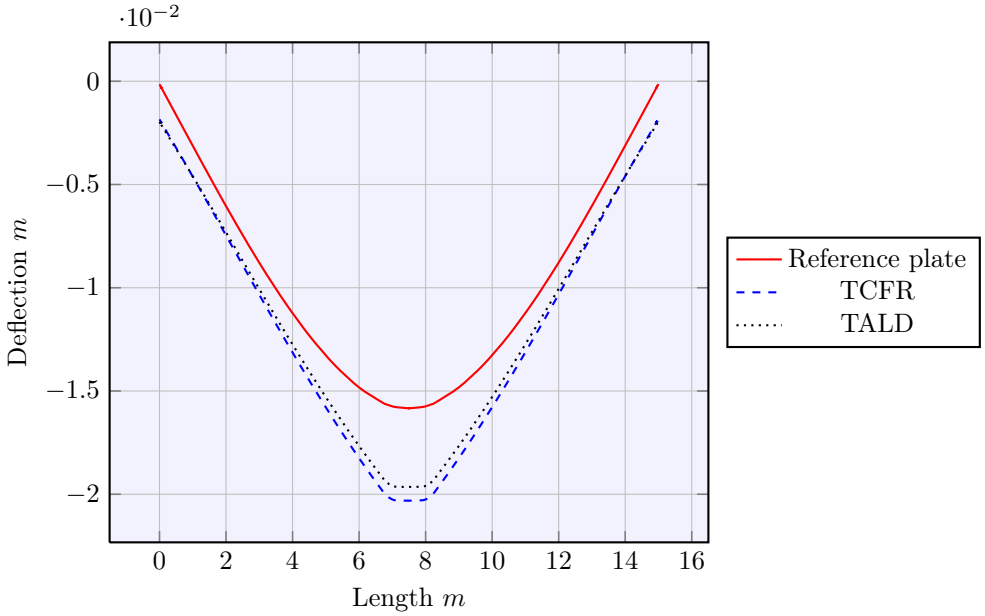

Figure 4.5.13: *Deflection U3 along x-direction for parameter set 7.*

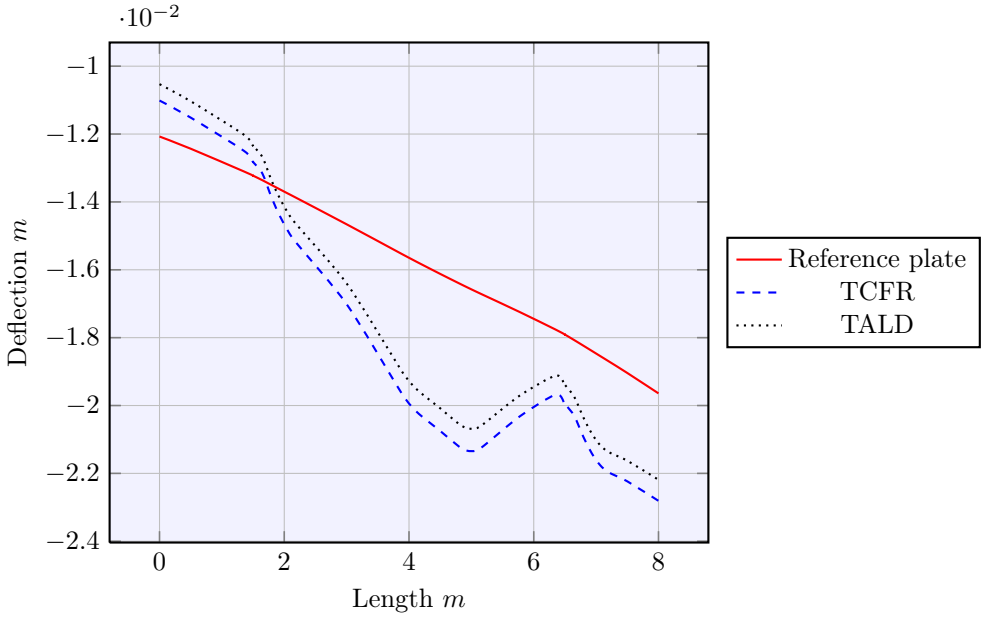

Figure 4.5.14: *Deflection U3 along y-direction for parameter set 7.*

4.6 Comment on the results

Better overall correlation is achieved according the previous results for the transformation based on constant flexural rigidity compared to the transformation based on axial loaded deformation. Close correlation is observed for TCFR in all sets except for set 7 where the core is much stiffer compared to the flanges, see table 4.4.20. This can be explained by a couple of different things; shear locking, round-off error in the stiffness matrix or maybe that the assumptions used when deriving the shear modulus do not hold true.

By adjusting the different material parameters for the equivalent plate calculated with TCFR, the problem area is identified. When increasing the transformed values of G_{13} and G_{23} the result is approaching the reference plate, see figure 4.6.1 and 4.6.2. By increasing G_{13} the global deflection of the total plate system is decreased. The deflection of the sandwich plate between the two main girders (local deflection) is instead affected by the parameter G_{23}. To obtain a result similar to the reference plate, both parameters have to be adjusted. This indicates that the equation for computing the equivalent shear modulus may not be valid when the difference in stiffness between the layers are too big.

The combined increase of both G_{13} and G_{23} plotted in figure 4.6.1 and 4.6.2 is calculated by taking the mean value of the three layers. The obtained result is almost identical to the reference plate.

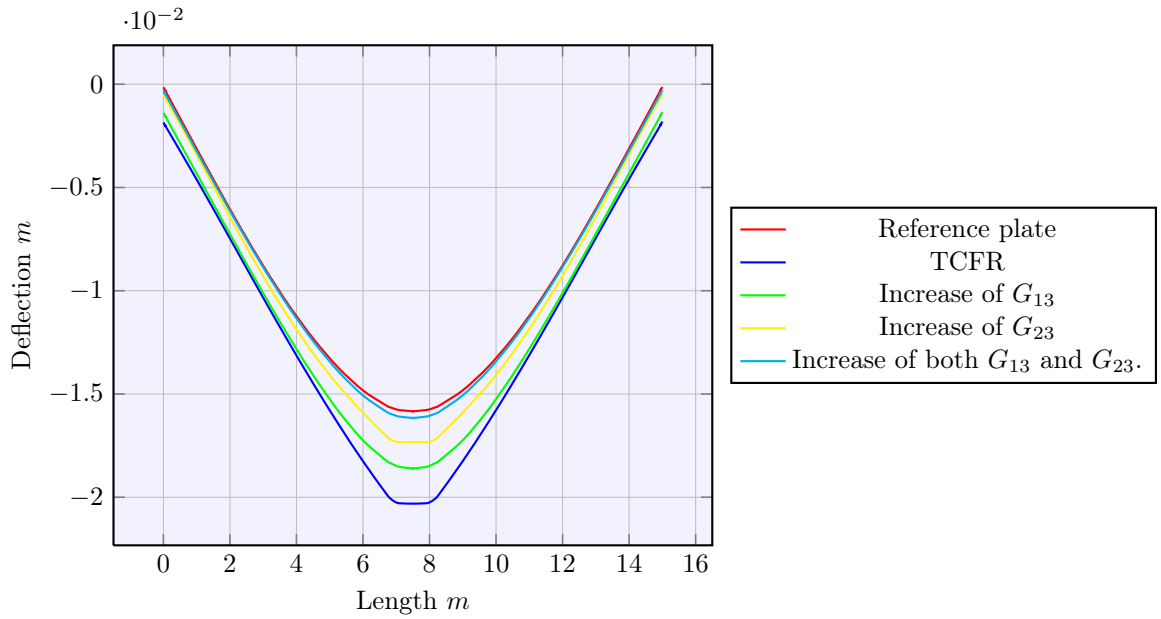

Figure 4.6.1: *Deflection U3 along x-direction for parameter set 7 when adjusting the values of the shear stiffness G_{13} and G_{23}.*

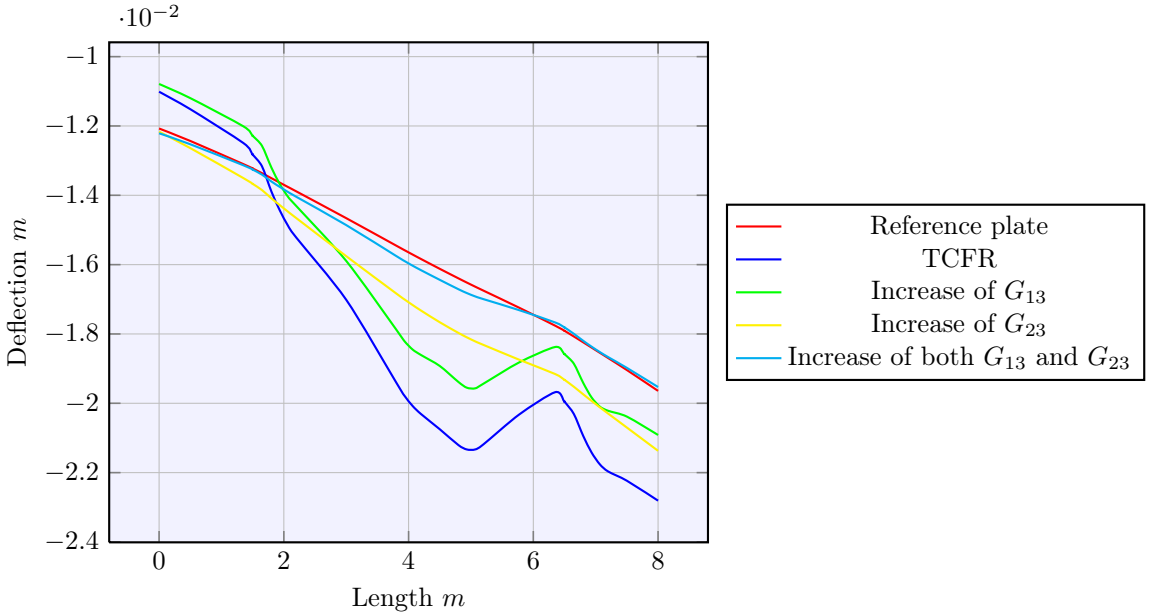

Figure 4.6.2: *Deflection in y-direction for parameter set 7 when adjusting the values of the shear stiffness G_{13} and G_{23}.*

4.6.1 Shear locking

Shear locking appears due to a geometric inconsistency in brick elements, which can propagate when the element is too large and is subjected to bending, Prathap (2001). The 8-node element cannot follow the curved shape forced by the bending and instead becomes more like a parallelogram which introduces shear stresses. This will increase the elements stiffness and corrupt the calculated result. A solution for this problem can be to increase the number of elements by using a finer mesh. When using 20-node second order quadratic elements instead of linear 8-node elements, shear locking is not a big problem. This 20-node element can more easily take the shape of a bent element due to its integration point in the middle between the corners of the rectangle. Though, this element has its own problem areas called hourglassing. This is when the element is too flexible and get distorted. However, this can be controlled by built in checks in the program. Due to the fairly fine mesh and the usage of 20-node elements, shear locking or hourglassing is probably not the problem behind the bad correlation for material set 7 in verification two. Another important factor to take into consideration is that an error like this one is tied to the mesh and the element type, which therefore should affect all results for the different parameter sets, at least to some extent. This is not the case which is another indication that shear locking or hourglassing is not the problem.

4.6.2 Round-off error

When there is a large difference in the material parameters, there is going to be a very large difference in magnitude for the different local stiffness matrices in the FE-calculation. When these matrices are assembled together, there is a risk of getting round-off errors in the global matrix. This may lead to singularity problems when trying to calculate the inverse of the global stiffness matrix. Abaqus has a build in system with warning messages for this kind of problem, and because no such message was received it is safe to assumed that this is not the problem which explains the bad correlation for parameter set 7.

4.6.3 Assumption error

Another explanation is that the assumptions used when deriving the equivalent shear modulus does not hold true for set 7. Since it was noted before that the reason for the bad correlation for set 7 could be explained by an underestimation of the shear moduli G_{13} and G_{23}, the assumption regarding the transformation of these parameters must be checked. When deriving the expression for G_{13} and G_{23}, it is assumed that the shear stress is equal in all layers. This may not be the case, and will be investigated and verified in section 4.6.4. If the

assumption does not hold true, it is possible to adjust the hypothesis and instead assume that, for example 80% of the shear is transfered down to the bottom plate.

4.6.4 Follow up checks of the assumption for shear stiffness G_{13} and G_{23}

The verification of the assumption regarding parameters G_{13} and G_{23} is done by dismounting the sandwich deck structure from the main girders and fixing the bottom side in all directions while keeping the top side free. A shear load is then applied at the top surface of the plate in order to investigate if the shear stress is transfered equally through all layers, i.e. if the shear stress is constant through the whole cross section. This procedure was done for the reference plate and the TCFR-plate. The stress S_{13} and the displacement u_1 were measured over the height of the cross section and plotted.

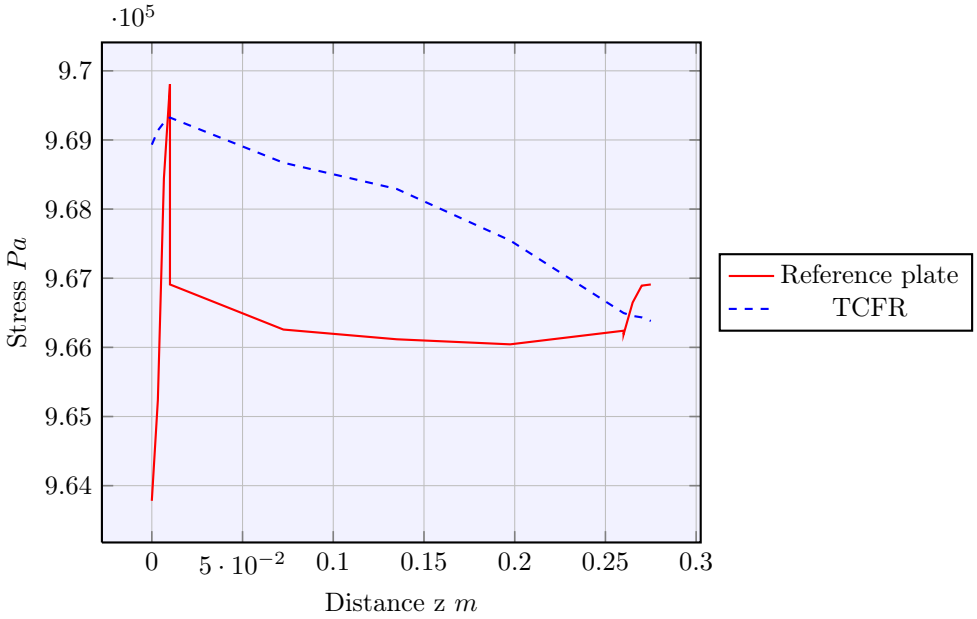

Figure 4.6.3: *Shear stress S13 along z-direction in the mid span for parameter set 7, where z is defined from the bottom up.*

As seen in figure 4.6.3, the stress varies much less than 1 percent over the cross section, both for the reference plate and the equivalent TCFR-plate. Due to this result it's obvious that the assumption of the derivation of both G_13 and G_{23} holds true.

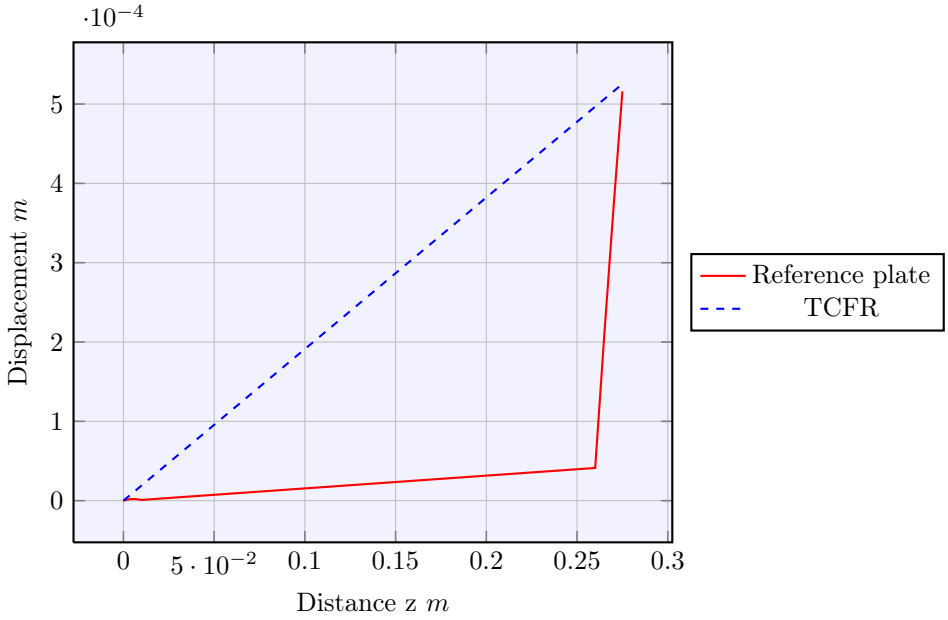

Figure 4.6.4: *Displacement $U1$ along z-direction in the mid span for parameter set 7.*

The displacement turns out to be almost the same at the upper side of the plate for both reference and TCFR-plate, which also confirms that the transformation of $G13$ and $G23$ holds. It is easily seen that the major part of the displacement takes place in the most upper layer of the reference plate and that the displacement is linear for the transformed TCFR-plate.

4.6.5 Estimation error of the plate's bending stiffness

The assumption, that the plate's individual bending stiffnesses are equal to the equivalent's one, is true as long as the strain distribution, before and after transformation, is linear. If the resulting shear stiffness, G_{13} or G_{23}, from the transformation is too low, the elastic bending resistance cannot be fully utilized. The resulting strain over the cross section will no longer be linear, see figure 4.6.5. Since the strain and stress are directly related to each other, the bending capacity is therefore reduced. This in turn leads to a larger deflection of the plate than what it actually should be.

There could also exist cases where the reference plate has some layer that has too low shear stiffness in comparison with the corresponding elastic modulus. This would give an overestimation of the summation of the individual bending stiffnesses, i.e. the transformed plate would show a lesser deflection than the reference plate.

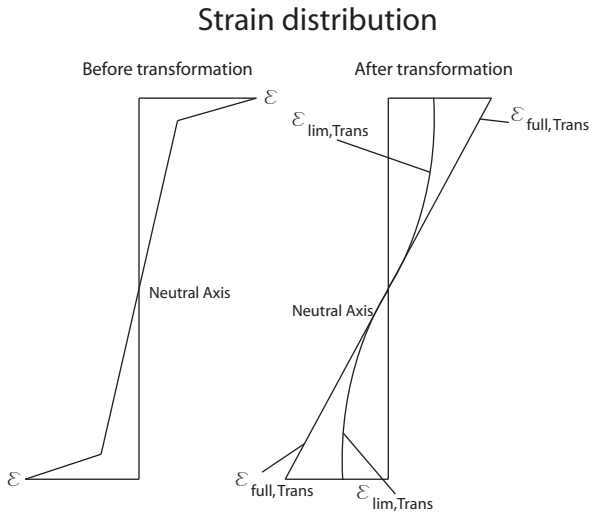

Figure 4.6.5: *Possible cases of strain distribution before/after transformation with TCFR.* $\epsilon_{full,Trans}$ *represents fully utilized strain distribution and* $\epsilon_{lim,Trans}$ *represents limited strain distribution.*

4.7 Final remarks and conclusions after verification 1 and 2

There is a difference in accuracy between the two methods, where TCFR generally correlates significantly better in both verification 1 and 2. The obtained difference between the equivalent plates and the reference plate is usually on the same side for both transformation methods, either an underestimation or overestimation. This means that the possible third method, where the two methods would be combined, cannot be used to improve the margin of error for the transformation.

Linear strain depends on the relation between the elastic and shear modulus in the concerned direction. This relation is not conserved during transformation from three layers to one. This can be explained by the different methods of transforming the elastic modulus (E_{11} and E_{22}) and the shear modulus (G_{13} and G_{23}). After further investigation, it is found that the strain for the transformed plate of material parameter set 7 is non-linear. This is therefore believed to be the major reason why the correlation of deflection, between the equivalent and the reference plate, is so low.

The transformation based on constant flexural rigidity is chosen as the transformation algorithm on the basis that this method shows better accuracy and a more stable result range.

5 Parametric Study

A parametric study of the equivalent plate resting on two steel girders is performed to establish important relations between different stiffnesses and also to investigate how these affects the general behavior of the plate system. This is done for a specific case where the bridge girders are working compositely with the sandwich deck plate. The three important aspects considered in the parametric study are:

- A linear strain (ϵ_{11}) distribution over the height of the cross section including the steel beams in the xz-plane. This will lead to a good composite action between the steel beams and the sandwich plate, where the plate section is contributing as much as possible to the global stiffness.
- A linear strain (ϵ_{22}) distribution over the height of the cross section in the yz-plane.
- Minimize the strain deviation of (ϵ_{11}) over the width of the cross section.

Optimizing these parameters will result in better usage of the material due to the linear strain over the cross sections.

5.1 Linear strain ϵ_{11} over the height of the main girder and sandwich plate

To be able to obtain a linear strain ϵ_{11} over the total cross section, the force has to be transported by shear from the steel beams to the plate and up to the top side. This shear is named G_{13} and is transformed by a parallel coupling between the layers into the equivalent plate. This means that all layers has to have a high enough shear stiffness to be able to get a good linear global relationship. If one layer is very weak, the strain will not be able to be transfered.

The magnitude of the load does not affect the shape of the strain, only the scale of the values in the graph. When a linear relationship is reached, there is no point in increasing the shear stiffness even more. If a higher stiffness is needed, E_{11} has to be increased. This will change the shape of the strain relationship to be non-linear. If the affected shear stiffness is increased to fit the new E_{11}, the strain will once more be linear which will lead to an increase of the section's bending stiffness. The other parameters besides E_{11} and G_{13} have no effect.

The strain is measured in the middle of the span according to figure 5.1.1. By assuming that the relationship seen in graph 5.1.2 is linear and using this as a reference it's possible to obtain the relation between E_{11} and G_{13}. This is done by assuming a stiffness E_{11} and adjusting the shear stiffness G_{13} until a similar linear strain distribution as for the reference strain is obtained. This is done for eight different assumed elastic moduli.

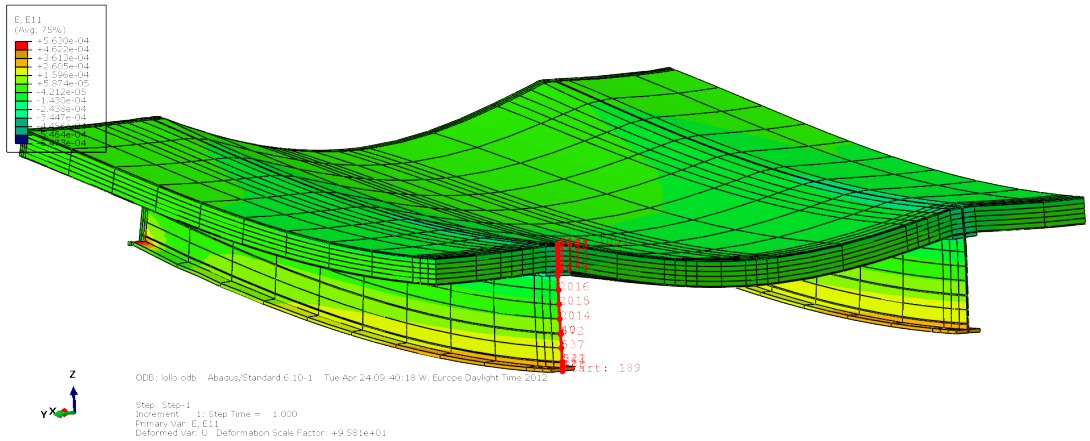

Figure 5.1.1: *The path created for measuring* ϵ_{11}.

By applying a curve fitting function to the measured values, as seen in figure 5.1.3, the following expression is obtained:

$$G_{13}(E_{11}) = 10^{4.4626} \cdot E_{11}^{\frac{1}{2.5472}} \text{ [Pa]} \tag{5.1.1}$$

Using this relation between G_{13} and E_{11} result in a linear strain relation through the cross section which leads to a more optimized material usage.

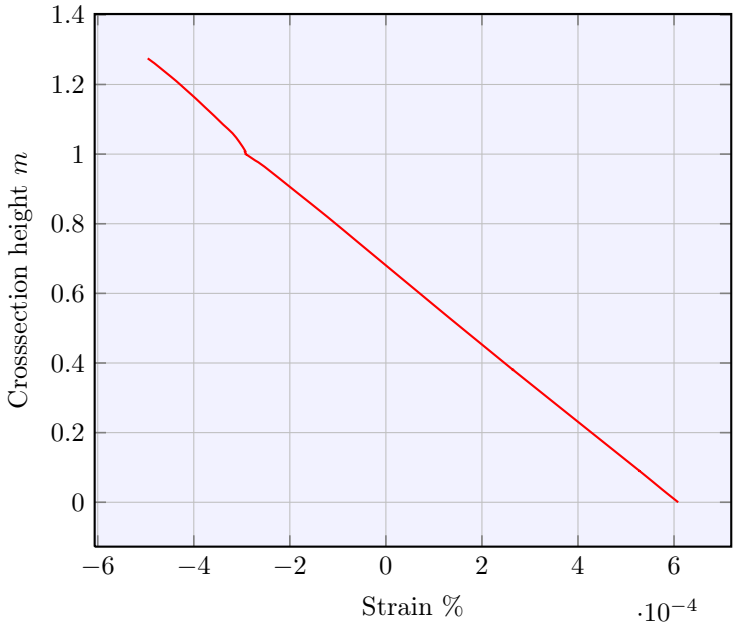

Figure 5.1.2: *Strain ϵ_{11} over the total crosssection, where z spans from the lower to the upper side.*

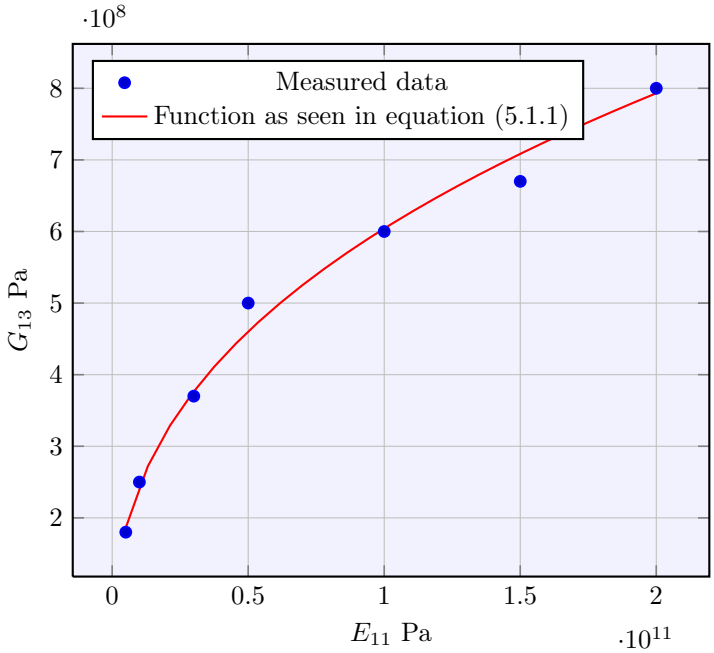

Figure 5.1.3: *Relation between E_{11} and G_{13}.*

5.2 Linear strain ϵ_{22} over the height of the sandwich plate

The same basic principle also applies in y-direction. This case present almost pure bending of the element without too much involvement of other parts of the bridge. There is a certain moment resistance from the longitudinal main steel girders that acts as supports in this direction. This is due to the flanges and their width in y-direction. However, this contribution will be small and consequently ignored.

The parameters that affect the strain in this direction are E_{22} and G_{23} and the measurements are made according to figure 5.2.1 in the middle span. This measurement position is chosen because it is the section with the maximum moment.

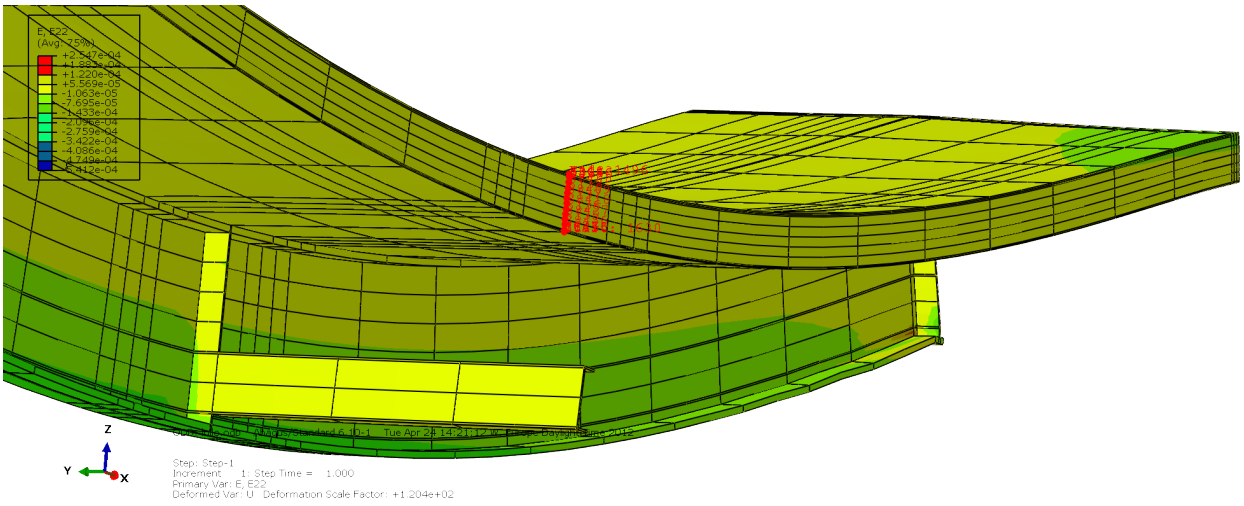

Figure 5.2.1: *Location of the path used for the investigation of* ϵ_{22}.

By adjusting the shear stiffness, a linear strain over the cross section is obtained, as seen in figure 5.2.2. Here the shear stiffness is changed from 0.05 GPa to 0.5 GPa and the strain is plotted. As seen in the figure, the strain is approaching a linear relationship. An elastic modulus E_{22} is assumed and the shear stiffness G_{23} is adjusted until a linear relationship is obtained. This is done for nine different elastic moduli. The obtained relation is plotted in figure 5.2.3. A curve fitting is once again applied which results in the relation expressed in equation (5.2.1). It is noteworthy to mention that the units in this equation should be always expressed in Pa, otherwise the results might be misleading.

$$G_{23}(E_{22}) = 1.3164 \cdot 10^8 e^{5.7292 \cdot 10^{-11} E_{22}} \text{ [Pa]} \tag{5.2.1}$$

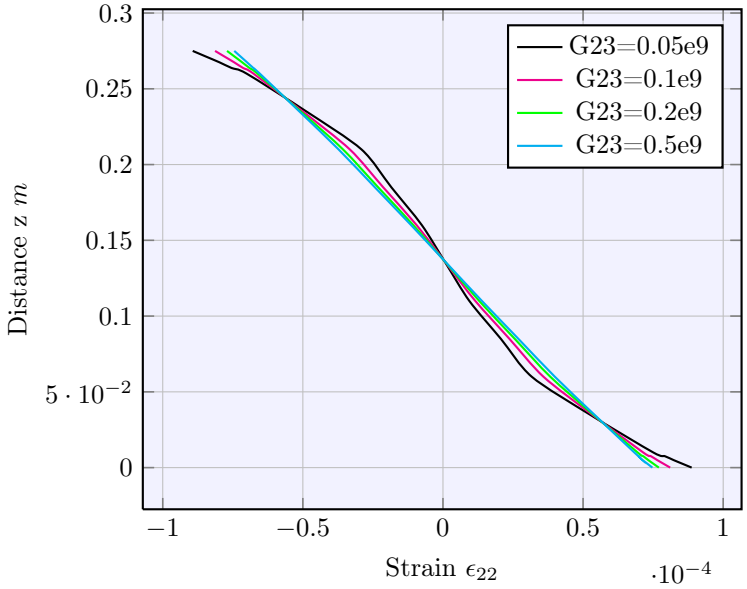

Figure 5.2.2: *Strain ϵ_{22} along z-direction in the mid span, where z spans from the lower to the upper side of the plate.*

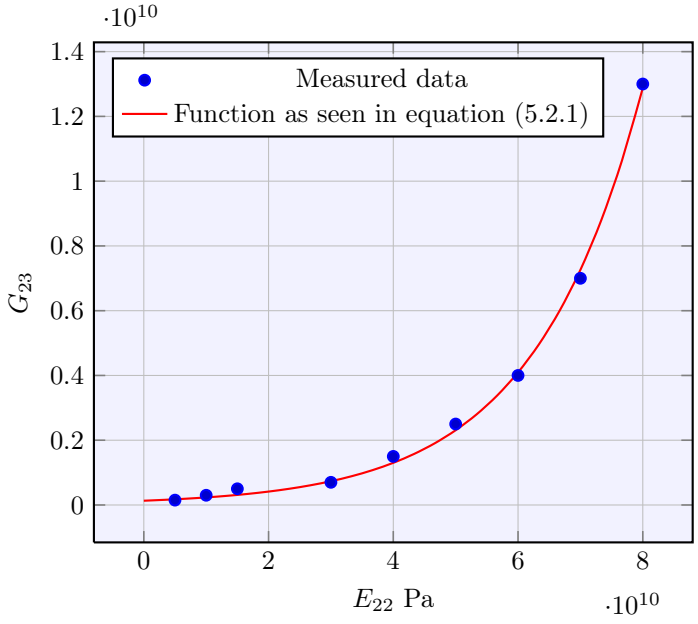

Figure 5.2.3: *Relation between E_{22} and G_{23}.*

5.3 Optimization of the effective width of the cross section

In order to utilize the material as much as possible, it is of big importance to have a wide contributing "flange" of the bridge frame system, in other words, have a large part of the sandwich plate contributing to the bending stiffness on a global scale. However, concrete decks resting on girders for example, often experiences shear lag. This is taken into account in calculations by reducing the width to an effective width. It would be of value to be able to increase the effective width to increase the material efficiency.

By examining the strain of ϵ_{11}, along the width for the sandwich plate, one could examine and obtain the contribution from it to the global system. The goal is to have a strain distribution that varies as little

as possible, i.e. that the forces are distributed effectively over the whole width of the sandwich plate. The location of the measurements are illustrated in figure 5.3.1. Do note that the values of E_{11} and G_{13} are set so they give linear strain over the height of the cross section, according to equation 5.1.1. This means that it does not matter at what height the strain is measured for the effective width.

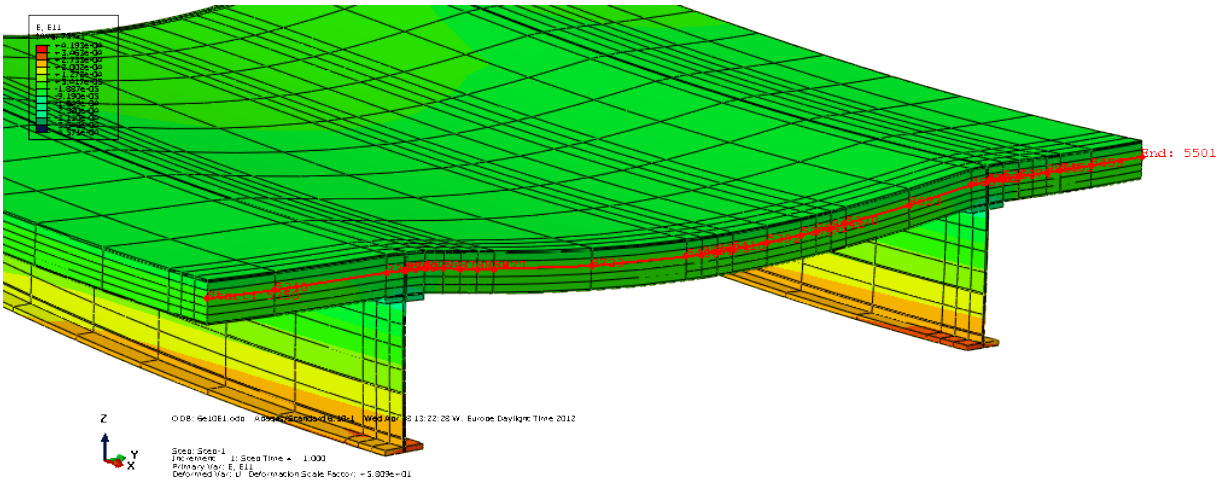

Figure 5.3.1: *Location of the path used for the investigation of* ϵ_{11}.

By changing one material parameter at a time, it is possible to determine which of them that affects the desired strain, ϵ_{11}. Doing so made it obvious that G_{12} and E_{11} is the only parameters that affects ϵ_{11}. To further investigate the influence of these parameters, they were adjusted and the strain was plotted, see figure 5.3.2 and 5.3.3.

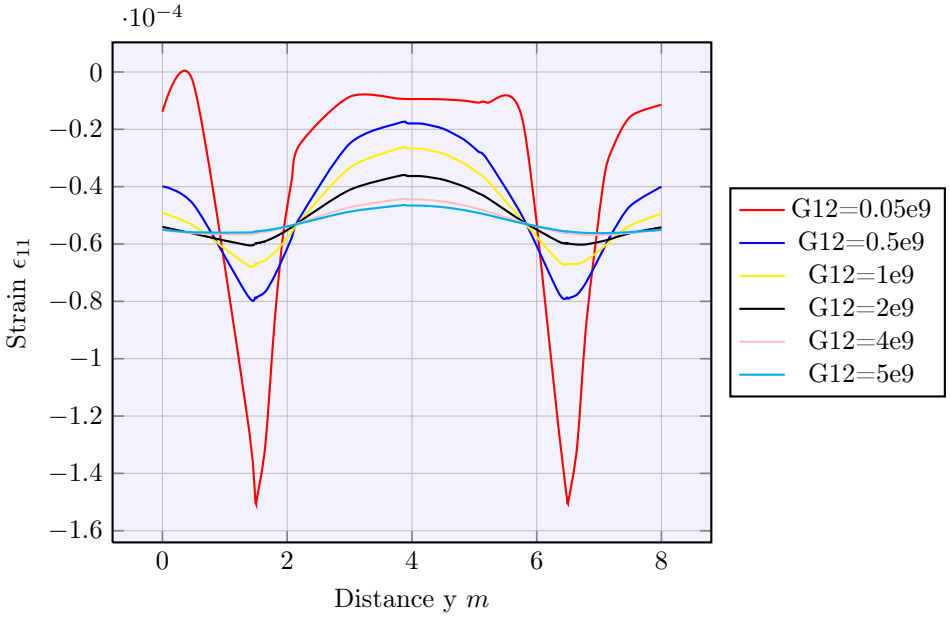

Figure 5.3.2: *Strain* ϵ_{11} *along y-direction in the mid span.*

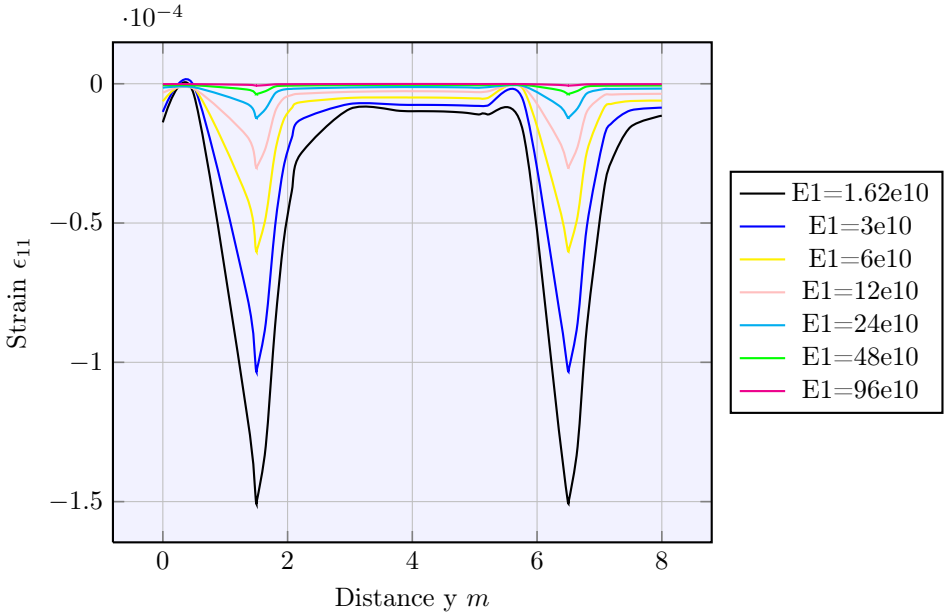

Figure 5.3.3: *Strain ϵ_{11} along y-direction in the mid span.*

From figure 5.3.2 it is seen that the strain distribution tends to be more uniform with increasing stiffness of G_{12}, i.e. activates more of the flange width.

As seen in figure 5.3.3 the strain decreases with increasing E_{11}, which is expected. The curve is not changing its behavior and is just scaled, i.e. the relative deviation from the mean value is the same for all different E_{11} tested. Judging from this, the only parameter that affect the effective width is the shear modulus G_{12}. By adjusting the parameter and measuring the difference between top and bottom value for the strain, an equation expressing the percentage of difference is obtained where the shear is inserted in $[Pa]$, see equation (5.3.1):

$$Relative\ strain(G_{12}) = 10^{7.4638} \cdot G_{12}^{-\frac{1}{1.5175}}\ [\%] \tag{5.3.1}$$

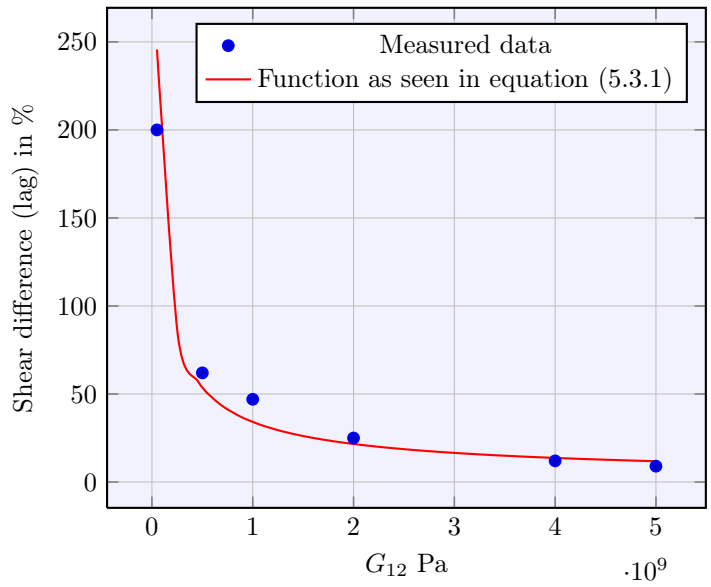

Figure 5.3.4: *Shows how the shear difference varies with varying shear stiffness G_{12}.*

6 Optimization of sandwich deck structures

The optimization is performed in accordance with the conclusions made in chapter 5. Different orthotropic plate systems are modeled with Abaqus CAE and loaded in different ways to obtain the equivalent properties. The deflection of a plate is a combination of shear and bending deflection. The analytical model for a plate supported on four supports is derived in previous section 2.3. To be able to solve the equation for the elastic modulus in the different directions, the plate has to be supported on only two supports. This will reduce the number of unknown values in the analytical expression for the deflection.

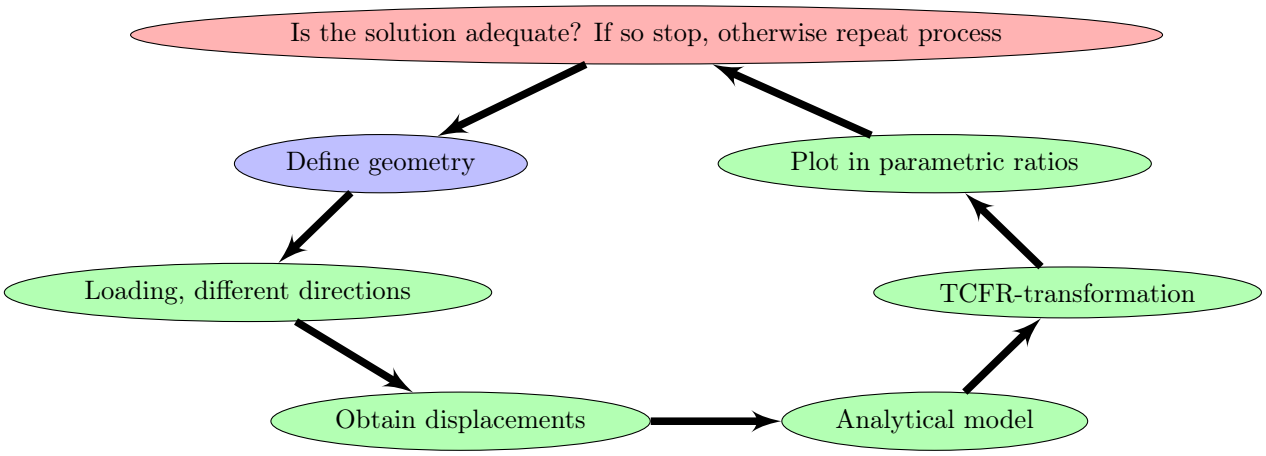

Figure 6.0.1: *Optimization iteration for a geometry with the parametric ratios.*

The analytical model for a plate supported on two supports is obtained from *DIAB Sandwich handbook* (2003) where the deflection is a function of the shear modulus and the elastic modulus in the direction where bending takes place. The plate is modeled in a similar fashion as a beam subjected to a line load. The width of the plate is taken into account by replacing the elastic modulus E_{ii} with $\frac{E_{ii}}{1-\nu_i^2}$, where i is either x or y depending on the direction of the bending. The expression for the deflection reads:

$$w = \frac{5ql^4}{384D} + \frac{ql^2}{8V} \tag{6.0.1}$$

With D and V:

$$D = \frac{E_1}{1-v_1^2}\left(\frac{bt_1^3}{12} + bt_1d_1^2\right) + \frac{E_2}{1-v_2^2}\left(\frac{bt_2^3}{12} + bt_2d_2^2\right) + \frac{E_3}{1-v_3^2}\left(\frac{bt_3^3}{12} + bt_3d_3^2\right) \tag{6.0.2a}$$

$$V = A \cdot G \tag{6.0.2b}$$

Where 1-3 denotes the different layers of the sandwich structure (1 - upper flange, 2 - core, 3 - bottom flange). The expression of the elastic modulus for the core is found by inserting equations (6.0.2a-b) into equation (6.0.1):

$$E_2 = -\frac{\left(\frac{384\,E_1\left({d_1}^2\,t_1+\frac{{t_1}^3}{12}\right)}{{v_1}^2-1} + \frac{384\,E_3\left({d_3}^2\,t_3+\frac{{t_3}^3}{12}\right)}{{v_3}^2-1}\right)\left({v_2}^2-1\right)}{384\left({d_2}^2\,t_2+\frac{{t_2}^3}{12}\right)} - \frac{5\,l^4\,q\,\left({v_2}^2-1\right)}{384\left(w-\frac{l^2\,q}{8\,A\,G}\right)\left(b\,{d_2}^2\,t_2+\frac{b\,{t_2}^3}{12}\right)} \tag{6.0.3}$$

The full orthotropic material properties for the plate system is obtained by first loading the plate in shear and calculating the shear moduli in the different directions with equation (6.0.4).

$$G = \frac{Fl}{A\Delta x} \tag{6.0.4}$$

The plate system is then subjected to a uniformly distributed load supported first in x-direction, then in y-direction on two supports to obtain the deflection. The obtained values are then inserted into equation (6.0.3) to solve the bending elastic moduli for the core in the different directions. This constitutes the first part of the transformation, where a sandwich structure is transformed into a three layered homogeneous plate. Equivalent properties for the one layered plate is calculated with the algorithm by means of MATLAB where the source code can be found in appendix 10.2. The program is constructed on the basis presented in chapter 3.1. The obtained equivalent stiffnesses are then plotted into the graphs derived in chapter 5. This will give an indication of which stiffnesses are too high or too low and will guide the optimization and be a basis for the recalibration of stiffnesses and geometric changes.

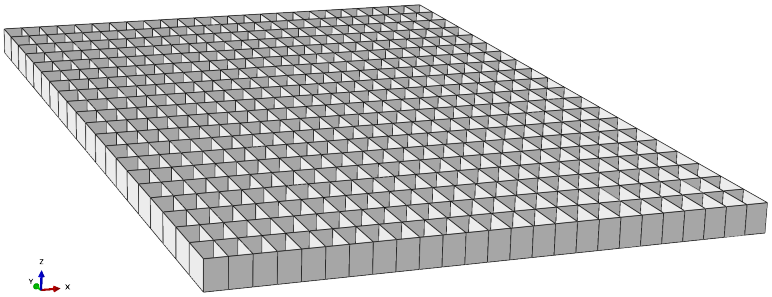

Figure 6.0.2: *Layout of the grids for the Rektoplate.*

This procedure is performed for three different specimens for evaluation and identification of general geometric properties that affect the stiffness ratios. It is also done in order to illustrate the work flow of an optimization by means of the ratios obtained from the parametric study. The modeled structures are all made of steel, which is an isotropic material. However, it is possible to perform the optimization on plates with orthotropic material properties as well.

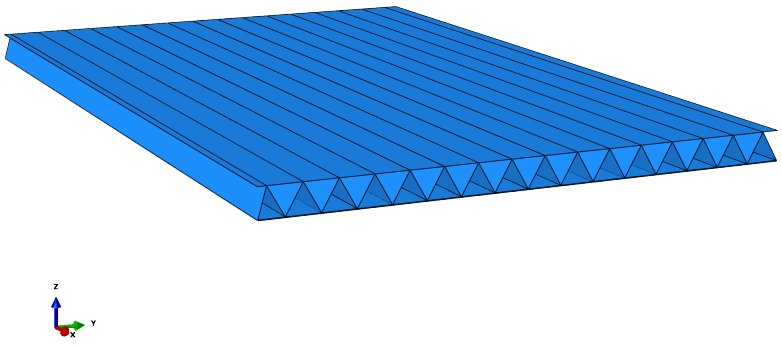

Figure 6.0.3: *Layout of the Truss* 60° .

The thickness of the flanges for Truss 60° is 7 mm and the core 4.9 mm and all is made of steel.

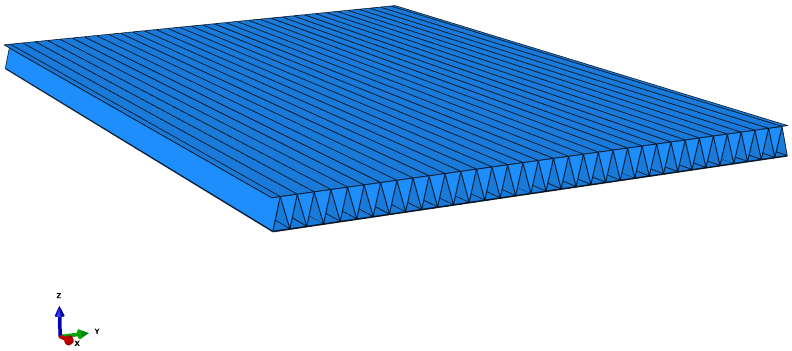

Figure 6.0.4: *Layout of the Truss* 75° .

The thickness of the flanges for Truss 75° is 7 mm and the core 2.5 mm and all is made of steel.

Two of the structures are truss plate systems, see figure 6.0.3 and 6.0.4, with varying angle of the core studs and the third is a cell-based plate system, similar to honeycomb but instead with rectangular cells (Rektoplate), see figure 6.0.2. The steel's Young's modulus is set to $E = 210$ GPa and $\nu = 0.3$. The result is found in table 6.0.1 and 6.0.2. Note that all directions and properties are expressed in global coordinates if nothing else is stated.

Table 6.0.1: Stiffness of the different cores $[GPa]$.

System	E_{11}	E_{22}	E_{33}	G_{12}	G_{13}	G_{23}
Truss 60°	0.233	5.54	6	2.425	1.45	2.05
Truss 75°	0.472	5.50	7	2.48	0.524	2.62
Rektoplate	0.166	4.35	6.875	2.59	0.95	1.96

The values of table 6.0.1 is computed by utilizing expression 6.0.3 and 6.0.4.

Table 6.0.2: Stiffness of the total equivalent plate transformed using TCFR-method $[GPa]$.

System	E_{11}	E_{22}	E_{33}	G_{12}	G_{13}	G_{23}
Truss 60°	30.73	35.31	6.217	6.217	1.522	2.152
Truss 75°	30.93	35.27	7.34	6.269	0.550	2.749
Rektoplate	30.7	34.3	7.21	6.37	1.00	2.06

Since the flanges stiffnesses are known and the core's stiffness is found in table 6.0.1, it is now possible to use the TCFR method to transform these into a single layered equivalent one. To verify the results a comparison of the deflection between the equivalent plate and the original plate is performed. The results are found in tables 6.0.3 - 6.0.5. The deflections are compared in Abaqus CAE. As seen in the graph, the correlation is very good with less than 1% difference for most cases.

Table 6.0.3: Difference in deflection between equivalent plate (EQ-P) and original plate truss 60° (OR-PT60).

Supports	Load $[\frac{N}{m^2}]$	Deflection OR-PT60 $[m]$	EQ-P $[m]$	Diff [%]
2(x-direction)	5000	0.00363285	0.00364927	0.45
2(x-direction)	7000	0.00509213	0.00511084	0.37
2(x-direction)	15000	0.0108967	0.0109518	0.50
4	15000	0.00121966	0.00122544	0.47

Table 6.0.4: Difference in deflection between equivalent plate (EQ-P) and original plate truss 75° (OR-PT75).

Supports	Load $[\frac{N}{m^2}]$	Deflection OR-PT75 $[m]$	EQ-P $[m]$	Diff [%]
2(x-direction)	5000	0.00362169	0.00364001	0.50
2(x-direction)	7000	0.00507158	0.00509602	0.48
2(x-direction)	15000	0.010901	0.010920	0.17
4	15000	0.00134855	0.00137322	1.8

Table 6.0.5: Difference in deflection between equivalent plate (EQ-P) and original plate Rektangular plate (Rektoplate).

Supports	Load $[\frac{N}{m^2}]$	Deflection Rektoplate $[m]$	EQ-P $[m]$	Diff [%]
2(x-direction)	5000	0.00374753	0.0037602	0.3
4	15000	0.0012756	0.00127315	0.2

Furthermore, the stiffness of these decks are compared with the optimization graphs obtained in section 5. As seen in figure 6.0.5, there is no need to increase the shear stiffness G_{12}. There is even a possibility of decreasing the amount of material to decrease the shear strength in this direction in favor of a higher bending stiffness in E_{11} or E_{22}. Since G_{12} is added up as a serial coupling of the individual shear stiffness of the members, the total G_{12} tends to be of adequate size.

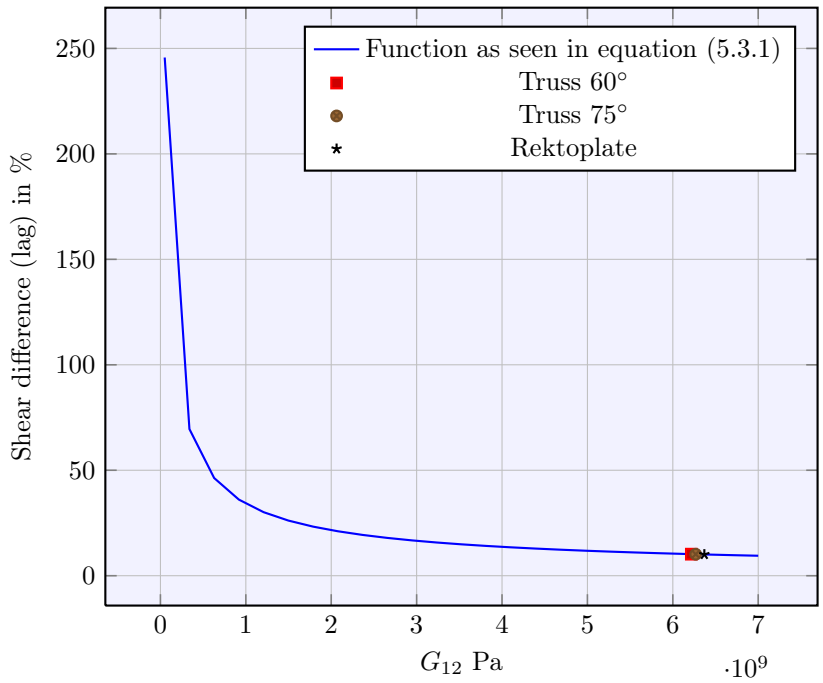

Figure 6.0.5: *Plotted values of the different plate systems in relation to the optimized relation of* G_{12}.

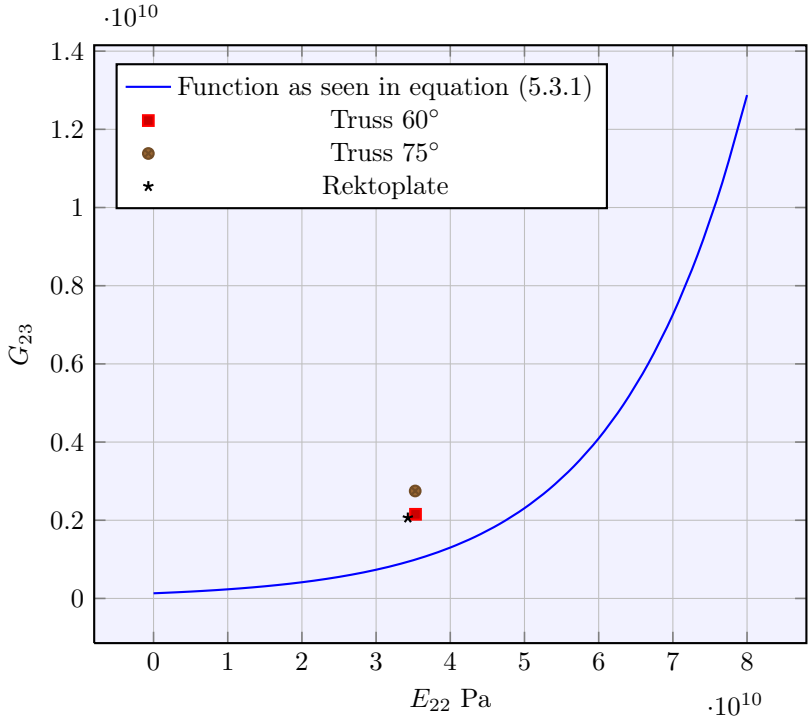

Figure 6.0.6: *Relation between E_{22} and G_{23}.*

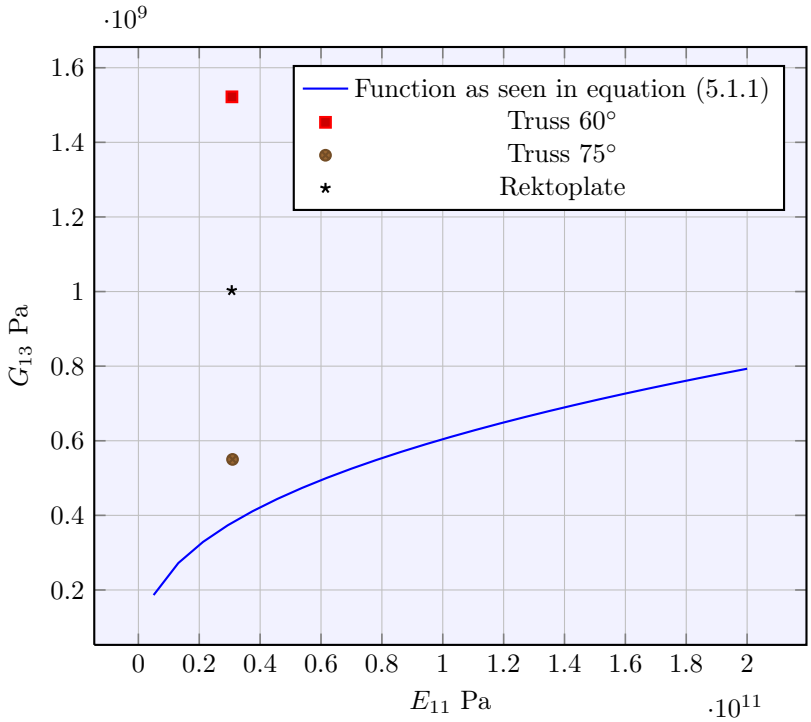

Figure 6.0.7: *Relation between E_{11} and G_{13}.*

As seen in the graphs 6.0.6 and 6.0.7, the change in geometry of the core gives different shear moduli, which makes the plotted values to move almost on a vertical line. Since no material is exchanged between the flanges and the core, the bending stiffness of the plates will be constant as long as the shear moduli fulfills linear strain distribution over the cross section. The change of geometry from 60° to 75° inclination of the core studs for the two truss examples, lowered G_{13} on a straight vertical line and did the opposite for G_{23}. For these examples with excessive amount of G_{13} and G_{23}, it is possible to transfer more material to the flanges in order to increase bending stiffness. This would lead to lower shear modulus and a higher elastic modulus, see figure 6.0.8.

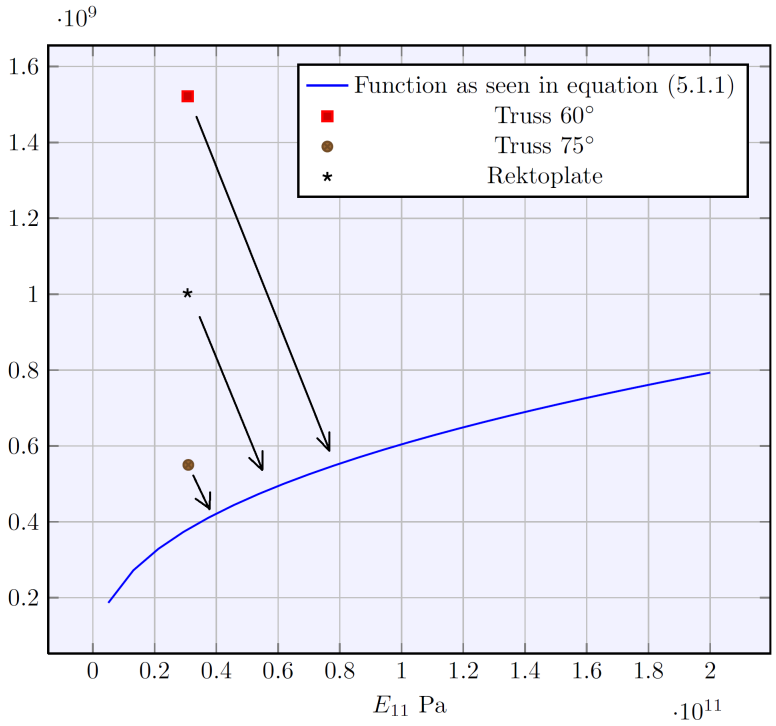

Figure 6.0.8: *Assumed direction when material is transfered from the core to the flanges.*

The inclination of the arrows in 6.0.8 shows the general direction of the stiffness change if material would be transfered from the core to the flanges. If no interchange of material is taken place, it is probable to end up with one of the shear modulus optimized and the other one too large/insufficient. Note that this only applies to cores that are linear symmetric around the neutral axis, i.e. same material distribution of a distance from the neutral axis, such as OR-PT60-75 and Rektoplate.

6.1 Optimized relation between E_{11} and E_{22}

When dealing with an orthotropic material or structure it is possible to change the stiffness in different directions by for example, changing the fiber direction in different sections of the sandwich plate if made of FRP or similar. It is also possible to add ribs or other stiffness altering features to change the global stiffness of the plate. When the sandwich plate system is placed on two main girders, the two main direction of stiffness E_{11} and E_{22} affect the deflection in different ways. The stiffness in the main direction (E_{11}), parallel to the steel beams, affects the longitudinal deflection because of the interaction between the main girders and the sandwich plate where the plate works as an upper flange to the global beam system. The transverse deflection between the two main girders is affected by the stiffness in the other direction (E_{22}) where the beam is subjected to almost pure bending.

A parametric study is performed to find a relation between E_{11} and E_{22} that minimize the deflection. This is done for a evenly distributed load where the magnitude only scales the deflection and thus have no influence on the ratios between the two stiffnesses. E_{11} was fixed and E_{22} were varied in 9 interval between 4 and 50 GPa. The affected shear moduli in the different directions were calculated and set to obtain full linear strain according to the equations derived from the parametric study in chapter 5. Then E_{11} was raised one step and all E_{22} run through again. For every material set the largest deflection was measured and plotted together with E_{11} and E_{22} which formed a surface plot as seen in figure 6.0.8. In total 81 combinations were measured and plotted. This few measured values results in a rough plot appearance. Therefore, the function Gridfit in MATLAB was used in order to smoothen up the surface area. Gridfit is an approximant which builds a surface on top of the input data. This means that noise and other distortions does not get removed due to numerical interpolation, *Understandning Gridfit* (2006).

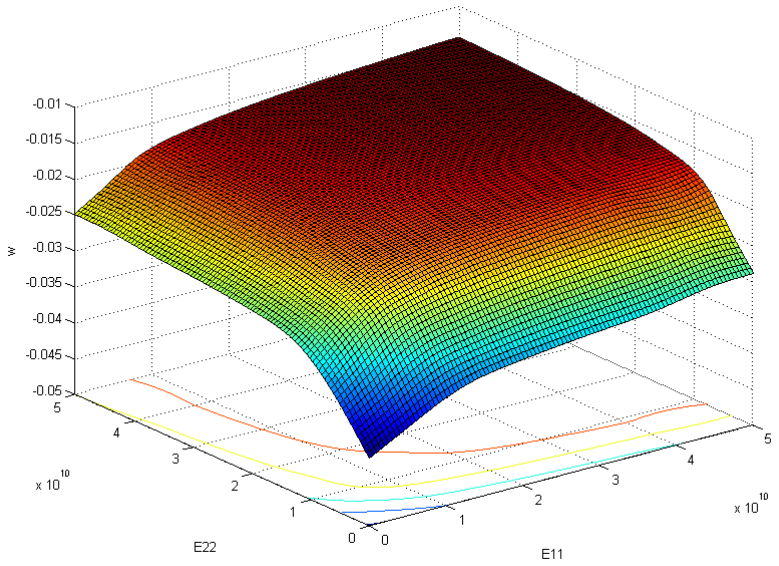

Figure 6.1.1: *Surface plot of E_{11}, E_{22} and displacement w.*

To be able to optimize a structure it is necessary to establish the current stiffness ratio in order to know how to alter the parameters, as seen in 6.1.1. For example if E_{11}=3e10 and E_{22}=0.5e10, it is much more viable to increase E_{22} instead of E_{11} to decrease the deflection, and vice versa for a case with opposite stiffness division.

To illustrate this further, a vector field is created from the surface plot, see figure 6.1.2. The behavior of the plate is improved by recalibration of the stiffnesses in the direction of the vectors. This will improve the overall deflection in an optimized way. It is also possible to establish a start ratio between the elastic modulus by considering the maximum deflection allowed and plotting the two dimensional relation of E_{11} and E_{22} for this specific case. The ratio can be chosen by comparing the absolute value of the total stiffness in both directions or in a similar fashion.

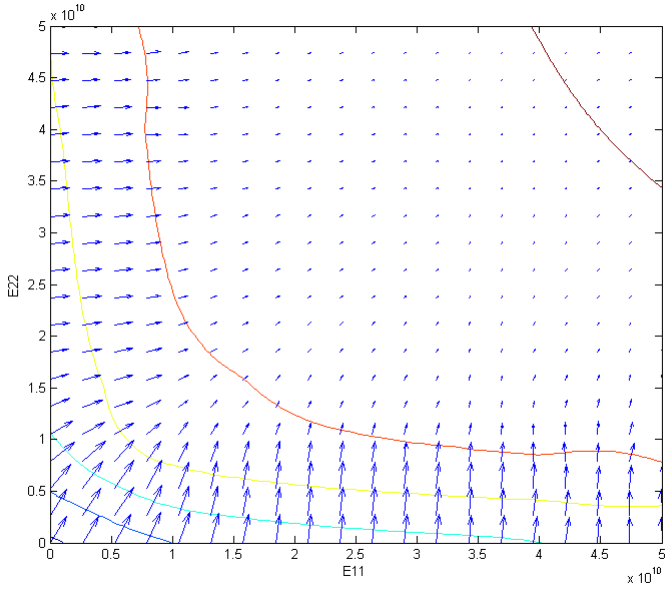

Figure 6.1.2: *Gradient vector field for the surface from figure 6.1.1.*

6.2 Optimization of Asset deck

To further illustrate the optimization method presented in the beginning of chapter 6, an existing commercial product Asset is to be modeled and evaluated. The method used is very similar to the one presented in figure 6.0.1, but with the starting geometry of the Asset bridge deck instead of a geometry defined from scratch. The objective is to optimize the structure with regard to global deflection and material efficiency. This is done with regard to the relations obtained from the parametric study found in chapter 5.

The Asset deck is a commercially available FRP bridge deck, produced by Fiberline in Middelfart, Denmark, *Fiberline webpage* (2012). The deck is based on truss action and consists of diagonal plates between two face sheets. The sandwich plate is most suited to carry the load in one main direction. Therefore the deck is to be placed with the pultruded direction transverse to the main girders of the bridge. Full interaction between the sandwich plates and main girders are assumed in all directions. The specific stiffness properties can be found in table 6.2.1, which is a result of how the fibers are situated, i.e. the distribution of fibers in different directions.

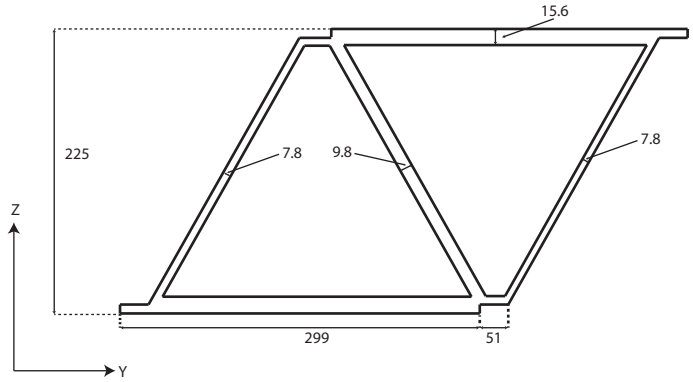

Figure 6.2.1: *Dimensions for the Asset deck, single element* [*mm*]*, (local coordinates).*

As seen in figure 6.2.1, the inner web is slightly thicker than the outer web. When the structure is assembled, see figure 6.2.2, the outer webs doubles which makes them much thicker than the inner web.

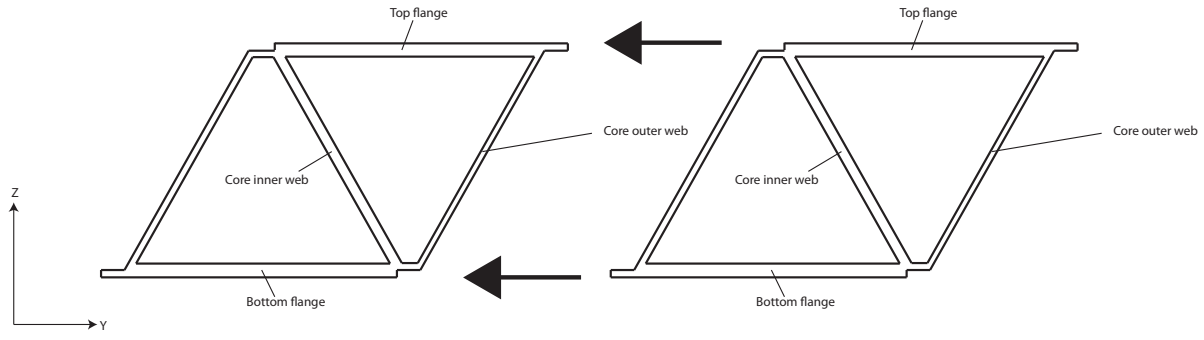

Figure 6.2.2: *Assembly of multiple Asset elements (local coordinates).*

The deck modules can be assembled together as far as desired. The joining between the modules is done by gluing them together at the slots. In reality the Asset profile is rounded at some edge spots, this is not modeled since it results in a too complicated mesh construction. Sharp edges are used instead.

The results are presented in local and global coordinates similar to the previous chapter. The plates are situated

cross the steel beams in the global structure, see figure 4.1.1, which means that the local x-direction translates to the global y-direction and the local y-direction translates to the global x-direction.

There are three versions of the Asset FRP deck used in this study, the first one is the original design and is the starting point of the optimization. The second version have an adjusted angle of the truss system in the core. This adjustment is done after careful evaluation of the plotted result from version one, where it could be found that an increase of the shear stiffness G_{13} (global coordinates) was needed. This is obtained by decreasing the inclination of the truss studs in the core from 61° to 55°. In version two, the thickness of the truss studs in the core is the same as for version one. This will lead to a lower total volume because of the geometric properties. Version three has the same structure as version two with the decrease in the inclination of the truss studs in the core, but with an adjusted thickness of the studs. The thickness is increased by 10% to match the total volume of version one. The Poisson's ratio of the total core structure is assumed to be $\nu = 0.3$.

In table 6.2.2 the stiffness in y-direction is set to zero, this is due to the results obtained from the calculations according to equation (6.0.3). When the bending stiffness of the core is very low, it is possible to obtain a negative value of the core stiffness. This can be explained by internal shear lag or other assumption errors for the derived analytical expression used in the transformation. In this case the stiffness of the core is set to zero as seen in table 6.2.2.

Table 6.2.1: Original stiffness for the material of the Asset deck parts (local coordinates) $[GPa]$.

System	E_{11}	E_{22}	E_{33}	G_{12}	G_{13}	G_{23}
Top flange	23	18	4.14	2.6	0.6	0.6
Core outer webs	17.3	22.7	4.14	3.15	0.6	0.6
Core inner webs	16.5	25.6	4.14	2	0.6	0.6
Bottom flange	23	18	4.14	2.6	0.6	0.6

Table 6.2.2: Stiffness of the core transformed into one orthotropic layer (local coordinates) $[GPa]$.

System	E_{11}	E_{22}	E_{33}	G_{12}	G_{13}	G_{23}
Asset version 1	0.874	0.103	7	0.307	0.193	0.051
Asset version 2	0.646	0*	6	0.332	0.143	0.125
Asset version 3	0.822	0*	6	0.336	0.155	0.130

* The stiffness in y-direction for the core is negligible and is set to zero.

Table 6.2.3: Stiffness of the equivalent plate (local coordinates) $[GPa]$.

System	E_{11}	E_{22}	E_{33}	G_{12}	G_{13}	G_{23}
Asset version 1	10.15	7.567	6.388	0.625	0.214	0.0585
Asset version 2	10.00	7.500	5.648	0.647	0.160	0.140
Asset version 3	10.12	7.500	6.65	0.650	0.173	0.146

To ensure a good transformation and a valid result, the transformed sections are compared once again with the original reference plate in table 6.2.4, 6.2.5 and 6.2.6. The deflection of the structures are compared for three different boundary conditions, two supports in x-direction (local coordinates), two supports in y-direction and the plate resting on four supports. Comparison is also carried out in two steps, first the original structure compared to the three layered sandwich plate and then the original structure compared to the one layered equivalent plate. This is done to be able to distinguish where possible errors occur and to better understand the total transformation process.

Table 6.2.4: Deflection for the Asset version 1 (AV-1), 3-layered equivalent plate (3-P) and the 1-layered equivalent plate (1-P) (local coordinates).

Supports	Load $[\frac{N}{m^2}]$	OR-P $[m]$	3-P $[m]$	1-P $[m]$	Diff AV-1 - 3-P [%]	Diff AV-1 - 1-P [%]
2(x-direction)	5000	0.0297675	0.0317499	0.0274049	6.24	7.94
2(y-direction)	5000	0.0073026	0.00747626	0.00644502	2.38	11.7
4	10000	0.0106598	0.0107973	0.00957696	1.3	10

Table 6.2.5: Deflection for the Asset version 2 (AV-2), 3-layered equivalent plate (3-P) and the 1-layered equivalent plate (1-P) (local coordinates).

Supports	Load $[\frac{N}{m^2}]$	OR-P $[m]$	3-P $[m]$	1-P $[m]$	Diff AV-2 - 3-P [%]	Diff AV-2 - 1-P [%]
2(x-direction)	5000	0.0305727	0.0325629	0.0280207	6.5	8.3
2(y-direction)	5000	0.00686316	0.00673103	0.00570962	1.9	16.8
4	10000	0.0102092	0.00976707	0.00853028	4.3	16.4

Table 6.2.6: Deflection for the Asset version 3 (AV-3), 3-layered equivalent plate (3-P) and the 1-layered equivalent plate (1-P) (local coordinates).

Supports	Load $[\frac{N}{m^2}]$	OR-P $[m]$	3-P $[m]$	1-P $[m]$	Diff AV-3 - 3-P [%]	Diff AV-3 - 1-P [%]
2(x-direction)	5000	0.0301046	0.0320748	0.02777152	6.5	7.7
2(y-direction)	5000	0.00685663	0.00671071	0.00569058	2.1	17
4	10000	0.010118	0.00969525	0.00847383	4.2	16.2

As previously mentioned, the stiffness in y-direction for the core is set to zero, though to obtain a reasonable material behavior it is set to 0.065 GPa in Abaqus. This stiffness will most likely not influence the deflection due to the low value and the zero level on for the moment of inertia.

As seen in tables 6.2.4 to 6.2.6, the difference between the original plates and the equivalent can be large. After studying column six and seven, its apparent that the difference in deflection is obtained due to the model translating the three layered sandwich plate into one layer. The difference reaches close to 20% in some cases which can be a source of error and misinterpretation if treated in the wrong way. It is important to keep this in mind in further conclusions.

The core transformation seem to hold true with only a small margin of error. This can be observed by studying column six in tables 6.2.4 to 6.2.6 with an error of maximum 5%. However, the difference between the original plates and the equivalent can be large and reaches up to 17%. After further study of column six and seven, it is apparent that the difference in deflection is obtained due to the model transforming the three layered sandwich plate into one equivalent layer. This may be a source of error and misinterpretation if treated the wrong way. It is important to keep this in mind in further conclusions.

The shear modulus of G_{12} for the asset deck gives a relative strain of approximately 50 %, as seen in figure 6.2.3. This value is much larger than the previous analyzed decks, such as the Rektoplate. This is obvious since the material of the Asset deck is fiber reinforced glass, which has a much lower elastic module than steel, which in turn was the material used for the other plates. The amount of material also differs between these plates, hence the results cannot be compared fairly. Since the Asset deck has this large value of relative strain, the effective width of the deck is rather low, which gives just a small contribution to the longitudinal stiffness of the whole bridge structure. Due to the small effective width, it could be of interest to increase the stiffness parameter G_{12} depending on the cost. This can be achieved by adding material and/or increasing the shear stiffness G_{12} of the flanges.

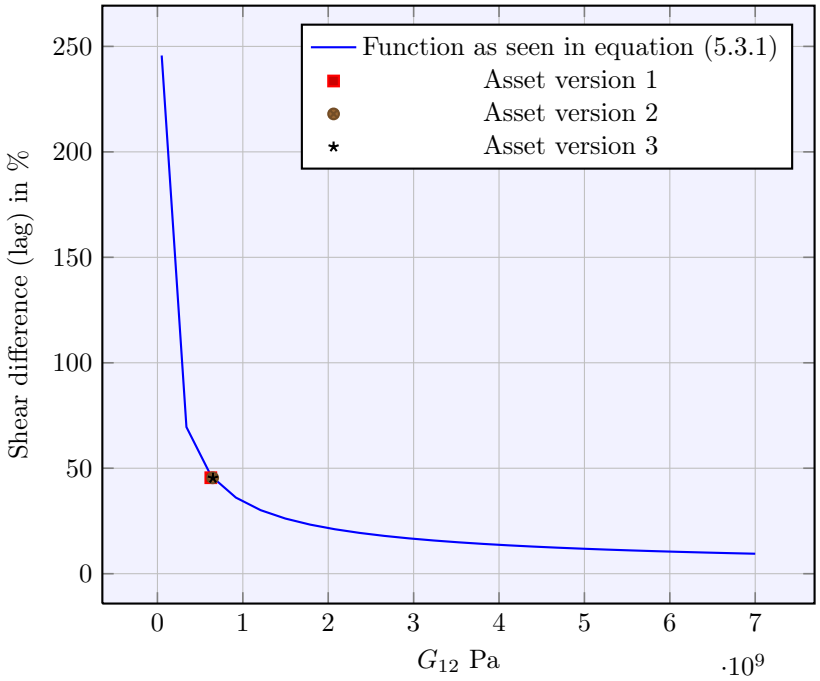

Figure 6.2.3: *Plotted values of the different plate systems in relation to the optimized relation of* G_{12}.

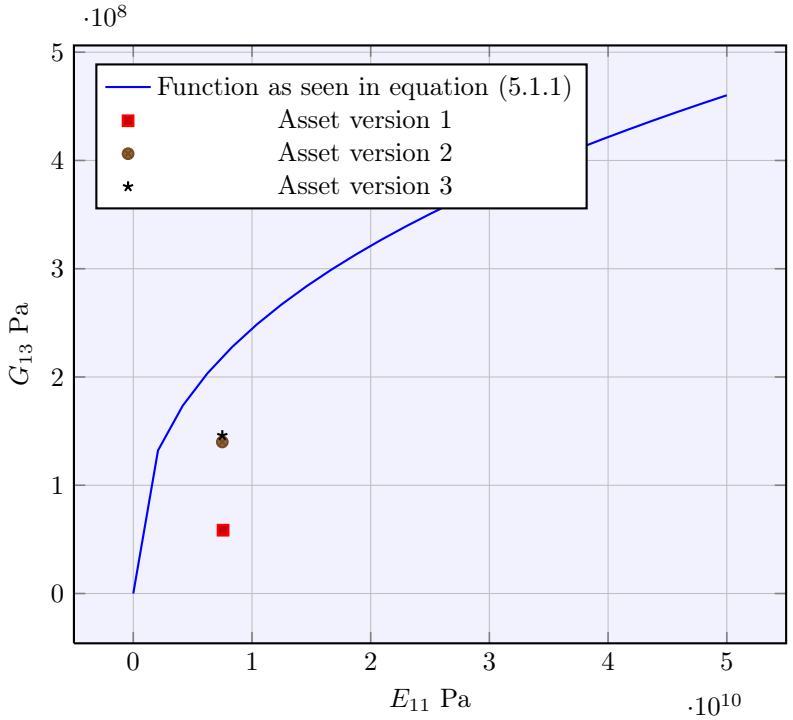

Figure 6.2.4: *Plotted values of the different plate systems in relation to the optimized relation of* E_{11} *and* G_{13}.

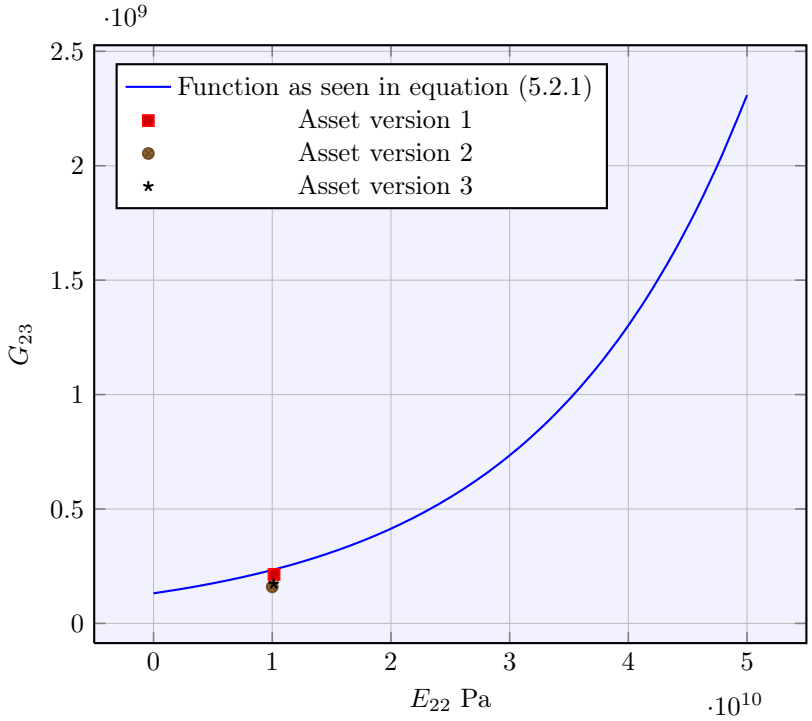

Figure 6.2.5: *Plotted values of the different plate systems in relation to the optimized relation of E_{22} and G_{23}.*

The relation between G_{23} and E_{22} is found to be almost optimal, just slightly below the curve as seen in figure 6.2.5. Since the Asset deck is supposed to work in single action transverse the bridge, hence it is not surprising that it behaves well in this area.

As seen in figure 6.2.4 G_{13} is too small for Asset version one, and has to be increased by almost 400 % in order to give a linear strain distribution over the height of the deck, i.e. effective height. This is done by increasing the inclination of the core studs for version two and three, where an improvement can be noted. When increasing the shear stiffness G_{13} the shear stiffness G_{23} will decrease slightly and loose its optimized relation. This can be explained by internal shear lag in the sandwich structure which may be introduced when the distance between the studs and the angle are increased. Hence, to obtain an even better relation between E_{11} and G_{13} more material or higher stiffness for the core material is needed.

7 Discussion

7.1 The generality of the result

The main result for this thesis is based on a very specific load case and geometry of the bridge. Therefore, the resulting parametric ratios are only valid and can only be applied for this specific case.

The load case has a big influence on the parametric study. However it is not the magnitude of the load but instead the load variation, for example different load lanes and point loads which are included in Eurocode load models. These will affect the ratio between E_{11} and E_{22} by having localized maximum deflections in different points depending on the load case, which will lead to a more complicated relation. Furthermore, when constructing the ratio between E_{11} and E_{22}, linear strain is assumed and obtained by the ratios between the elastic moduli and the shear moduli. These ratios are also affected by the load case which present some problem areas when measuring the strain. For example, the strain ϵ_{11} will not be symmetrical over the width of the plate and will change depending on the load calibration which makes the expression regarding G_{12} hard to approximate. This is also partly true for the strain ϵ_{22} which makes the ratio between E_{22} and G_{23} very dependent on the loading conditions.

All relationships are established for a certain height of the sandwich plate and stiffness of the underlying longitudinal steel beams. A change in the stiffness ratio between the steel beams and the sandwich plate could greatly affect the strain ϵ_{11} over the height of the total sandwich-beam structure. An increase of the height of the sandwich will also affect the other parameters due to the increase in stiffness of the member. Furthermore, the interaction between the sandwich plate and the main girders is assumed to be full. This is another parameter affects the ratios between the different stiffnesses.

For a realistic load case, all different load calibrations should be investigated and checked. A situation may occur where the calculated ratio between E_{11} and E_{22} for a certain allowed deflection is not stiff enough, and result in a larger deflection for another load calibration.

7.2 Validity of the results and possible error sources

When performing the parametric study, limited readings were done due to time constraints. This might have lead to a rather low resolution and few points for the curve fitting to approximate. It is also hard to judge what is linear enough since the new set of E_{11} and G_{13} is just compared with the reference by visual inspection. So both the curve fitting itself has too few readings and the visual inspection lacks accuracy. Even though that all this could have been done more accurate, this still proves that there is a relation between the affected stiffness ratios derived.

The TCFR transformation gives more accurate result than the TALD. Even though the result from it differs substantially from the reference one in some cases. Since TCFR is used for the optimization it must be remembered that the obtained result, when transforming before plotting in the parametric, ratios might differ to some extent.

The transformation methods are only verified by comparison of the deflection. The measured deflection is, as earlier said, a combination of bending and shear deflection. However, deflection caused by bending usually contributes much more to the total deflection, compared to shear deflection. If the shear moduli are transformed with very bad accuracy, but still end up being high enough to support fully developed linear strain, the comparison of the deflection is an invalid parameter to verify it by. This is due to the bending mainly being a function of the elastic moduli in the different directions. In other words, if the verification is done blindly without reflection and close inspection of the indata, the verification method can be an invalid comparison tool to evaluate the accuracy of the shear transformations. The shear transformation were though evaluated and tested, which showed a very good accordance between it and the reference plate, see section 4.7. Therefore, this is believed not to be a major problem for the somewhat inaccurate transformation.

When the truss plates were optimized, see section 6, they all had a large overcapacity of shear G_{13} and

G_{23}. Therefore they all probably had a fully developed linear strain distribution both before and after the TCFR transformation was performed. The transformed plates were compared with equivalent plates and the result showed very low difference in deflection, less than 1 %. However for the Asset deck optimization, see section 6.2, the regarded shear stiffnesses was too low to approve for linear strain. The transformation also showed much higher deviance of the result before and after transformation. In this case the plotted equivalent value may differ substantially from the actual correct one, making it very hard to be able to tell how far away it is from full linear strain. The relation between G_{23} and E_{22} is almost enough to provide for linear strain. This can also be observed by looking at the difference of deflection before/after transformation where it showed around 8 % wrong, compared with G_{13} and E_{11} where this value is around 16 %.

The transformation of the Asset deck to a three layered asset also had some problems. For the two modified Asset deck concepts it was impossible to get positive result of the core stiffness of E_{22} (local). Therefore this value was set to zero instead. This problem can be partly explained by that the strain ϵ_{22} (local) for the Asset deck is not linear over the cross section during bending. In equation 6.0.1 the D value is computed to allow for full linear strain. If this is not the case for the analyzed structure, an overestimation of the bending stiffness is obtained. When modeling bending of the Asset deck in Abaqus, the program takes care of shear lag of the face sheets between the studs. This is not the case when establishing D in the analytical model, where the face sheets are set to handle full strain all over. This, in combination with non-linear strain, is the reason why it is impossible to fit the measured deflection from Abaqus to solve the analytical expression to get the core's individual stiffness, i.e. the core gets a negative elastic modulus instead.

When optimizing a concept it is wise to design a concept that has overcapacity of shear stiffness G_{13} and G_{23}, and then decrease it to utilize the material better until linear strain in both cases. Doing it this way results in a proper transformation in both steps. If this is done the other way around, i.e. increasing the shear stiffnesses until linear strain, there might be errors. It was noted before that the Asset deck had insufficient shear stiffness, which resulted in bad transformations and inaccuracy when comparing the elastic and shear stiffness relations with the optimized relation. This error will decrease as long as strains tends to be more linear. However if the increments are too large, the last step may give a result that is believed to be linear, but it might not be since the method gives too large inaccuracy of the transformations. Therefore it is more safely to start with overcapacity of shear and decrease it rather than the vice versa.

The surface plot, see figure 6.1.1, is made with a fixed value of G_{12}, which affects the effective width. If this shear stiffness is changed, the surface plot will change. By increasing the effective width, the elastic modulus E_{11} will become more important.

7.3 Different types of optimization

The optimization of the sandwich plate structure can be divided into four different steps. They are organized with regard to the parameters affecting the different cases. The four identified steps are:

- Initial geometry
- Fully developed material strain, i.e maximized usage of material
- Stiffness in different directions
- Local behavior

The initial geometry affect the behavior of the sandwich plate in different ways. By changing the thickness of different layers and/or the total thickness, it is possible to find a more or less optimized geometry in relation to the steel beams. Another important factor is to design a structure that does not have internal shear lag between the core and the flanges, which may be the case for different truss structures with too large distance between the studs.

The two middle steps are addressed in this thesis by obtaining ratios from the parametric study. In other words, the obtained ratios between the shear and elastic moduli, and the relation between E_{11} and E_{22}. An improvement with regard to these ratios can be carried out by changing the structure, as exemplified in chapter

6, or by changing the stiffness in different directions for the elements in the sandwich structure with ribs or rearrangement of fiber layers in FRP-type materials.

Local behavior can be optimized with regard to buckling, delamination or other localized problems. This can be done by, for example, choosing a minimum thickness of a member to withstand buckling without overcapacity. There is no reason to believe that these four different optimizations have a similar result and can be combined, except for the two middle ones. This means that a complete optimized solution is hard to obtain and will most likely be a compromise. However, by aiming for an optimized relation between the stiffnesses, a better solution which is closer to an optimum structure will be obtained.

7.4 Assumptions and modeling

The FE modeling in this thesis has only been made with linear analysis. Buckling and local plasticity of the material has therefore been neglected which could have lead to unrealistic final result. The measured deflections might not have been possible to reach if this was considered, which gives an overestimation of the stiffness of the plates. Interaction of the sandwich and the girders has not been modeled in any way and the parts are just set to have full interaction.

Modeling in Abaqus CAE with shell elements can be dangerous and tricky. Defining shell offset directions has often turned up to be of opposite direction to what was believed because of localized coordinate systems for each individual part. This could have led to problems, especially for the optimization of different concepts where this had to be reconsidered several times until the desired and correct result was found.

8 Conclusions

- The TCFR method is a more stable and accurate transformation compared to the TALD method.
- There are four different levels of optimization for a sandwich plate resting on two longitudinal girders, where this thesis address two of them. Consequently the relations and concepts presented is insufficient data to perform a full scale optimization of a sandwich plate system.
- It is possible to establish usable relations between the different analyzed parameters, even though that they are only valid for this specific case. Otherwise the ratios could easily be adjusted to fit another type of geometric shape of the bridge, in the same manner as was done in this thesis.
- The derived parametric ratios can only be used as an evaluation tool and does not offer any design suggestions. It is up to the engineer to know how to alter the structure to fit the ratios better for an improved structural behavior.
- Several sandwich deck concepts suffered from overcapacity of shear stiffness, which was corrected and compensated by the help from the parametric ratios that were developed.
- An effective and accurate optimization should start with overcapacity of shear stiffness for the concept. This is done in order to ensure a good transformation with linear strain over the cross section in all directions.
- The procedure for optimization by hand is too tedious to perform for a single bridge. However, it could be useful if some parts of the optimization was to be automated.

8.1 General method for deck optimization

The results from this thesis could be used to establish a method of how to construct an optimized sandwich deck concept. Observe that the parametric ratios and relations from this thesis cannot be used in reality, since they are derived with a non-existing load case. These ratios would have to be done properly for LM1 from Eurocodes or equivalent. However the work methodology would be the same.

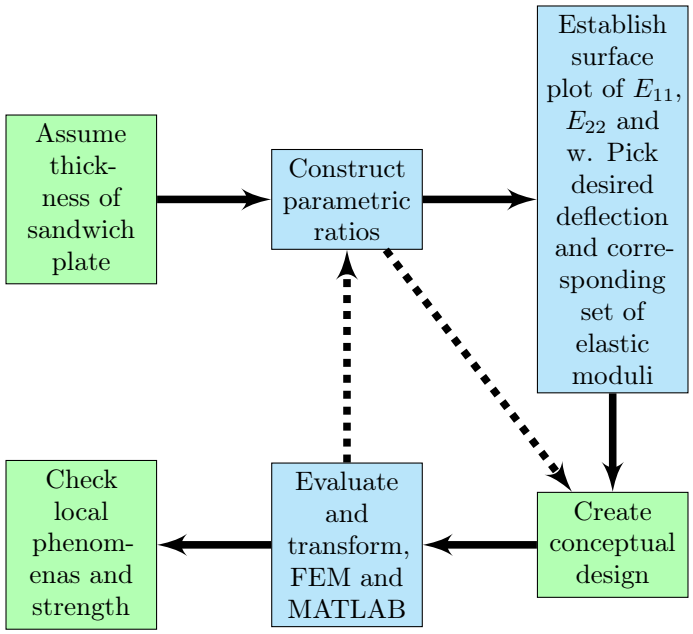

Figure 8.1.1: *Proposed optimization method, blue boxes indicates possibility of automation by computer software.*

- Start by assuming a thickness or use the one from the old bridge deck.

- Construct the parametric ratios for the specific case in question. This could be done by an automated process in e.g. Abaqus CAE by scripting, to give accurate relations.
- Next step would be to construct the E_{11}, E_{22} and w surface plot. From this a set of elastic moduli that fulfills the deflection requirement should be chosen.
- A conceptual design that is believed to serve the chosen elastic moduli and has overcapacity of shear stiffness should be constructed. By loading this concept in different directions, all elastic and shear moduli needed are obtained. Use the analytical model to simplify the structure to three different orthotropic homogeneous layers. Transform the three layered sandwich into one equivalent plate with the TCFR method. Compare resulting stiffness with the parametric ratios. Evaluate result and modify structure if not sufficiently optimized. Repeat this process until adequate relations are obtained.
- Evaluate the final conceptual design with regard to strength and local phenomena.

9 Future Research

- A deeper analysis where the optimization of the overall geometry is studied, both locally and globally.
- Model the interaction between the steel girders and the sandwich plate deck.
- Further verification and development of the transformation from a structured sandwich plate to a one layered plate. The TCFR method needs further calibration and verification. It might also need a limitation for which interval of parameters that could be used for it in order to get reliable results.
- Try to establish a more general solution for the parametric ratios, where sizes of beam members and height of sandwich plate can be changed.
- In the far future it could be of interest to study single walled carbon nano tube structure, instead of FRP, which holds a Young's modulus of approximately 5 times the one of steel and a strength of around 3 times, even though that the density is a fifth, Meo and Rossi (2006). These could be used for ultra light weight structures.

References

DIAB Sandwich handbook (2003). DIAB Group.

EUROPEAN STANDARD EN 1991-2:2003 (2003). *Eurocode 1: Actions on structures - Part 2: Traffic loads on bridges*. Version September 2003. EUROPEAN COMMITTEE FOR STANDARDIZATION.

Fiberline webpage (2012). Fiberline. URL: http://www.fiberline.com/about-us.

Meo, Michele and Marco Rossi (2006). "Prediction of Young's modulus of single wall carbon nanotubes by molecular-mechanics based finite element modelling". In: *Composites Science and Technology* 66.11âĂŞ12, pp. 1597 –1605. ISSN: 0266-3538. DOI: 10.1016/j.compscitech.2005.11.015. URL: http://www.sciencedirect.com/science/article/pii/S0266353805004367.

Prathap, Gangan (2001). *Finite element analysis as computation*. Scientific report. CSIR Center for Mathematical Modelling and Computer Simulation, Bangalore.

Szilard, Rudolph (2004). *Theories and applications of plate analysis*. John Wiley & Sons, Inc. ISBN: 0-471-42989-9.

Understandning Gridfit (2006). John R. D'Errico. URL: http://www.mathworks.com/matlabcentral/fileexchange/8998.

väg (2012). Nationalencyklopedin. URL: http://www.ne.se/vag/historik/sverige.

Zhou, Aixi (2002). "Stiffness and strength of fiber reinforce polymer composite bridge deck system". In: pp. 78–83.

10 Appendix

10.1 Load calculation

The load calculation is performed in Mathcad in accordance with the bridge section of Eurocode EC2 (*EUROPEAN STANDARD EN 1991-2:2003* 2003). The applied loads are divided into point loads and distributed loads. This is done to simulate axle loads from heavy vehicles (point loads) and a general traffic load in the different driving lanes (distributed loads). There are four different load models, Load model 1,2,3 and 4 (LM1-4) that are created to simulate different types of load the bridge can be subjected to. Load model 1 is made to simulate an universal traffic load and is to be used for general and local calculations. This is the load model used in the following calculations to make a preliminary sizing of the steel beams in the bridge model.

There are three different load cases where the loads are applied in different combinations to obtain the highest moment and reaction forces to be able to determine the design load (worst case). Ordinary a national annex with safety factors and specific values of constants is to be used in design, but because this is a preliminary sizing no such values are used. The self weight of the structure is also neglected.

Geometric input:

$l_{bridge} := 15m$ $l_{axle} := 1.2m$

$l_{ele} := 8m$

$l_{side} := 0.5m$

$l_{con} := 1.5m$

Other input

Self weight of sandwich element

$q_{sandwich} := 0\frac{kN}{m^2}$

Load model

Table 1: Number and width of notional lanes (EC1 part 2 table 4.1)

Carriageway width w	Number of notional lanes	Width of a notional lane w_l	Width of the remaining area
$w < 5{,}4$ m	$n_1 = 1$	3 m	w - 3 m
5,4 m $\leq w <$ 6 m	$n_1 = 2$	$\frac{w}{2}$	0
6 m $\leq w$	$n_1 = Int\left(\frac{w}{3}\right)$	3 m	$w - 3 \times n_1$
NOTE For example, for a carriageway width equal to 11m, $n_1 = Int\left(\frac{w}{3}\right) = 3$, and the width of the remaining area is 11 - 3×3 = 2m.			

$w := l_{ele} - 2 \cdot l_{side} = 7m$

$$n_1 := \begin{cases} 1 & \text{if } w < 5.4m \\ 2 & \text{if } 5.4m < w < 6m \\ \text{floor}\left(\frac{w}{3m}\right) & \text{if } w \geq 6m \end{cases} \quad = 2$$

$$w_l := \begin{cases} 3m & \text{if } w < 5.4m \\ \frac{w}{2} & \text{if } 5.4m < w < 6m \\ 3m & \text{if } w \geq 6m \end{cases} \quad = 3\,m$$

$$w_{ra} := \begin{cases} w - 3m & \text{if } w < 5.4m \\ 0 & \text{if } 5.4m < w < 6m \\ w - 3m \cdot n_1 & \text{if } w \geq 6m \end{cases} \quad = 1\,m$$

$w_p := 0.5m$

Load model 1 LM1

Table 2: Load Model 1, characteristic values (EC1 part 2, table 4.2)

Location	Tandem system *TS*	*UDL* system
	Axle loads Q_{ik} (kN)	q_{ik} (or q_{ik}) (kN/m^2)
Lane Number 1	300	9
Lane Number 2	200	2,5
Lane Number 3	100	2,5
Other lanes	0	2,5
Remaining area (q_{rk})	0	2,5

$q_{1k} := 9 \frac{kN}{m^2}$ $Q_{1k} := 300kN$

$q_{2k} := 2.5 \frac{kN}{m^2}$ $Q_{2k} := 200kN$

$q_{rak} := 2.5 \frac{kN}{m^2}$ **Observe, no safety factors applied!**

Transverse direction

Load case A (LM1)

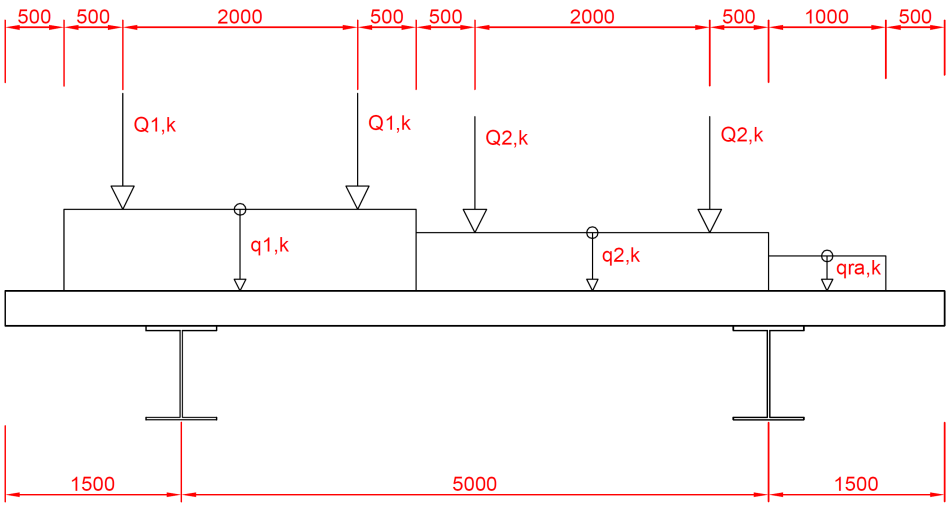

$$S_{A1} := \left| l_{ele} - l_{con} - l_{side} - \frac{w_l}{2} \right| = 4.5\,\text{m}$$

$$S_{A2} := \left| l_{ele} - l_{con} - l_{side} - \frac{3}{2}\cdot w_l \right| = 1.5\,\text{m}$$

$$S_{A3} := \left| l_{ele} - l_{con} - l_{side} - 2\cdot w_l - \frac{w_{ra}}{2} \right| = 0.5\,\text{m}$$

$$S_{Ap1} := \left| l_{ele} - l_{con} - l_{side} - w_p \right| = 5.5\,\text{m}$$

$$S_{Ap2} := \left| l_{ele} - l_{con} - l_{side} - \left(w_l - w_p\right) \right| = 3.5\,\text{m}$$

$$S_{Ap3} := \left| l_{ele} - l_{con} - l_{side} - w_l - w_p \right| = 2.5\,\text{m}$$

$$S_{Ap4} := \left| l_{ele} - l_{con} - l_{side} - w_l - \left(w_l - w_p\right) \right| = 0.5\,\text{m}$$

$$M_{A2q} := q_{sandwich}\cdot l_{ele}\cdot\frac{\left(l_{ele} - 2l_{con}\right)}{2} + q_{1k}\cdot w_l\cdot S_{A1} + q_{2k}\cdot w_l\cdot S_{A2} - q_{rak}\cdot w_{ra}\cdot S_{A3} = 131.5\cdot\frac{\text{kN}\cdot\text{m}}{\text{m}}$$

$$M_{A2Q} := Q_{1k}\cdot S_{Ap1} + Q_{1k}\cdot S_{Ap2} + Q_{2k}\cdot S_{Ap3} + Q_{2k}\cdot S_{Ap4} = 3.3\times 10^{3}\cdot\text{kN}\cdot\text{m}$$

The distributed load and point load have to be divided into different parts to be able to preform global calculations without unit related inconsistencies.

$$R_{A1} := \frac{M_{A2q}\cdot m + M_{A2Q}}{l_{ele} - 2\cdot l_{con}} = 686.3\cdot\text{kN}$$

$$R_{A1Q} := \frac{M_{A2Q}}{\left(l_{ele} - 2\cdot l_{con}\right)} = 660\cdot\text{kN}$$

$$R_{A2} := 2\cdot Q_{1k} + 2\cdot Q_{2k} + \left(q_{1k} + q_{2k}\right)\cdot w_l\cdot m + q_{rak}\cdot w_{ra}\cdot m - R_{A1} = 350.7\cdot\text{kN}$$

$$R_{A2Q} := 2\cdot Q_{1k} + 2\cdot Q_{2k} - R_{A1Q} = 340\cdot\text{kN}$$

$$R_{Al1} := \frac{M_{A2q}}{l_{ele} - 2\cdot l_{con}} = 26.3\cdot\frac{\text{kN}}{\text{m}}$$

$$R_{Al2} := \left(q_{1k} + q_{2k}\right)\cdot w_l + q_{rak}\cdot w_{ra} - R_{Al1} = 10.7\cdot\frac{\text{kN}}{\text{m}}$$

Load case B (LM1)

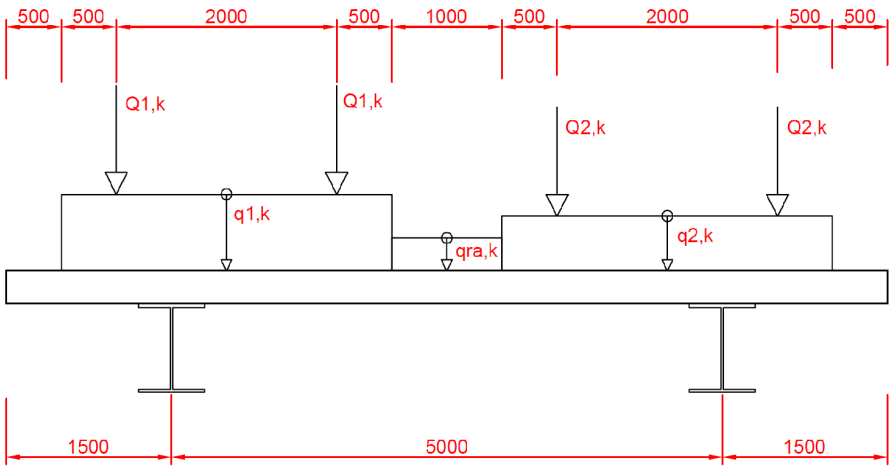

$$S_{B1} := \left| l_{ele} - l_{con} - l_{side} - \frac{w_l}{2} \right| = 4.5\,\text{m}$$

$$S_{B2} := \left| l_{ele} - l_{con} - l_{side} - w_l - \frac{w_{ra}}{2} \right| = 2.5\,\text{m}$$

$$S_{B3} := \left| l_{ele} - l_{con} - l_{side} - w_l - w_{ra} - \frac{w_l}{2} \right| = 0.5\,\text{m}$$

$$S_{Bp1} := \left| l_{ele} - l_{con} - l_{side} - w_p \right| = 5.5\,\text{m}$$

$$S_{Bp2} := \left| l_{ele} - l_{con} - l_{side} - \left(w_l - w_p \right) \right| = 3.5\,\text{m}$$

$$S_{Bp3} := \left| l_{ele} - l_{con} - l_{side} - w_l - w_{ra} - w_p \right| = 1.5\,\text{m}$$

$$S_{Bp4} := \left| l_{ele} - l_{con} - l_{side} - w_l - w_{ra} - \left(w_l - w_p \right) \right| = 0.5\,\text{m}$$

$$M_{B2q} := q_{sandwich} \cdot l_{ele} \cdot \frac{\left(l_{ele} - 2 \cdot l_{con} \right)}{2} + q_{1k} \cdot w_l \cdot S_{B1} + q_{rak} \cdot w_{ra} \cdot S_{B2} + q_{2k} \cdot w_l \cdot S_{B3} = 131.5 \cdot \frac{\text{kN} \cdot \text{m}}{\text{m}}$$

$$M_{B2Q} := Q_{1k} \cdot S_{Bp1} + Q_{1k} \cdot S_{Bp2} + Q_{2k} \cdot S_{Bp3} + Q_{2k} \cdot S_{Bp4} = 3.1 \times 10^{3} \cdot \text{kN} \cdot \text{m}$$

$$R_{B1} := \frac{M_{B2q} \cdot m + M_{B2Q}}{l_{ele} - 2 \cdot l_{con}} = 646.3 \cdot \text{kN}$$

$$R_{B1Q} := \frac{M_{B2Q}}{\left(l_{ele} - 2 \cdot l_{con} \right)} = 620 \cdot \text{kN}$$

$$R_{B2} := 2 \cdot Q_{1k} + 2.Q_{2k} + \left(q_{1k} + q_{2k}\right) \cdot w_l \cdot m + q_{rak} \cdot w_{ra} \cdot m - R_{B1} = 390.7 \cdot kN$$

$$R_{B2Q} := 2 \cdot Q_{1k} + 2.Q_{2k} - R_{B1Q} = 380 \cdot kN$$

$$R_{Bl1} := \frac{M_{B2q}}{l_{ele} - 2.l_{con}} = 26.3 \cdot \frac{kN}{m}$$

$$R_{Bl2} := \left(q_{1k} + q_{2k}\right) \cdot w_l + q_{rak} \cdot w_{ra} - R_{Bl1} = 10.7 \cdot \frac{kN}{m}$$

Load case C (LM1)

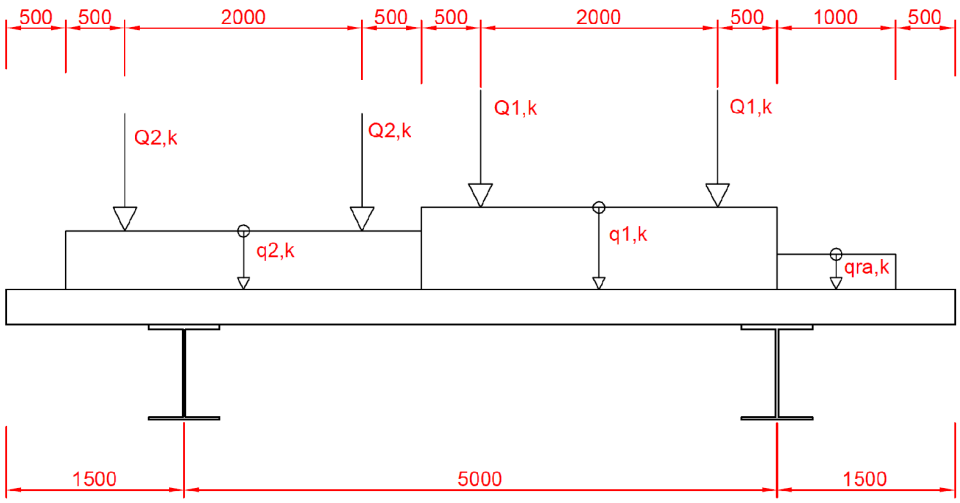

$$S_{C1} := \left| l_{ele} - l_{con} - l_{side} - \frac{w_l}{2} \right| = 4.5\,m$$

$$S_{C2} := \left| l_{ele} - l_{con} - l_{side} - w_l - \frac{w_l}{2} \right| = 1.5\,m$$

$$S_{C3} := \left| l_{ele} - l_{con} - l_{side} - 2 \cdot w_l - \frac{w_{ra}}{2} \right| = 0.5\,m$$

$$S_{Cp1} := \left| l_{ele} - l_{con} - l_{side} - w_p \right| = 5.5\,m$$

$$S_{Cp2} := \left| l_{ele} - l_{con} - l_{side} - \left(w_l - w_p\right) \right| = 3.5\,m$$

$$S_{Cp3} := \left| l_{ele} - l_{con} - l_{side} - w_l - w_p \right| = 2.5\,m$$

$$S_{Cp4} := \left| l_{ele} - l_{con} - l_{side} - w_l - \left(w_l - w_p\right) \right| = 0.5\,m$$

$$M_{C2q} := q_{sandwich} \cdot l_{ele} \cdot \frac{\left(l_{ele} - 2 \cdot l_{con}\right)}{2} + q_{2k} \cdot w_l \cdot S_{C1} + q_{1k} \cdot w_l \cdot S_{C2} - q_{rak} \cdot w_{ra} \cdot S_{C3} = 73 \cdot \frac{kN \cdot m}{m}$$

$$M_{C2Q} := Q_{2k} \cdot S_{Cp1} + Q_{2k} \cdot S_{Cp2} + Q_{1k} \cdot S_{Cp3} + Q_{1k} \cdot S_{Cp4} = 2.7 \times 10^{3} \cdot kN \cdot m$$

$$R_{C1} := \frac{M_{C2q} \cdot m + M_{C2Q}}{l_{ele} - 2 \cdot l_{con}} = 554.6 \cdot kN$$

$$R_{C1Q} := \frac{M_{C2Q}}{\left(l_{ele} - 2 \cdot l_{con}\right)} = 540 \cdot kN$$

$$R_{C2} := 2.Q_{1k} + 2 \cdot Q_{2k} + \left(q_{1k} + q_{2k}\right) \cdot w_l \cdot m + q_{rak} \cdot w_{ra} \cdot m - R_{C1} = 482.4 \cdot kN$$

$$R_{C2Q} := 2.Q_{1k} + 2 \cdot Q_{2k} - R_{C1Q} = 460 \cdot kN$$

$$R_{Cl1} := \frac{M_{C2q}}{l_{ele} - 2 \cdot l_{con}} = 14.6 \cdot \frac{kN}{m}$$

$$R_{Cl2} := \left(q_{1k} + q_{2k}\right) \cdot w_l + q_{rak} \cdot w_{ra} - R_{Cl1} = 22.4 \cdot \frac{kN}{m}$$

Longitudinal direction

$$q_{dist} := \max\left(R_{Al1}, R_{Bl1}, R_{Cl1}, R_{Al2}, R_{Bl2}, R_{Cl2}\right) = 26.3 \cdot \frac{kN}{m}$$ Case A

$$Q_{conc} := \max\left(R_{A1Q}, R_{B1Q}, R_{C1Q}, R_{A2Q}, R_{B2Q}, R_{C2Q}\right) = 660 \cdot kN$$

$$R_{l1} := \frac{q_{dist} \cdot l_{bridge} + 2 \cdot Q_{conc}}{2} = 857.25 \cdot kN$$

$$M_{max} := \left| Q_{conc} \cdot \left(\frac{l_{axle}}{2} \right) + q_{dist} \cdot \frac{l_{bridge}^{2}}{8} - R_{l1} \cdot \frac{l_{bridge}}{2} \right| = 5.294 \times 10^{3} \cdot kN \cdot m$$ at lbridge/2

$$W_{xHEB1000} := 12900 \cdot 10^{-6} \cdot m^{3}$$

$$f_{yk} := 355 \cdot MPa$$

$$M_{cap.HEB1000} := W_{xHEB1000} \cdot f_{yk} = 4.58 \times 10^{3} \cdot kN \cdot m$$ Slightly smaller than Mmax which is fine beacuse the "deck flange" will contribute.

10.2 MATLAB source code

```
%%%%%%%%%%%%%%%%%%%%%%%%%%%%%%%%%%%%%%%%%%%%%%%%%%%%%%%%%%%%%%%%%%%%%%%%
%   E2-calculation
%       Calculates the elastic modulus for the core
%       INPUT:  w (deflection)
%               E_1 (elastic moduli for flange 1)
%               E_3 (elastic moduli for flange 2)
%               t_1 (thickness of flange 1)
%               t_2 (thickness of core)
%               t_3 (thickess of flange 2)
%               v_1 (poisons ratio flange 1)
%               v_2 (poisons ratio core)
%               v_3 (poisons ratio flange 3)
%               b (width of the plate)
%               d_1 (distance from flange1 to neutral axis)
%               d_2 (distance from core to neutral axis)
%               d_3 (distance from flange2 to neutral axis)
%               NOTE:d_1-d_3 is calibrated for a symmetric
%                    cross-section in the current setting
%               G (shear modulus in direction of bending)
%               q (distributed load)
%               w (deflection)
%               l (length of plate)
%
%   BY: Anderberg Viktor, Bjorhag Isak
%%%%%%%%%%%%%%%%%%%%%%%%%%%%%%%%%%%%%%%%%%%%%%%%%%%%%%%%%%%%%%%%%%%%%%%%
clc
close all
clear all
%% INPUT
E_1=18e9;
E_3=18e9;

t_1=0.0156;
t_2=0.1938;
t_3=0.0156;

t=t_1+t_2+t_3;

v_1=0.3;
v_2=0.3;
v_3=0.3;

b=8;

d_1=((t_1+t_2+t_3)/2-t_1/2);
d_2=0;
d_3=((t_1+t_2+t_3)/2-t_1/2);

A=(t_1+t_2+t_3)*b;
G=0.1300578035e9;
q=5000*b;
w=0.00685663;
l=5;

%% CALCULATION
E_2=- (((384*E_1*(d_1^2*t_1 + t_1^3/12))/(v_1^2 - 1) + (384*E_3*(d_3^2*t_3 + ...
    t_3^3/12))/(v_3^2 - 1))*(v_2^2 - 1))/(384*(d_2^2*t_2 + t_2^3/12)) - (5*l^4*q*(v_2^2 - ...
    1))/(384*(w - (l^2*q)/(8*A*G))*(b*d_2^2*t_2 + (b*t_2^3)/12))
D=E_1/(1-v_1^2)*(b*t_1^3/12+b*t_1*d_1^2)+...
    E_2/(1-v_2^2)*(b*t_2^3/12+b*t_2*d_2^2)+...
    E_3/(1-v_3^2)*(b*t_3^3/12+b*t_3*d_3^2)
Δ=5*q*l^4/(384*D)+q*l^2/(8*A*G)
disp('Shear deflection (in %):')
q*l^2/(8*A*G)/Δ*100
disp('Bending deflection (in %):')
5*q*l^4/(384*D)/Δ*100
```

```
%%%%%%%%%%%%%%%%%%%%%%%%%%%%%%%%%%%%%%%%%%%%%%%%%%%%%%%%%%%%%%%%%%%%%%%
%   E11E22-relation
%           Produces a 3d-plot of the relations between
%           E11, E22 and the deflection from the data
%           found in finaldata.dat. Gradient vector field
%           is also plotted to indicate how to change
%           the plate to optimize the material.
%           A curvefit is implemented using the function
%           gridfit which can be found in MATLAB-online
%           recource library.
%
%   BY: Anderberg Viktor, Bjorhag Isak
%%%%%%%%%%%%%%%%%%%%%%%%%%%%%%%%%%%%%%%%%%%%%%%%%%%%%%%%%%%%%%%%%%%%%%%
clc
close all
clear all
%%
load('finaldata.dat')
x=finaldata(1:9,2);
y=x;
z=[finaldata(1+9*0:9+9*0,3),finaldata(1+9*1:9+9*1,3),...
    finaldata(1+9*2:9+9*2,3),finaldata(1+9*3:9+9*3,3),...
    finaldata(1+9*4:9+9*4,3),finaldata(1+9*5:9+9*5,3),...
    finaldata(1+9*6:9+9*6,3),finaldata(1+9*7:9+9*7,3),...
    finaldata(1+9*8:9+9*8,3)];
xi=linspace(0,x(9),100);
yi=linspace(0,y(9),100);
zgrids = gridfit(finaldata(:,1),finaldata(:,2),finaldata(:,3),...
    xi,yi,'autoscale','on');
vx=linspace(0,x(9),20);
vy=linspace(0,y(9),20);
zgrad=gridfit(finaldata(:,1),finaldata(:,2),finaldata(:,3),vx,...
    vy,'autoscale','on');
[px,py] = gradient(zgrad);
surfc(x,y,z)
xlabel('E11')
ylabel('E22')
zlabel('w')
figure(2)
surfc(xi,yi,zgrids)
xlabel('E11')
ylabel('E22')
zlabel('w')
figure(3)
contour(xi,yi,zgrids)
hold on
quiver(vx,vy,px,py)
xlabel('E11')
ylabel('E22')
```

```
%%%%%%%%%%%%%%%%%%%%%%%%%%%%%%%%%%%%%%%%%%%%%%%%%%%%%%%%%%%%%%%%%%%%%%%
%   EEM-algoritm
%       Calculates the equivalent properties of a plate
%       from a three-layered sandwich plate. A check
%       is also performed to ensure realistic material
%       indata.
%           INPUT:  E-moduli in three directions for the three layers
%                   G-moduli in three directions for the three layers
%                   Poisons-ratio in three directions for the three layers
%                   Height of the three layers
%           OUTPUT: KINA_EQ - equivalent properties calculated
%                             according to Aixi Zhou
%                   EQ - equivalent properties calculated
%                        according to equatins obtained from
%                        bending stiffness
%                   NU - equivalent poisons ratios
%
%   BY: Anderberg Viktor, Bjorhag Isak
%%%%%%%%%%%%%%%%%%%%%%%%%%%%%%%%%%%%%%%%%%%%%%%%%%%%%%%%%%%%%%%%%%%%%%%
clc
close all
clear all
format('shortE')
%% INPUT
%% TOP FACE SHEET (UPPER FLANGE)
ET=[23e9, 18e9, 20e9];
NU1T=[0.3, 0.3, 0.3];
NUT=[NU1T, NU1T(1)/ET(1)*ET(2), NU1T(2)/ET(1)*ET(3), NU1T(3)/ET(2)*ET(3)];
GT=[2.6e9, 600e6, 600e6];
HT=0.0156;

%% INTERFACE (CORE)
EI=[0, 0, 7e9];
NU1I=[0.3, 0.3, 0.3];
NUI=[NU1I, NU1I(1)/EI(1)*EI(2), NU1I(2)/EI(1)*EI(3), NU1I(3)/EI(2)*EI(3)];
GI=[0.3333e9, 0.140625e9, 0.1046e9];
HI=0.1938;

%% BOTTOM FACE SHEET (BOTTOM FLANGE)
EB=[23e9, 18e9, 20e9];
NU1B=[0.3, 0.3, 0.3];
NUB=[NU1B, NU1B(1)/EB(1)*EB(2), NU1B(2)/EB(1)*EB(3), NU1B(3)/EB(2)*EB(3)];
GB=[2.6e9, 600e6, 600e6];
HB=0.0156;
%%
%% CHECK
EC=[ET;EI;EB];
NUC=[NUT;NUI;NUB];
for i=1:length(EC)
    if NUC(i,1) > sqrt(EC(i,1)/EC(i,2))
        disp('ERROR not valid material properties')
        i
    end
    if NUC(i,2) > sqrt(EC(i,1)/EC(i,3))
        disp('ERROR not valid material properties')
        i
    end
    if NUC(i,3) > sqrt(EC(i,3)/EC(i,2))
        disp('ERROR not valid material properties')
        i
    end
    if 1-NUC(i,1)*NUC(i,4)-NUC(i,3)*NUC(i,6)-NUC(i,2)*NUC(i,5)-...
            2*NUC(i,4)*NUC(i,6)*NUC(i,2) < 0
        disp('ERROR not valid material properties')
        i
    end
end
%% CHECK OF ASSUMPTIONS
H=HT+HI+HB;
xNx=(-EB(1)*HB^2+2*EB(1)*H*HB+ET(1)*HT^2+EI(1)*H*HI)/(2*(EB(1)*...
```

```
    HB+EI(1)*HI+ET(1)*HT));
xNy=(-EB(2)*HB^2+2*EB(2)*H*HB+ET(2)*HT^2+EI(2)*H*HI)/(2*(EB(2)*...
    HB+EI(2)*HI+ET(2)*HT));
if xNx>HT+HI | xNx<HT
    disp('ERROR neutral axis is not in the core in x-direction')
end
if xNy>HT+HI | xNy<HT
    disp('ERROR neutral axis is not in the core in y-direction')
end
%% CONTROL OF RELATIONS BETWEEN SHEAR VALUES FOR ACCURATE TRANSFORMATION
for e=2:3
    diffG=max([GT(e),GI(e),GB(e)])/min([GT(e),GI(e),GB(e)]);
    if diffG>=1e3
        disp('WARNING! LARGE DIFFERENCE IN SHEAR MODULUS. THIS MAY LEAD TO INACCURATE RESULT')
    end
end
%% ALGORITHM
at=HT/H;
ai=HI/H;
ab=HB/H;
E11=at*ET(1)+ai*EI(1)+ab*EB(1);
E22=at*ET(2)+ai*EI(2)+ab*EB(2);
E33=1/(at/ET(3)+ai/EI(3)+ab/EB(3));
Eeq11=(12*ET(1)*(HT^3/12 + (HT*(- EB(1)*HB^2 + 2*EB(1)*H*HB + ET(1)*HT^2 + ...
    EI(1)*H*HI)^2)/(4*(EB(1)*HB + EI(1)*HI + ET(1)*HT)^2)))/H^3 + (12*EB(1)*(HB^3/12 + ...
    HB*(H - (- EB(1)*HB^2 + 2*EB(1)*H*HB + ET(1)*HT^2 + EI(1)*H*HI)/(2*(EB(1)*HB + EI(1)*HI ...
    + ET(1)*HT)))^2))/H^3 + (12*EI(1)*(HI^3/12 + HI*(HI/2 + HT/2 - (- EB(1)*HB^2 + ...
    2*EB(1)*H*HB + ET(1)*HT^2 + EI(1)*H*HI)/(2*(EB(1)*HB + EI(1)*HI + ET(1)*HT)))^2))/H^3;
Eeq22=(12*ET(2)*(HT^3/12 + (HT*(- EB(2)*HB^2 + 2*EB(2)*H*HB + ET(2)*HT^2 + ...
    EI(2)*H*HI)^2)/(4*(EB(2)*HB + EI(2)*HI + ET(2)*HT)^2)))/H^3 + (12*EB(2)*(HB^3/12 + ...
    HB*(H - (- EB(2)*HB^2 + 2*EB(2)*H*HB + ET(2)*HT^2 + EI(2)*H*HI)/(2*(EB(2)*HB + EI(2)*HI ...
    + ET(2)*HT)))^2))/H^3 + (12*EI(2)*(HI^3/12 + HI*(HI/2 + HT/2 - (- EB(2)*HB^2 + ...
    2*EB(2)*H*HB + ET(2)*HT^2 + EI(2)*H*HI)/(2*(EB(2)*HB + EI(2)*HI + ET(2)*HT)))^2))/H^3;
G12=at*GT(1)+ai*GI(1)+ab*GB(1);
G21=G12;
G13=1/(at/GT(2)+ai/GI(2)+ab/GB(2));
G31=G13;
G23=1/(at/GT(3)+ai/GI(3)+ab/GB(3));
G32=G23;
test=at*GT(3)+ai*GI(3)+ab*GB(3);
NU12=at*NUT(1)+ai*NUI(1)+ab*NUB(1);
NU13=at*NUT(2)+ai*NUI(2)+ab*NUB(2);
NU23=at*NUT(3)+ai*NUI(3)+ab*NUB(3);
KINA_EG=[E11,E22,E33,G12,G13,G23]';
EQ=[Eeq11, Eeq22, E33, G12, G13, G23]';
NUU=[NU12, NU13, NU23]';

%% OUTPUT
KINA_EG
EQ
format('short')
NUU
```

```
%%%%%%%%%%%%%%%%%%%%%%%%%%%%%%%%%%%%%%%%%%%%%%%%%%%%%%%%%%%%%%%%%%%%%%%
%   EG-ratio
%       Produces graphs and equations for the relation between
%       shear and elastic moduli in different directions with
%       regard to linear strain over the crossection.
%       The equations are obtained from curve fitting functions
%       logfit and ezyfit(G23 and E22) which both can be found
%       on the online MATLAB recource library.
%       This is constructed from indata files:
%               G13E11data.dat
%               G23grejor.dat
%               G12shearlag.dat
%
%   BY: Anderberg Viktor, Bjorhag Isak
%%%%%%%%%%%%%%%%%%%%%%%%%%%%%%%%%%%%%%%%%%%%%%%%%%%%%%%%%%%%%%%%%%%%%%%
clc
close all
clear all
%% Test values
Ex=4.1517*10^9;
Ey=7.2311*10^9;
G12=6.9733*10^8;
G13=1.0676*10^8;
G23=1.0676*10^8;
%% G13 and E11
data=load('G13E11data.dat');
x=linspace(data(1,1),data(end,1),100);
[s,i]=logfit(data(:,1),data(:,2),'loglog');
waapprox=(10^i)*x.^(s);
format('shortE')
G13ratt=(10^i)*Ex^(s)
%% G23 and E22
data3=sort(load('G23grejor.dat'));
x3=linspace(data3(1,1),data3(end,1),100);
d3approx=1.3164*10^8*exp(5.7292*10^-11.*x3);
G23ratt=1.3164*10^8*exp(5.7292*10^-11*Ey)
%% G12 shear lag
data2=load('G12shearlag.dat');
x2=linspace(data2(1,1),data2(end,1),100);
figure(1)
[slope,intercept]=logfit(data2(:,1),data2(:,2),'loglog');
yapprox=(10^intercept)*x2.^(slope);
Shearp=(10^intercept)*G12^(slope)
%% PLOT
figure(2)
plot(data(:,1),data(:,2),'o',x,waapprox,'-')
hold on
xlabel('E11 [Pa]')
ylabel('G13 [Pa]')
figure(3)
plot(data2(:,1),data2(:,2),'o',x2,yapprox,'-')
xlabel('G12 [Pa]')
ylabel('Shear difference (lag) in %')
figure(4)
plot(data3(:,1),data3(:,2),'o',x3,d3approx,'-')
xlabel('E22 [Pa]')
ylabel('G23 [Pa]')
```

```
%%%%%%%%%%%%%%%%%%%%%%%%%%%%%%%%%%%%%%%%%%%%%%%%%%%%%%%%%%%%%%%%%%%%%%%
%   Plate isotropic
%        Calculates the deflection, moments in x,y and xy and
%        stresses in x, y and xy by means of fourier expansions
%        for an isotropic plate. Plots the results in graphs.
%               INPUT:  loop - number of itterations
%                       a - width
%                       b - length
%                       steg - step
%                       nu - poisons ratio
%                       E - E-modulus
%                       h - height
%                       P0 - load
%
%   BY: Anderberg Viktor, Björhag Isak
%%%%%%%%%%%%%%%%%%%%%%%%%%%%%%%%%%%%%%%%%%%%%%%%%%%%%%%%%%%%%%%%%%%%%%%
%%
clear all
close all
clc
%% INPUT
loop=10;
a=5;
b=2;
steg=0.05;
E=210*10^9;
nu=0.3;
h=0.01;
z=h/2;
P0=2*10^3;
%% CALCULATION
x=0:steg:a;
y=0:steg:b;
wadd=zeros(length(x),length(y));
mxadd=wadd;
myadd=wadd;
mxyadd=wadd;
wsum=wadd;
mxsum=wadd;
mysum=wadd;
mxysum=wadd;
D=E*h^3/(12*(1-nu^2));
for m=1:2:loop
    for n=1:2:loop
        for i=1:length(x)
            for j=1:length(y)
                wadd(i,j)=sin(m*pi*x(i)/a)*sin(n*pi*y(j)/b)/((m^2/a^2+n^2/b^2)^2*m*n);
                mxadd(i,j)=((m/a)^2+nu*(n/b)^2)*sin(m*pi*x(i)/a)*sin(n*pi*y(j)/b)/((m^2/a^2...
                +n^2/b^2)^2*m*n);
                myadd(i,j)=((n/b)^2+nu*(m/a)^2)*sin(m*pi*x(i)/a)*sin(n*pi*y(j)/b)/((m^2/a^2...
                +n^2/b^2)^2*m*n);
                mxyadd(i,j)=cos(m*pi*x(i)/a)*cos(n*pi*y(j)/b)/(a*b*(m^2/a^2+n^2/b^2)^2);
            end
        end
        wsum=wsum+wadd;
        mxsum=mxsum+mxadd;
        mysum=mysum+myadd;
        mxysum=mxysum+mxyadd;
    end
end
w=-16*P0/(pi^6*D).*wsum;
mx=16*P0/(pi^4).*mxsum;
my=16*P0/(pi^4).*mysum;
mxy=-16*P0/pi^4*(1-nu).*mxysum;
sigx=-192*P0*z/(h^3*pi^4).*mxsum;
sigy=-192*P0*z/(h^3*pi^4).*mysum;
sigxy=-192*P0*z/(h^3*pi^4)*(1-nu).*mxysum;
%% PLOT
figure(1)
surf(w')
```

```
xlabel('x')
ylabel('y')
axis([0 max(a,b)/steg+1 0 max(a,b)/steg+1 min(min(w)) max(max(w))])
title('Deflection')
figure(2)
surf(mx')
xlabel('x')
ylabel('y')
axis([0 max(a,b)/steg+1 0 max(a,b)/steg+1 min(min(mx)) max(max(mx))])
title('mx')
surf(my')
xlabel('x')
ylabel('y')
axis([0 max(a,b)/steg+1 0 max(a,b)/steg+1 min(min(my)) max(max(my))])
title('my')
figure(4)
surf(mxy')
xlabel('x')
ylabel('y')
axis([0 max(a,b)/steg+1 0 max(a,b)/steg+1 min(min(mxy)) max(max(mxy))])
title('mxy')
figure(5)
surf(sigx')
xlabel('x')
ylabel('y')
axis([0 max(a,b)/steg+1 0 max(a,b)/steg+1 min(min(sigx)) max(max(sigx))])
title('Sigma x')
figure(6)
surf(sigy')
xlabel('x')
ylabel('y')
axis([0 max(a,b)/steg+1 0 max(a,b)/steg+1 min(min(sigy)) max(max(sigy))])
title('Sigma y')
figure(7)
surf(sigxy')
xlabel('x')
ylabel('y')
axis([0 max(a,b)/steg+1 0 max(a,b)/steg+1 min(min(sigxy)) max(max(sigxy))])
title('Sigma xy')
```

```
%%%%%%%%%%%%%%%%%%%%%%%%%%%%%%%%%%%%%%%%%%%%%%%%%%%%%%%%%%%%%%%%%%%%%%%%%%%%
%   Plate orthotropic
%           Calculates the deflection, moment in x, y and xy and
%           stress in x, y and xy for an orthotropic plate. This
%           is done by means of fourier expansion.
%                   INPUT:  loop - number of itterations
%                           a - width
%                           b - length
%                           steg - step
%                           Ex - E-modulus in x-direction
%                           Ey - E-modulus in y-direction
%                           nux - poisons ratio in x-direction
%                           nuy - poisons ratio in y-direction
%                           h - height
%                           P0 - load
%
%   BY: Anderberg Viktor, Björhag Isak
%%%%%%%%%%%%%%%%%%%%%%%%%%%%%%%%%%%%%%%%%%%%%%%%%%%%%%%%%%%%%%%%%%%%%%%%%%%%
%%
clear all
close all
clc
%% INPUT
loop=40;
a=5;
b=2;
steg=0.1;
Ex=210*10^1;
Ey=210*10^10;
nux=0.3;
nuy=0.3;
h=0.01;
z=h/2;
P0=-2*10^3;
%% Stiffnesses
G=sqrt(Ex*Ey)/(2*(1+sqrt(nux*nuy)));
Dx=Ex*h^3/(12*(1-nux*nuy));
Dy=Ey*h^3/(12*(1-nux*nuy));
Dxy=Ex*h^3*nuy/(12*(1-nux*nuy));
Ds=G*h^3/12;
H=Dxy+2*Ds;
%% CALCULATION
x=0:steg:a;
y=0:steg:b;
wadd=zeros(length(x),length(y));
mxadd=wadd;
myadd=wadd;
mxyadd=wadd;
wsum=wadd;
mxsum=wadd;
mysum=wadd;
mxysum=wadd;
sigxadd=wadd;
sigxsum=wadd;
sigysum=wadd;
sigyadd=wadd;
for m=1:2:loop
    for n=1:2:loop
        for i=1:length(x)
            for j=1:length(y)
                wadd(i,j)=sin(m*pi*x(i)/a)*sin(n*pi*y(j)/b)/(m*n*(Dx*m^4/a^4+2*H*m^2*n^2/...
                    (a^2*b^2)+Dy*n^4/b^4));
                mxadd(i,j)=Dx*m^2*pi^2/a^2*sin(m*pi*x(i)/a)*sin(n*pi*y(j)/b)/(m*n*(Dx*m^4...
                /a^4+2*H*m^2*n^2/(a^2*b^2)+Dy*n^4/b^4))+Dxy*n^2*pi^2/b^2*sin(m*pi*x(i)/a)...
                    *sin(n*pi*y(j)/b)/(m*n*(Dx*m^4/a^4+2*H*m^2*n^2/(a^2*b^2)+Dy*n^4/b^4));
                myadd(i,j)=Dy*n^2*pi^2/b^2*sin(n*pi*y(j)/b)*sin(m*pi*x(i)/a)/(m*n*(Dx*m^4...
                /a^4+2*H*m^2*n^2/(a^2*b^2)+Dy*n^4/b^4))+Dxy*m^2*pi^2/a^2*sin(m*pi*x(i)/a)...
                    *sin(n*pi*y(j)/b)/(m*n*(Dx*m^4/a^4+2*H*m^2*n^2/(a^2*b^2)+Dy*n^4/b^4));
                mxyadd(i,j)=pi^2*cos(m*pi*x(i)/a)*cos(n*pi*y(j)/b)/(a*b*(Dx*m^4/a^4+2*H...
                    *m^2*n^2/(a^2*b^2)+Dy*n^4/b^4));
```

```
                sigxadd(i,j)=m^2*pi^2/a^2*sin(m*pi*x(i)/a)*sin(n*pi*y(j)/b)/(m*n*(Dx*m^4...
                /a^4+2*H*m^2*n^2/(a^2*b^2)+Dy*n^4/b^4))+nuy*n^2*pi^2/b^2*sin(m*pi*x(i)/a)...
                    *sin(n*pi*y(j)/b)/(m*n*(Dx*m^4/a^4+2*H*m^2*n^2/(a^2*b^2)+Dy*n^4/b^4));
                sigyadd(i,j)=n^2*pi^2/b^2*sin(m*pi*x(i)/a)*sin(n*pi*y(j)/b)/(m*n*(Dx*m^4...
                /a^4+2*H*m^2*n^2/(a^2*b^2)+Dy*n^4/b^4))+nux*m^2*pi^2/a^2*sin(m*pi*x(i)/a)...
                    *sin(n*pi*y(j)/b)/(m*n*(Dx*m^4/a^4+2*H*m^2*n^2/(a^2*b^2)+Dy*n^4/b^4));
            end
        end
        wsum=wsum+wadd;
        mxsum=mxsum+mxadd;
        mysum=mysum+myadd;
        mxysum=mxysum+mxyadd;
        sigxsum=sigxsum+sigxadd;
        sigysum=sigysum+sigyadd;
    end
end
w=16*P0/(pi^6).*wsum;
mx=16*P0/(pi^6).*mxsum;
my=16*P0/(pi^6).*mysum;
mxy=-G*h^3/12*16*P0/pi^6.*mxysum;
sigx=-Ex/(1-nux*nuy)*16*P0/pi^6*z.*sigxsum;
sigy=-Ey/(1-nux*nuy)*16*P0/pi^6*z.*sigysum;
sigxy=-2*G*z.*mxysum;
%% PLOT
figure(1)
surf(w')
xlabel('x')
ylabel('y')
title('w')
axis([0 max(a,b)/steg+1 0 max(a,b)/steg+1 min(min(w)) max(max(w))])
figure(2)
surf(mx')
xlabel('x')
ylabel('y')
title('mx')
axis([0 max(a,b)/steg+1 0 max(a,b)/steg+1 min(min(mx)) max(max(mx))])
figure(3)
surf(my')
xlabel('x')
ylabel('y')
title('my')
axis([0 max(a,b)/steg+1 0 max(a,b)/steg+1 min(min(my)) max(max(my))])
figure(4)
surf(mxy')
xlabel('x')
ylabel('y')
title('mxy')
axis([0 max(a,b)/steg+1 0 max(a,b)/steg+1 min(min(mxy)) max(max(mxy))])
figure(5)
surf(sigx')
xlabel('x')
ylabel('y')
title('sigma x')
axis([0 max(a,b)/steg+1 0 max(a,b)/steg+1 min(min(sigx)) max(max(sigx))])
figure(6)
surf(sigy')
xlabel('x')
ylabel('y')
title('sigy')
axis([0 max(a,b)/steg+1 0 max(a,b)/steg+1 min(min(sigy)) max(max(sigy))])
figure(7)
surf(sigxy')
xlabel('x')
ylabel('y')
title('sigxy')
axis([0 max(a,b)/steg+1 0 max(a,b)/steg+1 min(min(sigxy)) max(max(sigxy))])
```